

AFWAL-TR-86-4049

ADA 206426



CHARACTERIZATION OF ACETYLENE- TERMINATED RESIN CURE STATES

**A. C. Lind
C. G. Fry
R. L. Levy
T. C. Sandreczki**

**McDonnell Douglas Research Laboratories
St. Louis, Missouri 63166**

September 1986

Final Report for Period 1 June 1983 – 30 September 1985

Approved for public release; distribution is unlimited.

Best Available Copy

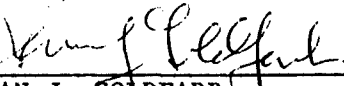
**MATERIALS LABORATORY
AIR FORCE WRIGHT AERONAUTICAL LABORATORIES
AIR FORCE SYSTEMS COMMAND
WRIGHT-PATTERSON AIR FORCE BASE, OHIO 45433-6533**

20040219033

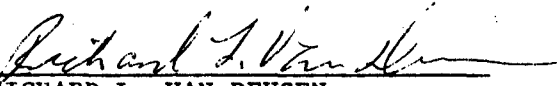
When Government drawings, specifications, or other data are used for any purpose other than in connection with a definitely related Government procurement operation, the United States Government thereby incurs no responsibility nor any obligation whatsoever; and the fact that the Government may have formulated, furnished, or in any way supplied the said drawings, specifications, or other data, is not to be regarded by implication or otherwise as in any manner licensing the holder or any other person or corporation, or conveying any rights or permission to manufacture use, or sell any patented invention that may in any way be related thereto.

This report has been reviewed by the Office of Public Affairs (ASD/PA) and is releasable to the National Technical Information Service (NTIS). At NTIS, it will be available to the general public, including foreign nationals.

This technical report has been reviewed and is approved for publication.



IVAN J. GOLDFARB
Project Scientist



RICHARD L. VAN DEUSEN
Chief, Polymer Branch

FOR THE COMMANDER



MERRILL L. MINGES
Director
Nonmetallic Materials Division

If your address has changed, if you wish to be removed from our mailing list, or if the addressee is no longer employed by your organization please notify AFWAL/MLBP, Wright-Patterson AFB OH 45433 to help us maintain a current mailing list.

Copies of this report should not be returned unless return is required by security considerations, contractual obligations, or notice on a specific document.

REPORT DOCUMENTATION PAGE					
1a. REPORT SECURITY CLASSIFICATION UNCLASSIFIED		1b. RESTRICTIVE MARKINGS			
2a. SECURITY CLASSIFICATION AUTHORITY		3. DISTRIBUTION/AVAILABILITY OF REPORT Approved for public release; distribution unlimited			
2b. DECLASSIFICATION/DOWNGRADING SCHEDULE					
4. PERFORMING ORGANIZATION REPORT NUMBER(S) MDC Report Q1273		5. MONITORING ORGANIZATION REPORT NUMBER(S) AFWAL-TR-86-4049			
6a. NAME OF PERFORMING ORGANIZATION McDonnell Douglas Research Laboratories		6b. OFFICE SYMBOL (If applicable)	7a. NAME OF MONITORING ORGANIZATION Materials Laboratory (AFWAL/MLBP) Air Force Wright Aeronautical Laboratories		
6c. ADDRESS (City, State and ZIP Code) P. O. Box 516 St. Louis, MO 63166		7b. ADDRESS (City, State and ZIP Code) Wright-Patterson Air Force Base, OH 45433-6533			
8a. NAME OF FUNDING/SPONSORING ORGANIZATION		8b. OFFICE SYMBOL (If applicable)	9. PROCUREMENT INSTRUMENT IDENTIFICATION NUMBER F33615-80-C-5170		
8c. ADDRESS (City, State and ZIP Code)		10. SOURCE OF FUNDING NOS.			
		PROGRAM ELEMENT NO.	PROJECT NO.	TASK NO.	WORK UNIT NO.
		61102F	2303	Q3	07
11. TITLE (Include Security Classification) CHARACTERIZATION OF ACETYLENE-TERMINATED RESIN CURE STATES					
12. PERSONAL AUTHOR(S) Lind, Arthur C., Fry, Charles G., Levy, Ram L., Sandreczki, Thomas C.					
13a. TYPE OF REPORT Final Technical		13b. TIME COVERED FROM 83 JUN TO 85 SEP	14. DATE OF REPORT (Yr., Mo., Day) September 1986	15. PAGE COUNT 108	
16. SUPPLEMENTARY NOTATION					
17. COSATI CODES			18. SUBJECT TERMS (Continue on reverse if necessary and identify by block number) Acetylene-terminated sulfone, Acetylene-terminated bisphenol A, Phenoxyphenoxyphenylacetylene		
FIELD	GROUP	SUB. GR.			
11	01				
11	04				
19. ABSTRACT (Continue on reverse if necessary and identify by block number) Acetylene-terminated (AT) oligomers are being considered for use in high service temperature adhesives and composites. Characterization of the cure states of these resins by Fourier transform infrared (FT-IR), nuclear magnetic resonance (NMR), and electron paramagnetic resonance (EPR) techniques was investigated. The AT resins 4,4-bis(3ethylphenoxy)diphenylsulfone (ATS), 4,4-bis(4-ethylphenoxy)-2,2-diphenylpropane (p-ATB), and 4,4-bis(3-ethylphenoxy)-2-diphenylpropane (m-ATB), and the monofunctional model compound phenoxyphenoxyphenylacetylene (PPPA), were studied as a function of cure and postcure conditions. These measurements provided parameters useful in characterising the cure states of AT resins. The results also provided additional insight to the cure mechanism.					
20. DISTRIBUTION/AVAILABILITY OF ABSTRACT UNCLASSIFIED/UNLIMITED <input checked="" type="checkbox"/> SAME AS RPT. <input type="checkbox"/> DTIC USERS <input type="checkbox"/>			21. ABSTRACT SECURITY CLASSIFICATION UNCLASSIFIED		
22a. NAME OF RESPONSIBLE INDIVIDUAL I. J. Goldfarb		22b. TELEPHONE NUMBER (Include Area Code) 513-255-2340	22c. OFFICE SYMBOL AFWAL/MLBP		

18. Subject Terms (continued)

Cure State	Electron paramagnetic resonance	Adhesive
Reaction	Fourier-transform infrared	Composite
Thermoset	Polymerization	Chemical Kinetics
Nuclear magnetic resonance	Free radical	Mechanisms

FOREWORD

This Final Technical Report covers work performed on Contract No. F33615-80-C-5170, Project No. 2303, entitled "Characterization of Acetylene-Terminated Resin Cure States," during the period 1 June 1983 through 30 September 1985. This program is sponsored by the Air Force Aeronautical Laboratories, Materials Laboratory, Wright-Patterson Air Force Base, Ohio. Dr. Ivan Goldfarb is the Project Monitor. Personnel contributing to the program are Dr. Donald P. Ames, Program Manager; Dr. Arthur C. Lind, Principal Investigator; Dr. Charles G. Fry, Co-Investigator; Dr. Ram L. Levy, Co-Investigator; and Dr. Thomas C. Sandreczki, Co-Investigator.

TABLE OF CONTENTS

SECTION	PAGE
I. INTRODUCTION	1
II. EXPERIMENTAL CONSIDERATIONS	2
1. MATERIAL AND CURE CONDITIONS	2
2. SAMPLE PREPARATION	3
a. NMR Sample Preparation	3
b. EPR Sample Preparation	4
c. FT-IR Sample Preparation	5
3. SPECTROMETRIC TECHNIQUES	5
a. NMR Techniques	5
b. EPR Techniques	6
c. FT-IR Techniques	7
III. RESULTS AND ANALYSES	9
1. ^{13}C NMR RESULTS	9
a. ^{13}C NMR Isothermal Cure Studies	9
b. ^{13}C NMR Postcure Studies	13
2. ^1H NMR RESULTS	17
3. EPR RESULTS	47
a. EPR Isothermal Cure Studies	47
b. EPR Postcure Studies	58
4. FT-IR RESULTS	62
a. FT-IR Isothermal Cure Studies	62
b. FT-IR Postcure Studies	80
IV. DISCUSSION OF RESULTS	83
V. CONCLUSIONS	91
VI. REFERENCES	95

LIST OF ILLUSTRATIONS

FIGURE	PAGE
1. ^{13}C NMR spectrum of solid, uncured, debulked ATS resin.	9
2. ^{13}C NMR acetylene intensity during isothermal cures.	11
3. ^{13}C NMR spectrum of p-ATB with tentative assignments shown by the arrows.	12
4. ^{13}C NMR spectra of ATS resin samples cured at 403 K (266°F) for the indicated times followed by a postcure for 2 h at the indicated temperatures.	14
5. ^{13}C NMR spectra of ATS resin samples cured at 423 K (302°F) for the indicated times followed by a postcure for 2 h at the indicated temperatures.	15
6. ^{13}C NMR spectra of ATS resin samples cured at 453 K (356°F) for the indicated times followed by a postcure for 2 h at the indicated temperatures.	16
7. Spin-lattice relaxation times for ATS resin during a cure at 423 K (302°F).	18
8. Early cure spin-lattice relaxation times for ATS resin during a cure at 423 K (302°F).	18
9. Spin-spin relaxation times for ATS resin during a cure at 423 K (302°F).	19
10. Component fractions for an ATS resin during a cure at 423 K (302°F).	20
11. Component fractions of ATS during isothermal curing at 403 K (266°F) for two samples.	21
12. Expanded view of Figure 11 with a linear scale for the cure time.	22
13. Spin-spin relaxation times of ATS during isothermal curing at 403 K (266°F) for two samples.	23
14. Expanded view of Figure 13 with a linear scale for the cure time.	24
15. The spectrum of spin-spin relaxation times plotted against their respective fractional intensities for ATS cured isothermally at 403 K (266°F) for two samples.	25
16. Approximate first-order uptake during early curing of ATS at 403 K (266°F).	30

LIST OF ILLUSTRATIONS (Continued)

FIGURE	PAGE
17. High-resolution ^1H NMR spectrum of ATS cured 19 minutes <u>in situ</u> at 423 K (302°F).	31
18. Component fractions of ATS during isothermal curing at 453 K (356°F); obtained with the 2+1 assumption.	33
19. Spin-spin relaxation times of ATS during isothermal curing at 453 K (356°F); obtained with the 2+1 assumption.	34
20. The spectrum of spin-spin relaxation times, T_2 , plotted against their respective fractional intensities for ATS cured isothermally at 453 K (356°F); obtained with the 2+1 assumption.	34
21. Component fractions of ATS during isothermal curing at 453 K (356°F); obtained with the 3+1 assumption	35
22. Spin-spin relaxation times, T_2 , of ATS during isothermal curing at 453 K (356°F); obtained with the 3+1 assumption.	36
23. The spectrum of spin-spin relaxation times, T_2 , plotted against their respective fractional intensities for ATS cured isothermally at 453 K (356°F); obtained with the 3+1 assumption.	37
24. Comparisons of 2+1 to 3+1 assumptions fitted to the raw data obtained <u>in situ</u> on ATS cured at 453 K (356°F) for 6.0 min.	38
25. Direct comparison of the 2+1 and 3+1 fitting assumptions.	39
26. Comparison of the fraction acetylene obtained from ^{13}C and ^1H NMR measurements.	40
27. Successive first-order reactions fitted to the early cure data shown in Figure 18.	41
28. Successive first-order reactions fitted to the early cure data shown in Figure 21.	42
29. Suggested reaction pathways for cis-trans free-radical polymerization of ATS assuming head-to-tail addition throughout.	43
30. Suggested reaction pathways for trans-trans free-radical polymerization of ATS assuming head-to-tail addition throughout.	44
31. Acetylene consumption in ATS cured isothermally at 423 K (306°F) predicted from ^1H spin-spin relaxation data.	45

LIST OF ILLUSTRATIONS (Continued)

FIGURE	PAGE
32. First- and second-derivative spectra of partially cured PPPA and m-ATB.	48
33. EPR signal intensities for ATS as a function of cure time at early stages of cure.	50
34. EPR signal intensities in ATS as a function of cure time.	51
35. Fits of Equation 22 to ATS curing data collected by EPR. Curing temperature is 403 K (266°F).	53
36. Fits of Equation 22 to ATS curing data collected by EPR. Curing temperature is 453 K (356°F).	54
37. Free-radical concentration as a function of cure time for m-ATB.	55
38. EPR signal intensity for m-ATB as a function of log cure time.	56
39. Radical concentrations of cured ATS samples before and after postcuring at 523 K (482°F).	58
40. Radical concentrations of cured ATS samples before and after postcuring at 543 K (518°F).	59
41. EPR signal intensity, both before and after postcuring at 573 K (572°F), as a function of degree of cure.	60
42. EPR spectra observed during curing/postcuring of selected ATS samples.	61
43. FT-IR spectrum of ATS monomer.	64
44. Superimposed FT-IR spectra of the 3295 cm^{-1} acetylene-band region of ATS at different stages of cure at 423 K (302°F).	65
45. Superimposed FT-IR spectra of the 941 cm^{-1} acetylene-band region of ATS oligomer in different stages of cure at 423 K (302°F).	65
46. Degree of cure determined from the average of 941 cm^{-1} and 3295 cm^{-1} FT-IR band-area measurements for the three different isothermal cures of ATS samples.	69
47. Superimposed FT-IR spectra: (a) m-ATB monomer and (b) p-ATB monomer.	70
48. Degree of cure in m-ATB isothermally cured at 433 K (320°F) determined with FT-IR. Normalized against 3010-2840 cm^{-1} band.	73

LIST OF ILLUSTRATIONS (Continued)

FIGURE	PAGE
49. Degree of cure in m-ATB isothermally cured at 433 K (320°F) determined with FT-IR. Normalized against 822-805 cm^{-1} band.	73
50. Degree of cure in m-ATB isothermally cured at 453 K (356°F) determined with FT-IR. Normalized against 3010-2840 cm^{-1} band.	74
51. Degree of cure in m-ATB isothermally cured at 453 K (356°F) determined with FT-IR. Normalized against 882-805 cm^{-1} band.	74
52. Superimposed difference FT-IR spectra of the 400 - 1400 cm^{-1} region.	75
53. Schematic illustration of a frequency-shifted band.	76
54. Superimposed FT-IR spectra m-ATB (700-1650 cm^{-1}) for 453 K (356°F) cure.	78
55. Superimposed FT-IR spectra m-ATB (2500-3500 cm^{-1}) for 453 K (356°F) cure.	79
56. Comparison of ^{13}C and ^1H NMR results to DSC and FT-IR results for acetylene uptake in ATS cured isothermally at 453 K (356°F).	83
57. Comparison of ^{13}C and ^1H NMR results to DSC and FT-IR results for acetylene uptake in ATS cured isothermally at 423 K (306°F).	84
58. Comparison of ^{13}C and ^1H NMR results to DSC and FT-IR results for acetylene uptake in ATS cured isothermally at 403 K (266°F).	85

LIST OF TABLES

TABLE	PAGE
1. Fractional Areas Beneath Resonance Peaks in ^{13}C NMR Spectra of p-ATB.	12
2. Changes in the Longest Relaxation Time, T_2^{vm} , and Its Corresponding Fractional Amplitude, f_{vm} , Due to Various Choices of the Baseline Parameter, C.	23
3. High Resolution ^1H NMR Results on ATS Cured at 423 K (302°F).	31
4. EPR Curing Parameters for ATS.	51
5. Parameters Determined from Least-Squares Fit of EPR Data.	53
6. Parameters Determined from Forced Least-Squares Fit of EPR Data.	54
7. EPR Curing Parameters for m-ATB.	57
8. Effects of Postcuring m-ATB Samples at 453 K (356°F).	62
9. Comparison of the Degree of Cure (DOC) Values for ATS Derived by Different Methods at 403 K (266°F).	67
10. Comparison of the Degree of Cure (DOC) Values for ATS Derived by Different Methods at 423 K (302°F).	67
11. Comparison of the Degree of Cure (DOC) Values for ATS Derived by Different Methods at 453 K (356°F).	68
12. Degrees of Cure (DOC) of p-ATB as a Function of Cure Time at 443 K (338°F).	69
13. Degrees of Cure (DOC) of m-ATB as a Function of Cure Time at 433 K (320°F).	71
14. Degrees of Cure (DOC) of m-ATB as a Function of Cure Time at 453 K (356°F).	72
15. FT-IR Results of Incomplete Cure of ATS at 403 K (266°F) Followed by 120 Min Postcure at 523 K (482°F), 543 K (518°F), and 573 K (572°F).	80
16. FT-IR Results of 423 K (302°F) Cure of ATS Followed by a 120 Min Postcure at 523 K (482°F), 543 K (518°F), and 573 K (572°F).	81
17. FT-IR of Incomplete Cure of ATS at 453 K (356°F) Followed by 120 Min Postcure at 523 K (482°F), 543 K (518°F), and 573 K (572°F).	81
18. Selected Cure Times Measured by EPR, ^1H NMR, and FT-IR.	86
19. ATS Resin Rate Constants for Radical Production (EPR) and Rigid Component Production (NMR).	88

I. INTRODUCTION

Acetylene-terminated oligomers are being considered for use in high-service-temperature adhesives and composites.^{1,2} It is thought that these resins cure via numerous pathways, resulting in the production of various chemical structures;² therefore, the time-temperature schedule employed during curing may strongly affect the properties of the cured resin. To better understand the acetylene-terminated system, to enable the specification of appropriate cure schedules for producing polymers with the desired properties, and to provide a means for assuring the quality of fabricated components containing these polymers, techniques are needed that utilize small laboratory-scale samples to obtain accurate measurements of a set of parameters that uniquely determines the polymer properties.

The objectives of an earlier part of this program were to

- (1) develop nuclear magnetic resonance (NMR), electron paramagnetic resonance (EPR), and Fourier-transform infrared (FT-IR) techniques for measuring parameters of acetylene-terminated sulfones (ATS) that had undergone a variety of cure schedules,
- (2) relate these parameters to the cure schedules, and
- (3) attempt a correlation of these parameters with the known mechanical properties.

The results of this earlier study were previously reported.³

The objectives of the current part of the program are to

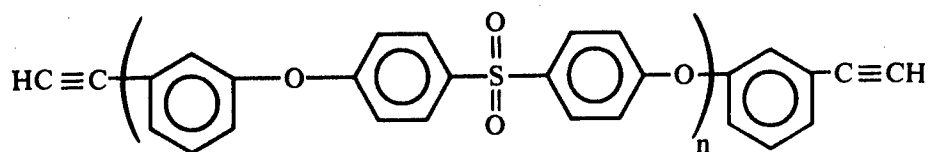
- (1) conclude the study of ATS,
- (2) apply the results of this study to other acetylene-terminated resins to validate their general utility, and
- (3) compare cure-state results for the different resins.

This report restates some results from the earlier study where they are needed for clarity.

II. EXPERIMENTAL CONSIDERATIONS

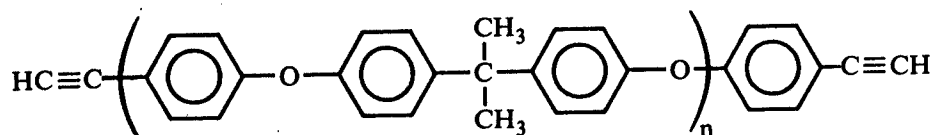
1. MATERIAL AND CURE CONDITIONS

Four acetylene-terminated (AT) resins, all supplied by AFWAL/ML, were used in this study. The first resin is based on the 4,4'-bis(3-ethynylphenoxy)-diphenylsulfone (ATS) monomer. This ATS resin contains about 80% monomer and 20% higher-order oligomers, and has 95% meta configuration and 5% para configuration.⁴



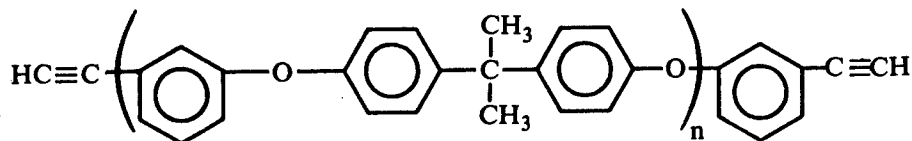
ATS

The second resin is based on the 4,4'-bis(4-ethynylphenoxy)-2,2-diphenylpropane monomer, also known as para-acetylene-terminated bisphenol A, (p-ATB). This resin was supplied containing some higher order oligomers.⁵



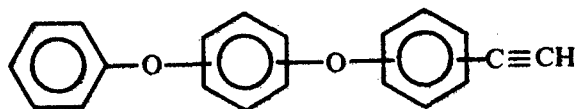
p-ATB

The third resin is based on the 4,4'-bis(3-ethynylphenoxy)-2,2-diphenylpropane monomer, also known as meta-acetylene-terminated bisphenol A, (m-ATB). This resin was supplied as a purified monomer, so higher order oligomers were negligible.⁶



m-ATB

The fourth resin is a monofunctional compound used in the EPR studies. It is purified phenoxyphenoxyphenylacetylene (PPPA).⁷



PPPA

The AT resins were stored in a desiccator at 253 K (-4°F). Prior to curing, the samples were degassed (debulked) at 393 K (248°F) in vacuum for 15 min and backfilled with nitrogen. Isothermal curing measurements and postcure measurements were conducted in nitrogen atmospheres.

2. SAMPLE PREPARATION

a. NMR Sample Preparation

¹³C NMR: Samples for carbon-13 nuclear magnetic resonance (¹³C NMR) measurements were prepared and cured in silicone rubber molds. The inside dimensions of the molds were 0.71 cm (0.28 in.) diameter by 1.66 cm (0.655 in.) length with wall thickness of 0.11 cm (0.045 in.). A sample was prepared by adding ~1.3 g (0.046 oz) of an AT resin to a mold, inserting the mold into a tightly fitting hole in an aluminum block preheated to 393 K (284°F), outgassing at 393 K (248°F) for 15 min in a vacuum oven, and backflushing the sample with cool nitrogen gas during rapid (< 1 min) cooling to room temperature.

Sample curing and postcuring were similarly performed in the silicone rubber mold. The mold containing the sample was inserted into a nitrogen-purged preheated aluminum block in a well-regulated forced-air oven. After the appropriate cure or postcure time, the mold was removed from the aluminum block and flushed with nitrogen gas to cause rapid (< 1 min) sample cooling. These samples were stored in stoppered glass vials in a freezer at 253 K (-4°F) when not being measured in the ¹³C NMR spectrometer.

¹H NMR: Samples for hydrogen nuclear magnetic resonance (¹H NMR) measurements were prepared in sealed glass tubes. About 0.1 g (0.0035 oz) of ATS was placed in each 5-mm-o.d. (0.20-in.-o.d.) Pyrex NMR tube. The samples were vacuum degassed at 393 K (248°C) for 15 min, backfilled with dry nitrogen, sealed, and stored at 253 K (-4°F) until use in an experiment. In situ ¹H NMR

measurements were obtained during curing by employing a heated NMR probe. This procedure contrasts with the ^1H NMR measurements that were made in the earlier part of this program in which ^1H NMR measurements were performed at room temperature on samples that had been cured in a separate heater for different times. In these experiments, some samples required very long cure times. Therefore, to better utilize the NMR spectrometer, the samples were cured in oil-filled wells in a preheated, thermally calibrated aluminum block for the longer cure times and then returned to the heated NMR probe for measurement. If it was necessary to delay an NMR measurement, the sample was stored in a freezer at 253 K (-4°F).

b. EPR Sample Preparation

Samples were prepared by warming the material from 253 K (-4°F) to ambient temperature, pulverizing the desired quantity, and placing the powder in 5-mm-o.d. Pyrex sample tubes. The samples were degassed for 15 min at 393 K (248°F), backfilled with nitrogen gas, and sealed. They were stored at 253 K (-4°F) until use in EPR experiments.

The samples were cured isothermally by placing them in a heated aluminum block containing ~ 6-mm diam holes filled with silicone oil. The block was brought to cure temperature prior to sample insertion and was maintained at cure temperature in a calibrated, forced-convection oven. With this system, samples came to within 1 K of the cure temperature within 1 min. Thermal lag of the sample (i.e., time spent during heat-up and cool-down) was sometimes minimized by using a series of two or three samples for each isothermal cure experiment, thus reducing the number of times each sample needed to be removed from the oven for measurement during its cure cycle.

For the postcuring experiments, samples were heated in a copper tube containing a gently flowing stream of nitrogen purge gas. In this way, inevitable sample tube breakage from thermal expansion of the ATS did not result in exposure of the sample to air at the postcure temperature. Following postcuring, the copper tube was cooled to ambient temperature prior to sample removal. The sample was then placed in a new EPR sample tube, degassed, backfilled with nitrogen, and sealed.

The samples were rapidly brought to the postcure temperature by the above technique because the copper tube was heated prior to sample insertion. It was not cooled until postcuring was completed.

c. FT-IR Sample Preparation

AT resin specimens suitable for sequential curing and recording of FT-IR spectra after each cure interval were prepared by the bulk-cure KBr pellet method, as follows. Bulk specimens weighing about 0.5 g were isothermally cured in nitrogen-purged test tubes inserted into oil-filled wells in a pre-heated aluminum block as described in Section 2b. The test tube was removed from the heated block after each cure interval and allowed to cool to room temperature. Then 5 to 15 mg of resin was removed from the bulk for preparation of KBr pellets (discs) according to standard procedures.⁸

Specimens for FT-IR study of the effect of post-cure heating were of the same origin as the ones used for ^{13}C NMR measurements. Specimen preparation is described in Section 2a.

3. SPECTROMETRIC TECHNIQUES

a. NMR Techniques

^{13}C NMR: Solid state ^{13}C NMR spectra of the AT resins were obtained on a JEOL FX60QS spectrometer operating at 15 MHz with magic-angle spinning,⁹ cross-polarization, and high-power decoupling.¹⁰ The magic-angle spinner bodies were fabricated from Kel-F; as a result, they produced no ^{13}C spectral lines that would interfere with those of the sample. The spinner was usually spun at a rate of 2.4 kHz, which was sufficient to reduce the area beneath the sideband peaks to less than 5%. The cross-polarization was accomplished with a Hartmann-Hahn double resonance at approximately 50 kHz. Cross-polarization contact times between 1 and 10 ms were investigated, and 4 ms was found to be optimal. The high-power hydrogen decoupling field was 1.2 mT. The data from 5000 pulse sequences usually were averaged before Fourier transforming the data to obtain the spectra.

The solid-state ^{13}C NMR spectra of the AT resins consisted of well-resolved lines whose assignments were determined by comparison with AT solution spectra.¹¹ Parameters were derived from these spectra by measuring the areas beneath the spectral lines at various stages of cure or by measuring the area beneath the lines in the difference spectra which were obtained by subtracting spectra at different stages of cure, as had been done in a study of acetylene-terminated polyimide resins.¹²

^1H NMR: The pulsed ^1H NMR measurements were performed on an MDRL-designed, single-coil spectrometer operating at 100 MHz. An external fluorine

lock sampled at 94 MHz was used to control the magnet (Varian V-4014) so that small signals could be signal averaged for long times without attendant drift. The 100-MHz and 94-MHz rf signals were derived from a frequency synthesizer (Hewlett Packard HP5100), and the 8-mT pulsed rf magnetic field was generated by a programmable digital pulser and a 100-W linear amplifier (Electronic Navigation Industries 3100L). The dead time of the receiver was $< 6 \mu\text{s}$. A digital oscilloscope (Nicolet 4094) was used to acquire and store the signals, and a computer (Digital Equipment PRO-380 or VAX 11/780) was used to analyze the signals.

Three different types of pulsed ^1H NMR experiments were performed:

- (1) a single 90° pulse experiment to determine the relative amounts of rigid and mobile phases and their spin-spin relaxation times T_2 ,
- (2) a $180^\circ, \tau, 90^\circ$ pulse experiment to determine the spin-lattice relaxation time T_1 , and
- (3) a $90^\circ_x, \tau, (180^\circ_y, 2\tau)_n$ pulse sequence, referred to as the CPMG¹³ sequence, to determine large spin-spin relaxation times, T_2 .

b. EPR Techniques

EPR spectra from ATS and the original set of m-ATB data (see Section III.3) were recorded on the Varian E-102 EPR spectrometer described previously.³ The corrected set of m-ATB data (see Section III.3) were recorded using an IBM ER-200 X-band EPR spectrometer and IBM 9000 data acquisition system. This acquisition system enabled signal averaging, spectral scaling, integration and subtraction.

Free radical concentrations were determined by comparing the AT resin signal with that of a strong pitch reference sample having a Lorentzian line shape and a radical concentration of 2.46×10^{15} spins per cm length. Any variations in spectrometer parameters were minimized by recording the reference spectrum along with each sample or group of samples observed within a short time period (≤ 30 min). Reproducible placement of sample and reference was achieved by using 5-cm-long samples that extended from the bottom of the cavity to beyond the top of the cavity where the microwave intensities were small.

Spectral intensities were calculated either by direct numerical integration or by using the expression

$$I \propto hw^2$$

(1)

when spectra having the same line shapes were compared. In this expression, I is the integrated intensity, h is the peak-to-peak amplitude of the recorded derivative spectrum, and w is the peak-to-peak linewidth.

Error in signal intensity resulting from improper signal phasing was possible during direct integration. Incorrect phasing occurred because the spectrometer was operated at low power to avoid saturation and distortion of the AT resin signal (AT resins saturated easily). At these low power levels, the spectra contained small amounts of dispersion signals and slightly reduced absorption signals. The integral of the former did not contribute to the integrated signal intensity, so that the overall intensity of the incorrectly phased EPR signal was reduced accordingly. To avoid the difficulties of direct integration, an integration procedure using Equation (1) was employed.

In Equation (1), it is essential for the spectra being compared to have the same spectral line shapes. Thus, two Lorentzian or two Gaussian lines can be compared, but a Lorentzian and a Gaussian line cannot be compared with each other. For example, if the intensities of a Lorentzian line and a Gaussian line having the same h and w (and I) values were determined by direct integration, the true integrated intensity of the Lorentzian would be a factor of 3.5 times greater than that of the Gaussian. The AT resin line shapes corresponding to > 20% cure are approximately Gaussian in shape. Since the strong pitch produced a Lorentzian signal, it was not possible to determine the intensity of AT resin relative to the reference simply by comparing the values of I calculated with Equation (1). Instead, these values of I were compared to intensities obtained by direct integration of the references and to selected AT resin spectra having very little dispersion-signal content. In this manner, the I values for the reference line shape and AT resin line shapes were calibrated by use of their true intensity values, enabling use of Equation (1) for the remaining ATS samples.

c. FT-IR Techniques

The transmission FT-IR spectra of AT resin specimens were obtained either on a Digilab FTS-20V FT-IR spectrometer or on a Nicolet 7199 spectrometer. Both spectrometers yielded identical spectra for a given specimen and, therefore, the spectra obtained were interchangeable. Nevertheless, any sequence

of spectra resulting from a particular series of experiments was recorded on the same spectrometer.

The raw single-beam spectra from both instruments were recorded in digital form on a magnetic tape with a Kennedy Model 9700 recorder and were transferred to a CDC Cyber mainframe computer for interactive processing via a Tektronix 4010 CRT terminal. The software for extensive off-line processing of spectral data on a mainframe computer was developed at MDRL. Spectra were recorded either from 300 scans (signal averaged) at a resolution of 1 cm^{-1} or from 100 scans at a resolution of 2 cm^{-1} . Both scan conditions yielded the same results for determination of band areas or band intensities. However, for the measurement of small cure-induced frequency shifts, spectra obtained from 300 scans at a resolution of 1 cm^{-1} produced greater accuracy and were therefore used. Transmission spectra were recorded at room temperature before curing and after each isothermal cure or post-cure stage of a given curing sequence.

Difference spectroscopy was used because it is a sensitive method for detecting and measuring minor cure-induced changes in polymers. Difference spectra, providing net changes in the AT resin after curing for a given increment of time, were obtained by digital absorbance subtraction as follows:

$$\Delta A(\nu) = A_2(\nu) - kA_1(\nu) , \quad (2)$$

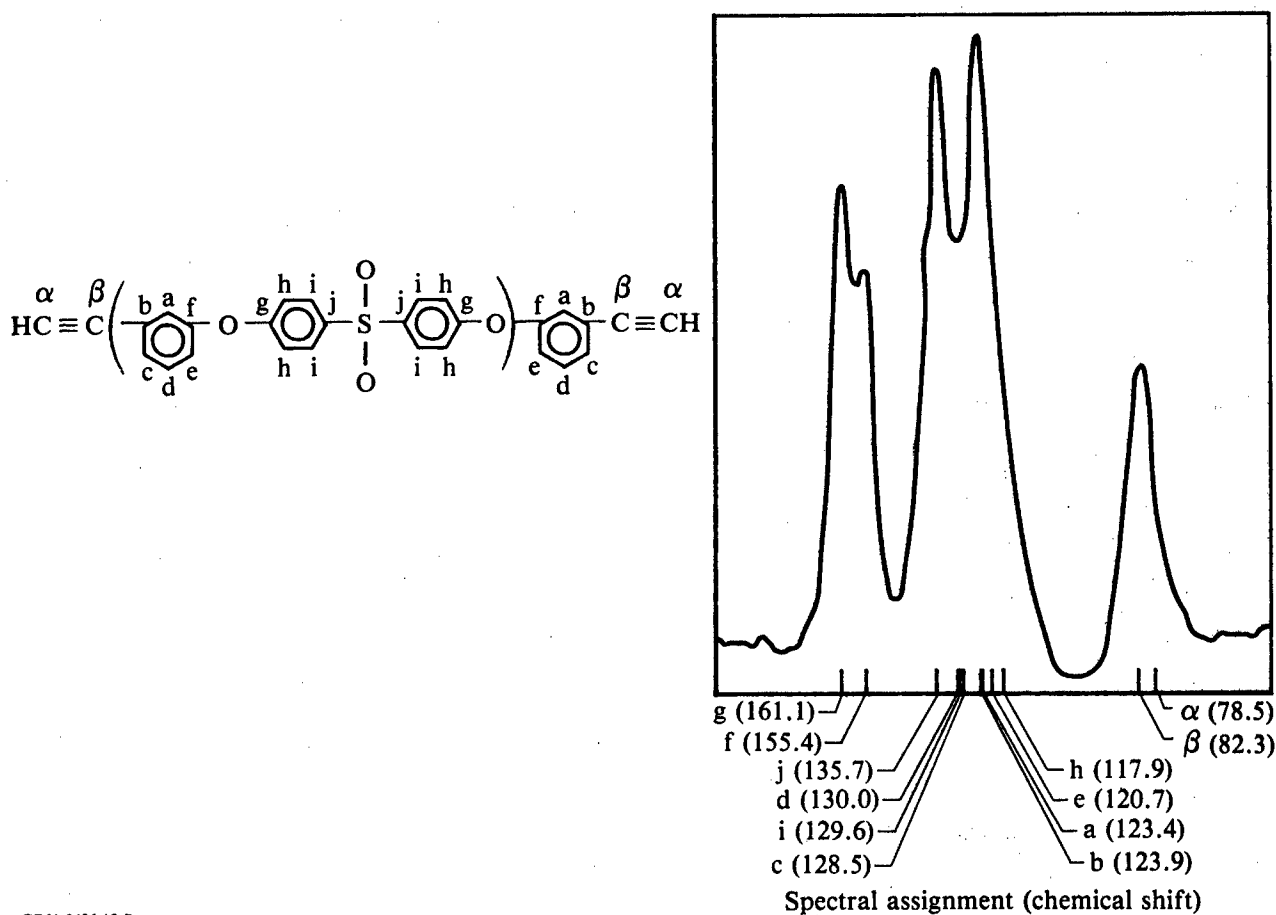
where $\Delta A(\nu)$ is the net absorbance change at frequency ν , k is an adjustable scaling factor to correct for changes in the thickness of the specimen, and $A_2(\nu)$ and $A_1(\nu)$ are the absorbances of the AT specimen at frequency ν for the two different cure states. The difference spectrum consists of a plot of $\Delta A(\nu)$ as a function of the frequency ν .

III. RESULTS AND ANALYSES

1. ^{13}C NMR Results

a. ^{13}C NMR Isothermal Cure Studies

Figure 1 shows the ^{13}C NMR spectrum of solid, uncured, debulked ATS resin. This spectrum was obtained using a cross-polarization contact time of 4 ms. Also shown in Figure 1 is the structure of the ATS monomer along with the spectral assignments that were obtained from solution ^{13}C NMR spectra.¹¹ The solution spectra are well resolved because the molecular motion present in the liquid averages conformational chemical shifts so that single, sharp spectral lines occur for nonequivalent carbons. In the solid spectra these conformational differences are not averaged, and broad spectral lines result. Because this sample contains higher order oligomers, there are a larger number of non-



GP61-0496-18-R

Figure 1. ^{13}C NMR spectrum of solid, uncured, debulked ATS resin. The chemical shifts of the spectral lines observed in the ^{13}C NMR spectrum of the resin dissolved in CDCl_3 are also shown along with the spectral assignments.

equivalent carbons than that in a pure monomer and additional spectral broadening occurs.

^{13}C NMR spectra of the type shown in Figure 1 were obtained on AT resin samples in various stages of cure. The spectra were analyzed by two procedures:

- (1) subtracting spectra obtained from samples at different stages of cure, and
- (2) obtaining the areas beneath the three well-resolved resonance peaks and expressing the three areas as a fraction of the total area beneath all three peaks.

While the first procedure yielded difference spectra that characterized the changes taking place during curing, the second procedure generated more useful cure-state parameters. The reason is that the second procedure required only a single spectrum of the AT resin sample being characterized, while the first procedure required a reference spectrum whose amplitude and chemical shift had to be manually adjusted to obtain valid difference spectra. The amplitude adjustment corrected for gain changes and differences in sample size, while the chemical shift adjustment corrected for shifts caused by spectrometer drift or slight changes in sample position in the magnet. While these adjustments could be performed in an objective manner for research applications, they are not suitable for routine measurement of cure-state parameters. Therefore, only area ratios were measured in this study.

At selected times during the isothermal cures, the samples were removed from the oven, and ^{13}C NMR spectra were obtained at room temperature for the optimum cross-polarization contact time of 4 ms. From these spectra, the fractional areas beneath the three well-resolved peaks were determined.

During cure, the following spectral changes were observed. First, the fractional area beneath the high-field peak (acetylenic carbons at ~ 80 ppm) decreases into the baseline (zero, within experimental error) during the cure. Second, the fractional area beneath the low-field peak (centered at 160 ppm) does not change significantly during the cure, indicating that the number of aryl carbons adjacent to oxygens remains constant during the cure. Third, the fractional area beneath the central-field peak (centered at 125 ppm) increases in correspondence to the decrease in the fractional area beneath the high-field peak during the cure; this suggests that acetylenic carbons are reacting

to form a conjugated polyene having either a linear or a trisubstituted benzene structure.

When the ^{13}C NMR data were reviewed, the area beneath the acetylene (high-field) resonance was found to be the most suitable result to use as a cure-state parameter. This resonance area was not as dependent upon contact time as were the areas beneath the other two resonances, and this acetylene peak experienced the greatest changes during curing. The area beneath the acetylene peak also presents the advantage of being approximately proportional to the number of unreacted acetylene groups in the sample. This cure-state parameter is plotted in Figure 2 for three isothermal cures.

The ^{13}C NMR technique was applied to the para-acetylene-terminated bisphenol A, (p-ATB), resin to determine if this technique was of general utility in characterizing the cure state of AT resins. The ^{13}C NMR spectrum of solid, uncured p-ATB resin is shown in Figure 3. The resolution does not permit a rigorous assignment of all the resonance lines to all the carbons in the resin, but general assignments are shown.

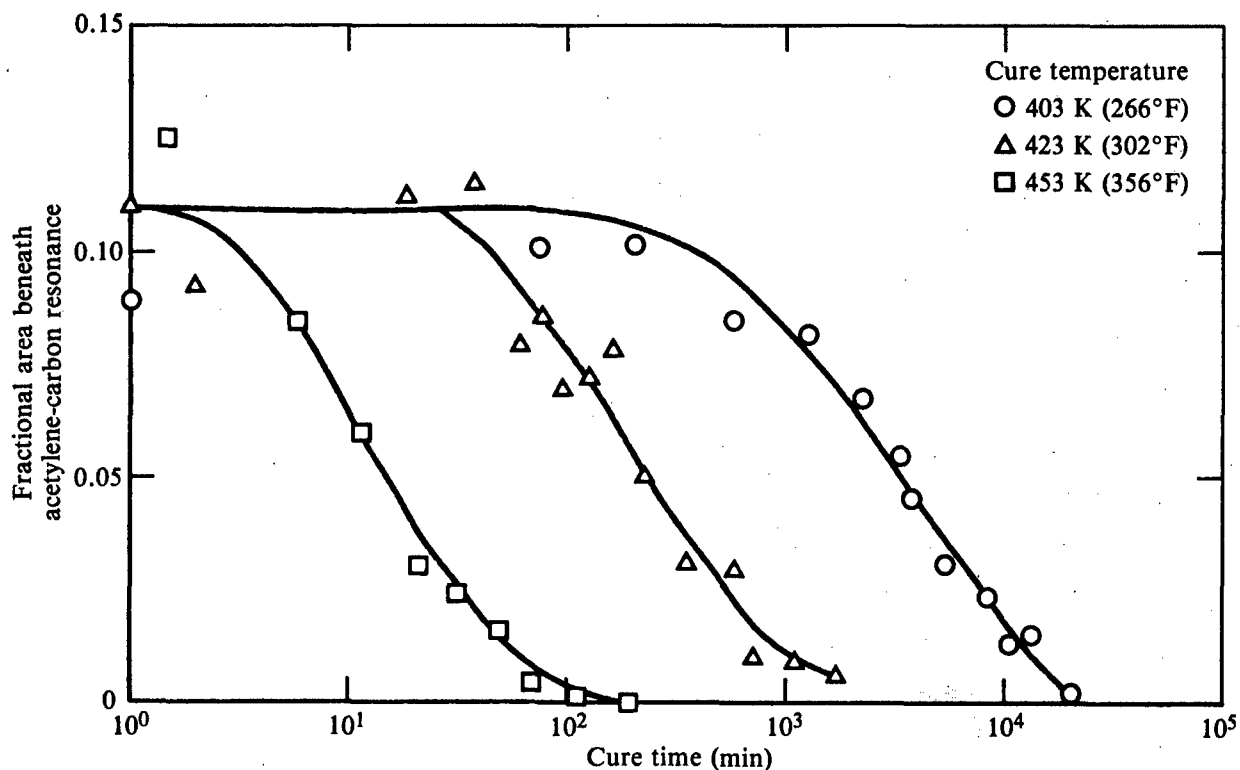


Figure 2. ^{13}C NMR acetylene intensity during isothermal cures.

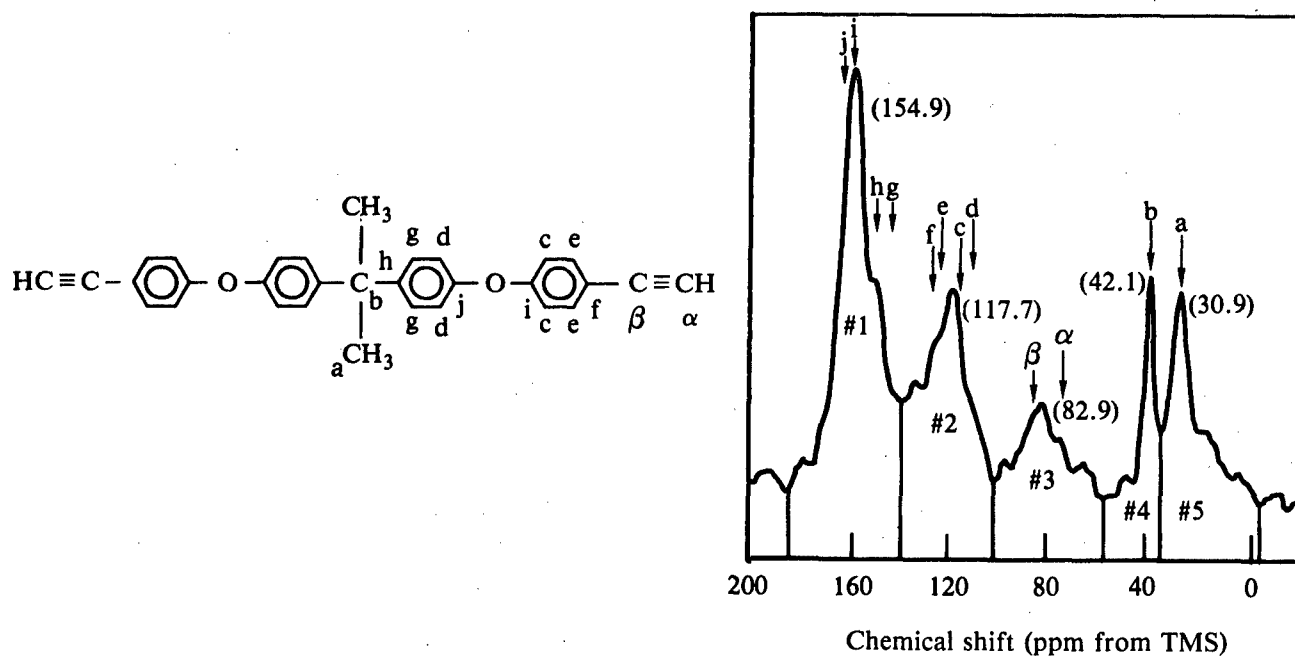


Figure 3. ^{13}C NMR spectrum of p-ATB with tentative assignments shown by the arrows.

GP61-0496-61-R

The fractional areas beneath the resonance peaks were measured in three different spectra and the results are shown in Table 1. Each one of these spectra required 5000 data accumulations over a period of seven hours. These results demonstrate the errors associated with quantitative ^{13}C NMR measurements of solids. Based on the three measurements shown in Table 1, the fractional area beneath the acetylene resonance is 0.099 ± 0.008 ($\pm 8\%$). The error in determining this quantity from a single spectrum is 14%. This error for the ATB resin was larger than that for the ATS resin because the resonances from the quaternary carbon (b) and the two methyl carbons (a) adjacent to the

TABLE 1. FRACTIONAL AREAS BENEATH RESONANCE PEAKS IN ^{13}C NMR SPECTRA OF p-ATB.

Spectrum number	Peak #1	Peak #2	Peak #3	Peak #4	Peak #5
374	0.397	0.304	0.091	0.085	0.124
375	0.374	0.296	0.107	0.055	0.176
376	0.446	0.262	0.098	0.069	0.140
Average	0.406	0.287	0.099	0.070	0.146
Standard deviation	0.037	0.022	0.008	0.015	0.027

GP61-0496-1-R

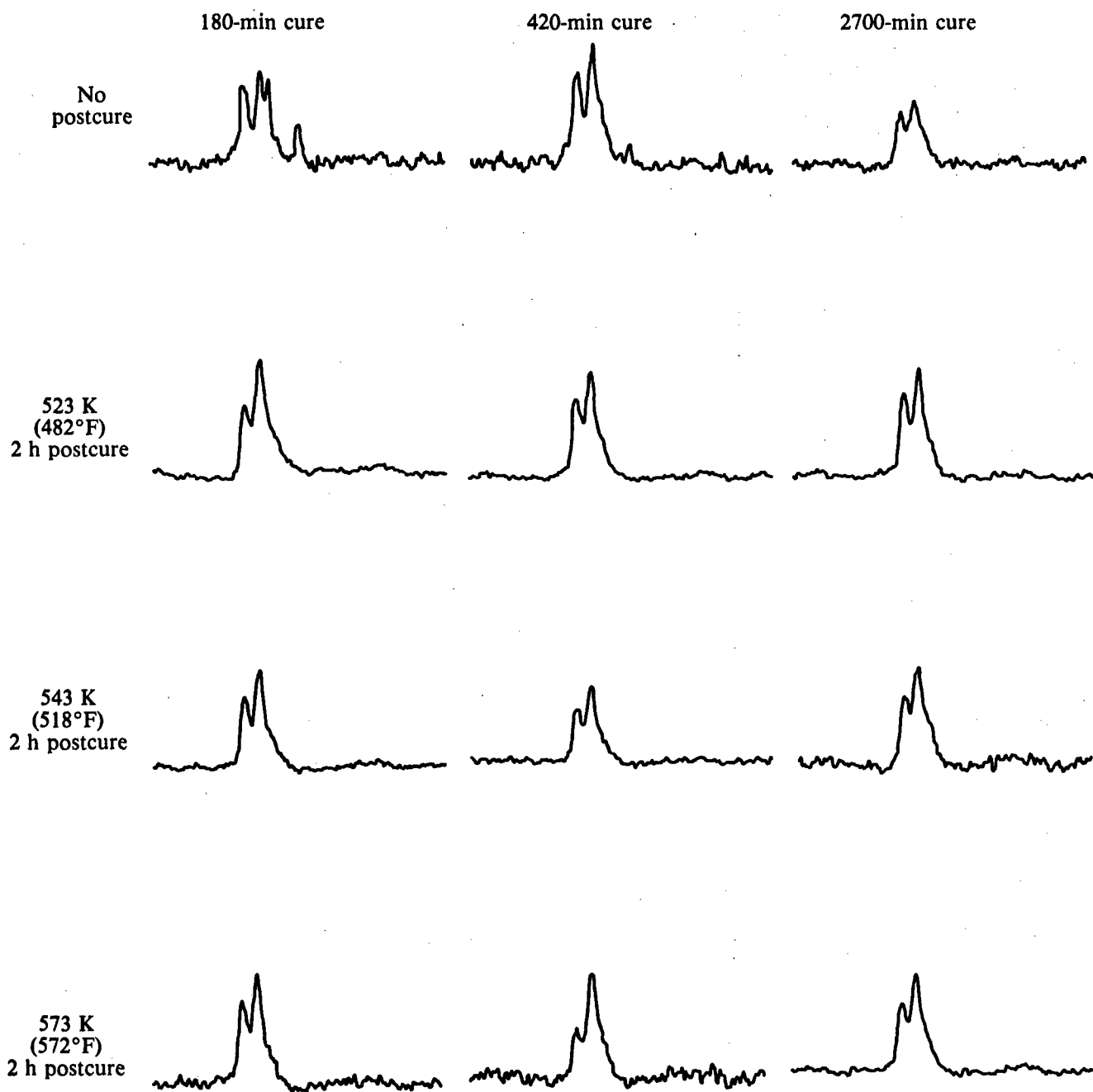
acetylene resonance make the area determination more difficult. Also, the large fractional area of the a and b resonances, not present in the ATS resin, reduced the fractional-area contribution from the acetylene carbons, thereby increasing the relative error. Because of the large error and the excessive time required to collect the data, the measurements on p-ATB were not continued.

The fractional area beneath the acetylene resonance peak can be used to estimate the oligomer content of the uncured resin if one assumes that the area beneath the peak is proportional to the number of carbons producing the peak. This was found to be a reasonable assumption for the ATS resin. Referring to Figures 1 and 2, one sees that ATS has $11 \pm 1\%$ acetylenic carbons. An oligomer of ATS contains $18n+6$ aromatic carbons and 4 acetylene carbons. The fraction of acetylene carbons, f , is $4/(18n+6)$. Therefore, $n=(4-6f)/18f$. The ^{13}C NMR results shown in Figure 2 thus predict that $n=1.7 \pm 0.2$ for ATS as obtained from AFWAL.⁴ Referring to Figure 3, an oligomer of p-ATB contains $18n+6$ aromatic carbons, $2n$ methyl carbons, n quaternary carbons, and 4 acetylene carbons. Thus, for p-ATB, the fraction of acetylene carbons, f , is $4/(21n+10)$, and n is equal to $(4-10f)/21f$. The data in Table 1 predict that $n = 1.45 \pm 0.15$ for p-ATB.⁵

b. ^{13}C NMR Postcure Studies

Postcure studies of ATS samples incompletely cured at 403 K (266°F) were performed. Magic-angle spinning ^{13}C NMR spectra were obtained and analyzed. These spectra, along with spectra obtained in earlier postcure studies of ATS samples incompletely cured at 423 K (302°F) and 453 K (356°F), are shown in Figures 4-6. The spectra of the samples before postcuring show the decrease in intensity of the upfield acetylene resonance peak as the curing time is increased. The relative areas beneath the acetylene peaks are in agreement with previous measurements. None of the spectra of the postcured samples contain the acetylene resonance peak. Analyses of the spectra of the postcured ATS samples cured and postcured at different temperatures have revealed no significant differences. Thus, the ^{13}C NMR results show no significant differences in the chemical structures of the postcured ATS samples for the cure times and the postcure temperatures used in these experiments.

It was observed that ATS samples which were postcured without prior curing at low temperature contained numerous voids, presumably the result of rapid outgassing.



GP61-0496-62-R

Figure 4. ^{13}C NMR spectra of ATS resin samples cured at 403 K (266°F) for the indicated times followed by a postcure for 2 h at the indicated temperatures.

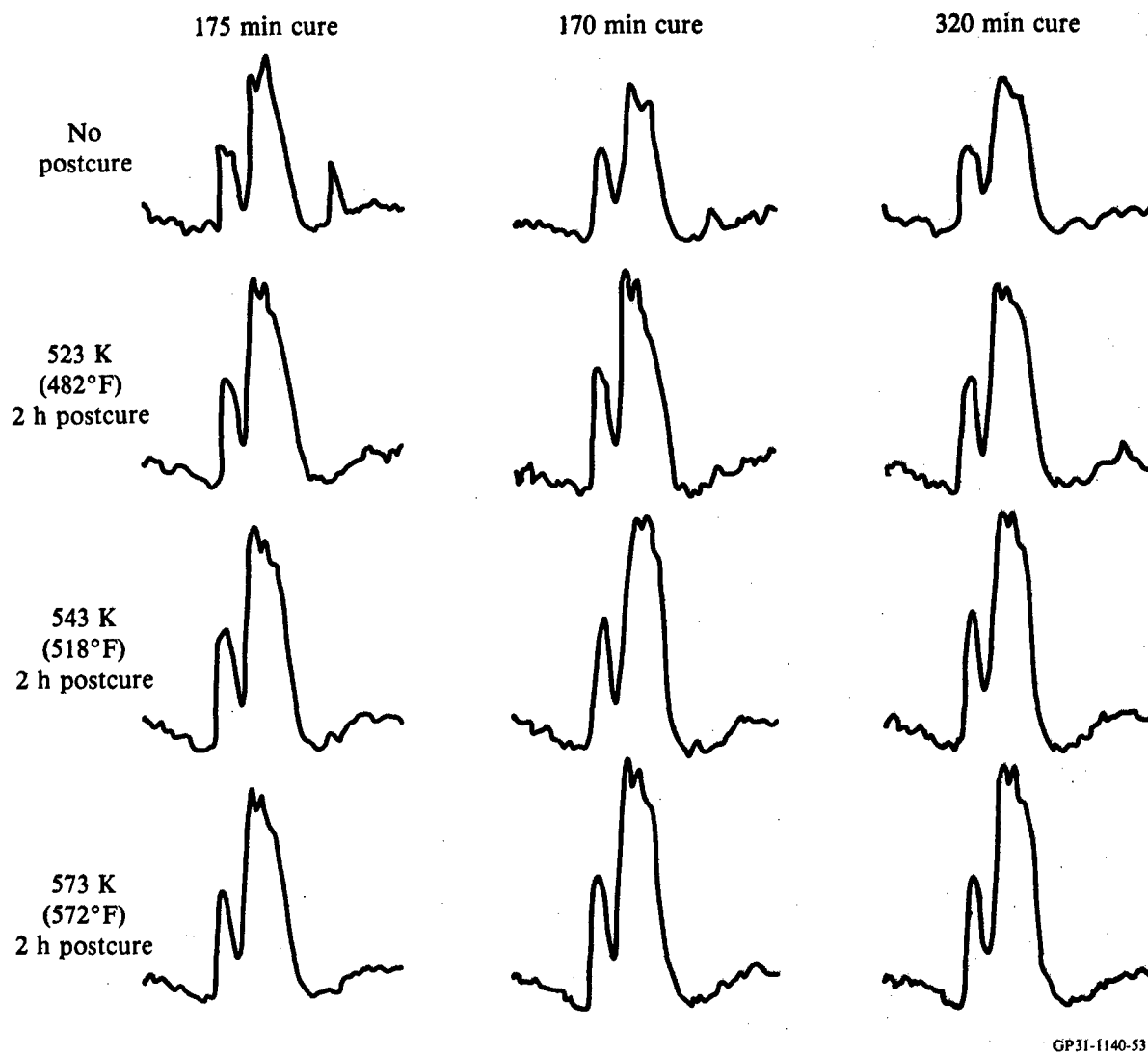


Figure 5. ^{13}C NMR spectra of ATS resin samples cured at 423 K (302°F) for the indicated times followed by a postcure for 2 h at the indicated temperatures.

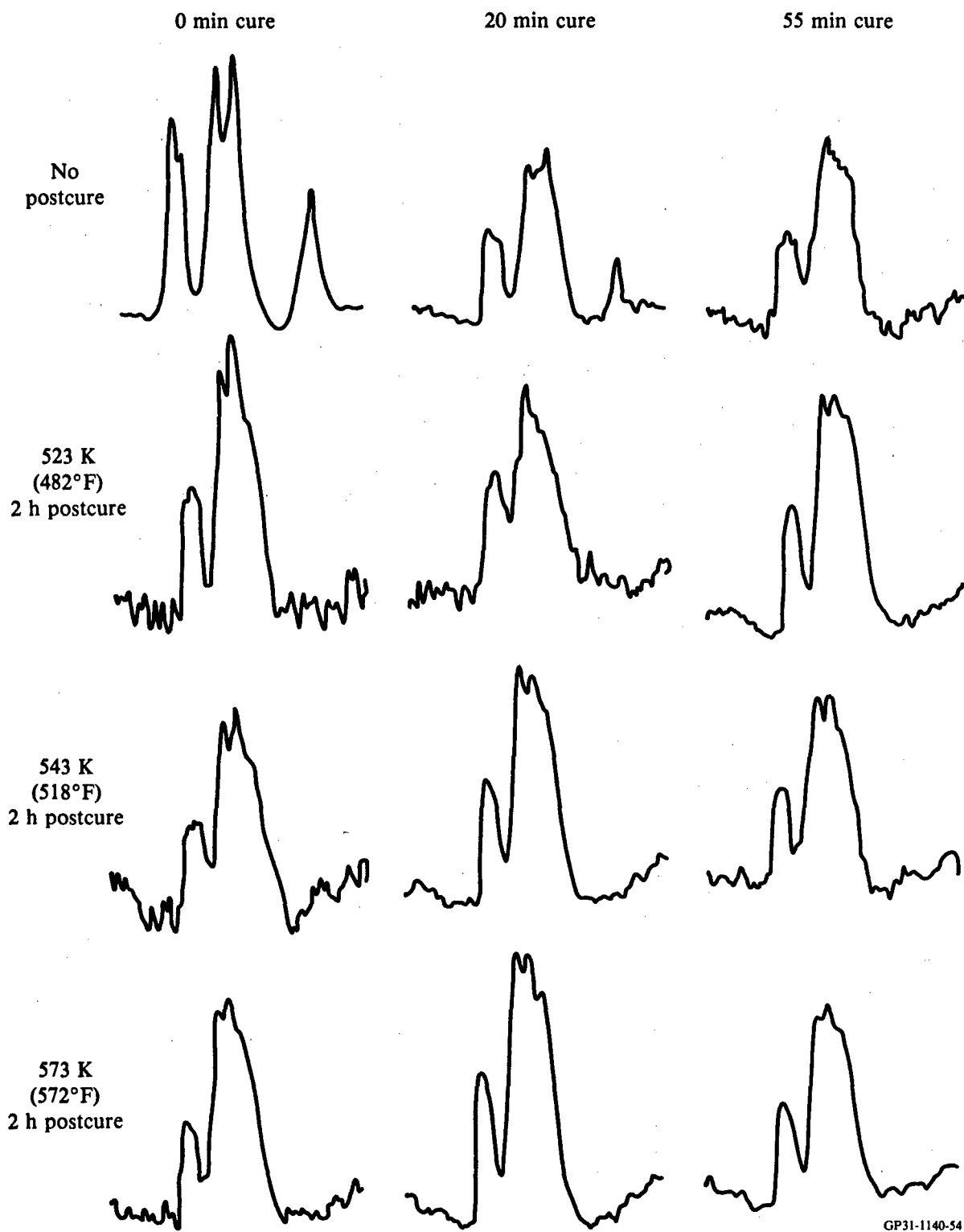


Figure 6. ^{13}C NMR spectra of ATS resin samples cured at 453 K (356°F) for the indicated times followed by a postcure for 2 h at the indicated temperatures.

2. ^1H NMR Results

In the earlier portion of this study, ^1H NMR experiments were conducted on ATS samples at room temperature after they had been cured at elevated temperatures for various times.³ The results of these measurements were not significantly different from those of the EPR measurements; therefore, in situ ^1H NMR measurements were made during curing while the sample was at the cure temperature. The results of these measurements provided additional information on the kinetics of cure, and also provided insights into the cure mechanism.

Several samples of uncured ATS resin were prepared in 5-mm-o.d. NMR tubes degassed at 393 K (248°F) for 15 min, backfilled with nitrogen gas, and sealed. Hot air was passed through the ^1H NMR probe to maintain the sample temperature within ± 2 K (3.6°F) of the desired cure temperatures, i.e., 403 K (266°F), 423 K (302°F), or 453 K (356°F).

The spin-lattice relaxation times measured during an in situ cure study at 423 K (302°F) are shown in Figures 7 and 8 for extended and early cure times, respectively. The increase in the spin-lattice relaxation time with cure time is caused by the decrease in molecular motion, and the decrease later in the cure is caused by an increase in free radicals, observed in EPR measurements. The spin-lattice results obtained at the cure temperature were similar to those previously obtained from room-temperature ^1H NMR measurements;³ hence, they were not continued.

The sampled signals obtained during the cure were computer analyzed to determine the spin-spin relaxation times and the component fractions. Our routine analysis technique showed that at least three components were present during the cure. The preliminary assignments of these components were as follows:

1. The component with a large spin-spin relaxation time is assigned to the mobile monomer and low-order oligomers, as these would be expected to have the highest mobility. This component is designated the mobile (m) component.
2. The component with the intermediate spin-spin relaxation time is assigned to either those parts of the higher-order oligomers that are free at one end so that they can execute semi-unrestricted motion, or to a polymer having an intermediate molecular weight. This component is designated the intermediate (i) component.

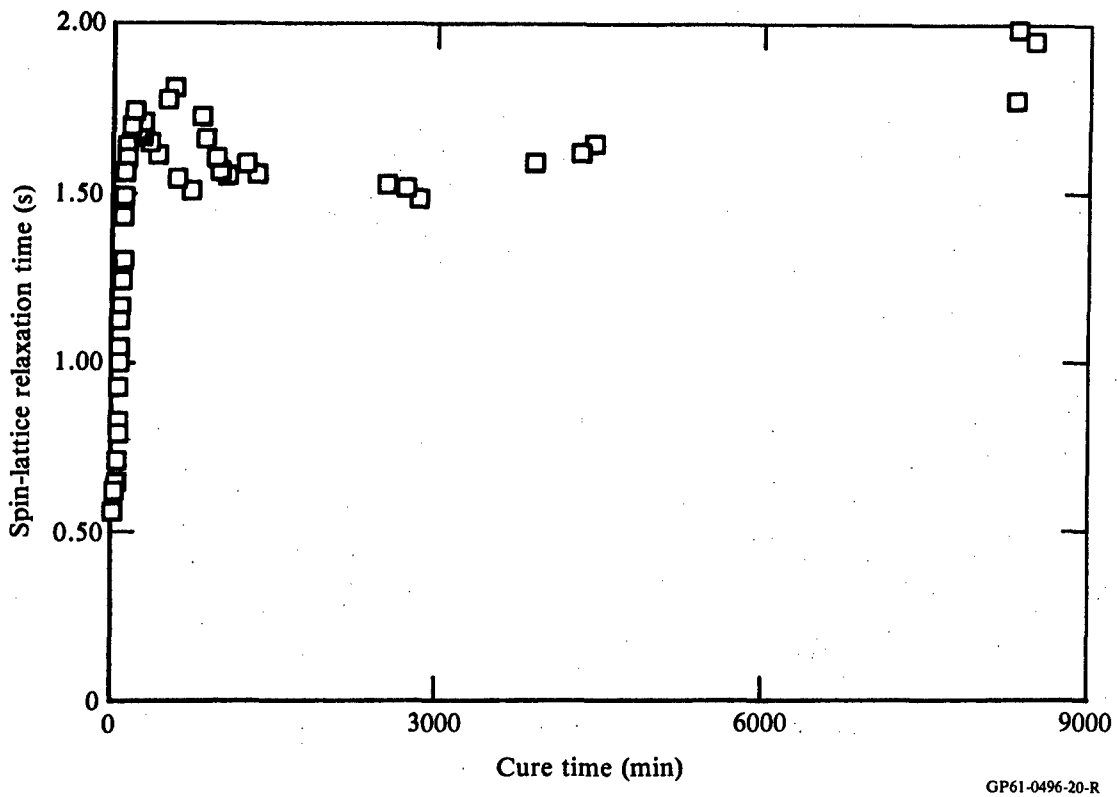


Figure 7. Spin-lattice relaxation times for ATS resin during a cure at 423 K (302°F).

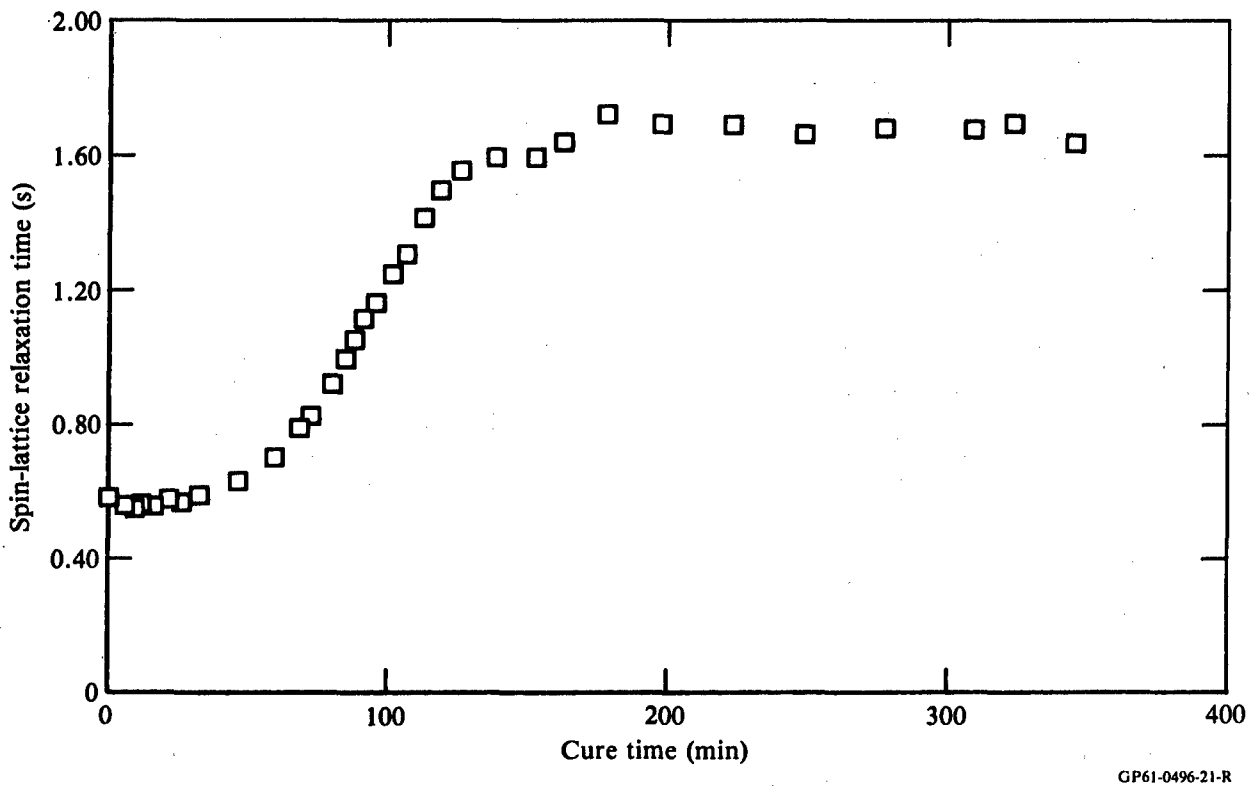
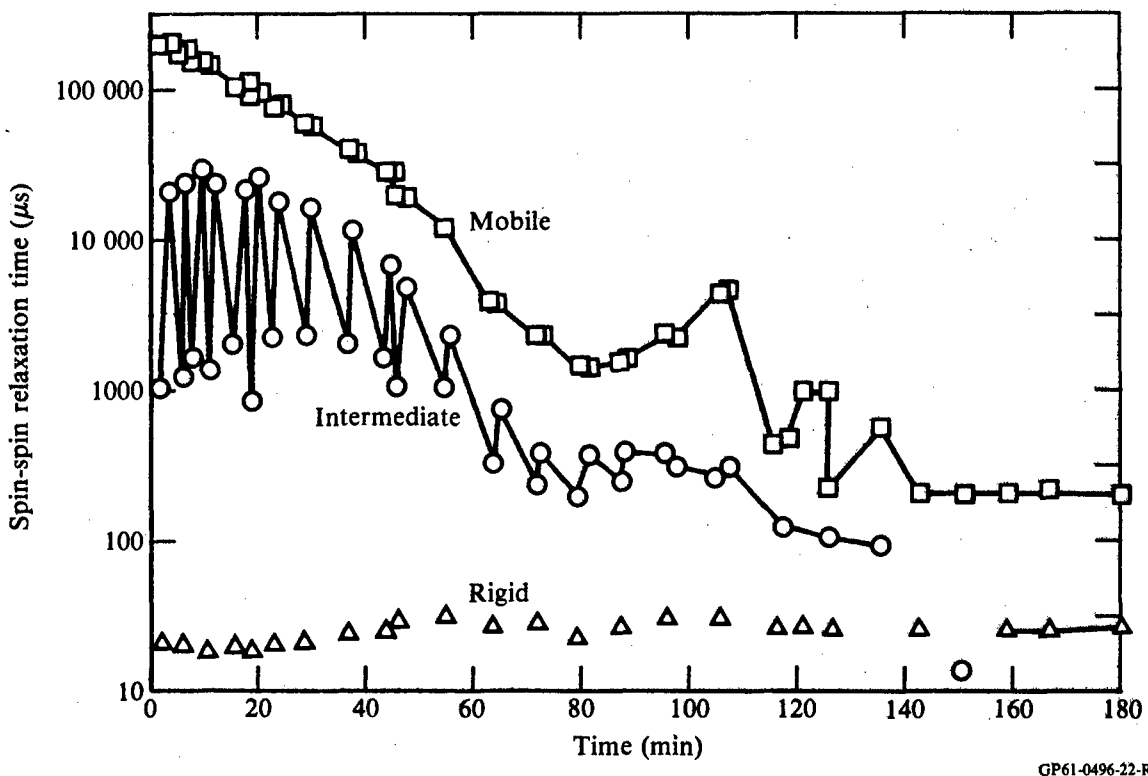


Figure 8. Early cure spin-lattice relaxation times for ATS resin during a cure at 423 K (302°F).

3. The component with the small spin-spin relaxation time is assigned to those parts of the polymer that have reacted at both ends and are embedded in a cross-linked matrix having a large molecular weight ($\geq 20,000$) so that their motion is highly restricted. This component is designated the rigid (r) component.

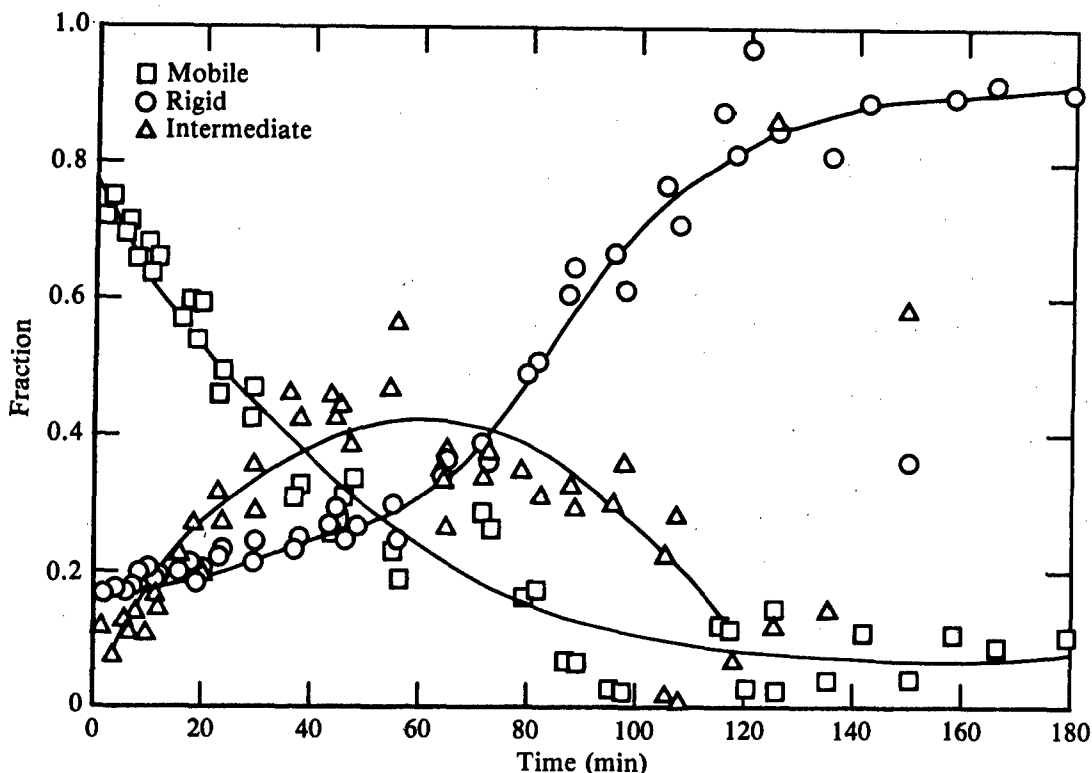
Our "routine" analysis technique for determining the components in an NMR spin-spin relaxation decay had been adequate for the study of epoxy resins where only two components are observed. However, the analysis technique was not adequate for the study of ATS resins which had three or more components. Figures 9 and 10 illustrate the uncertainties that resulted from use of our routine technique to analyze the NMR signals from an ATS sample during an in situ cure at 423 K (302°F).

The spin-spin relaxation times during the cure at 423 K (302°F) are shown in Figure 9. Throughout the entire cure at 423 K (302°F) three components were analyzed, but the intermediate component was not observed after 180 min of cure. The data for the most mobile and least mobile component have little experimental error, but the data for the intermediate component are subject to



GP61-0496-22-R

Figure 9. Spin-spin relaxation times for ATS resin during a cure at 423 K (302°F).



GP61-0496-23-R

Figure 10. Component fractions for an ATS resin during a cure at 423 K (302°F). Solid lines are drawn for visualization only.

considerable fitting error because of inadequacies inherent in the routine analysis technique.

Figure 10 shows the fractions of the total signal due to the three components. At zero cure time the rigid fraction is nonzero; it is initially equal to about 0.18. This initial observation of a "rigid" component was caused by contamination in the NMR probe; the contaminant was subsequently removed. After 1200 min of cure, the mobile fraction is about 0.03, but it appears to still be decreasing at a very slow rate.

A generalized fitting procedure was developed to analyze the complex NMR signals obtained from the ATS resin during *in situ* cure studies. A larger number of data points were obtained for each NMR signal, thus improving the uniqueness of the analysis. The generalized fitting procedure was used to analyze the ^1H spin-spin relaxation data obtained *in situ* on two ATS samples cured at 403 K (266°F). The results of this analysis are shown in Figures 11-15. Because of the importance the fitting routines have in any interpretation of the data, we present a discussion of the relative merits of the new fitting procedure as follows.

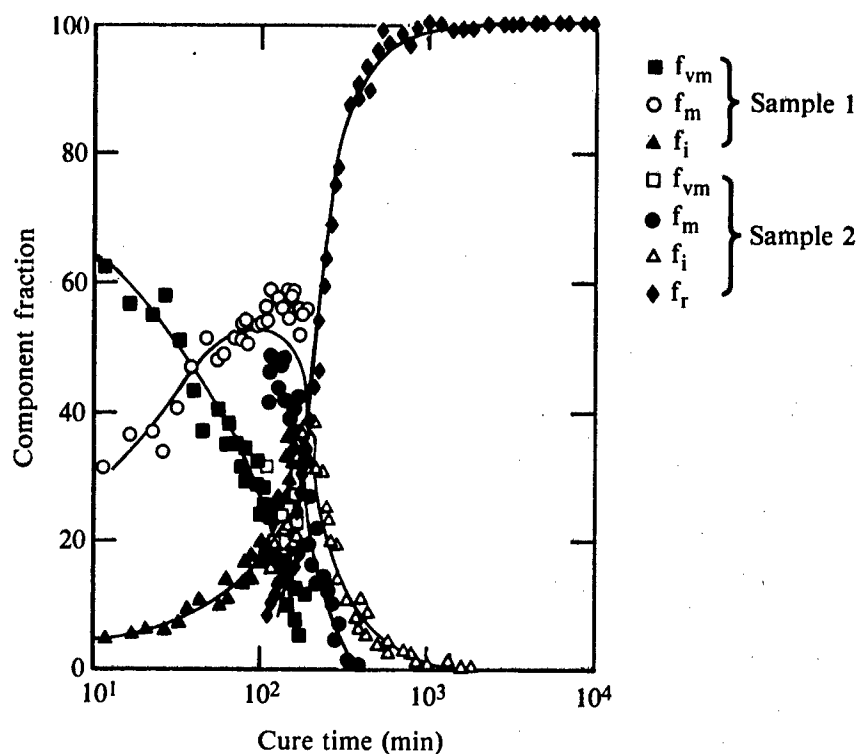


Figure 11. Component fractions of ATS during isothermal curing at 403 K (266°F) for two samples; all line shapes are assumed Lorentzian in character except f_r which is assumed Gaussian. The solid lines are drawn in for visualization only.

The new routine, FCDA, is built about a generalized fitting procedure called ZXSSQ, copyrighted by IMSL.¹⁴ FCDA allows the user to define up to five component decays to be included in the fit, along with a baseline parameter. The form of the fitted equation is then

$$f_1 \exp\left[\left(-t/T_2^1\right)^{n_1}\right] + f_2 \exp\left[\left(-t/T_2^2\right)^{n_2}\right] + \dots + C \quad (3)$$

where the parameters f_j , T_2^j and n_j are the fractional amplitude, spin-spin relaxation time, and lineshape parameter, respectively, for the j th component decay, and C is the baseline parameter. Each parameter can be fixed or fitted, depending on the user's input. The user can choose decays to be Lorentzian, $n=1$, Gaussian, $n=2$, or other, $n=(\text{user defined or fitted})$ in character.

The advantages of using FCDA over previous fitting procedures are the following:

- 1) FCDA can accept up to 16384 points, increasing the resolution capability of a single data set,

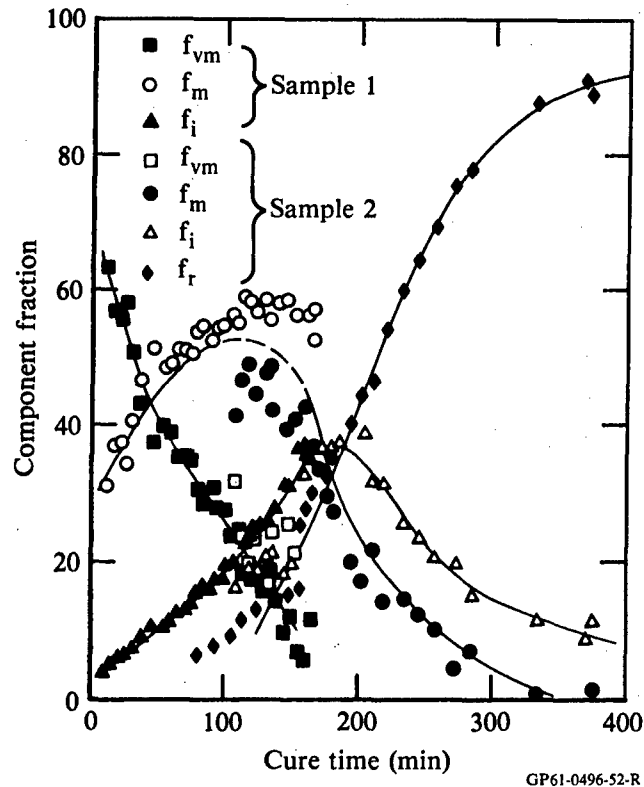


Figure 12. Expanded view of Figure 11 with a linear scale for the cure time. The discontinuities in f_m at cure times of 110 to 160 minutes are mainly due to the relatively small values of f_{vm} and f_r . When the amplitude of a component decay is small, the baseline offset affects the fit to a much greater degree, increasing the fitting errors. The solid lines are drawn for visualization only.

- 2) FCDA releases the user from many hours of work compared to the previous iterative method, and
- 3) most important, FCDA will not be affected by possible subjective input in initial estimates of relaxation times. The previous iterative procedure required breaking the data into sections, and the method chosen to section the data could affect the results, sometimes dramatically.

In cases where the spin-spin relaxation times differ by a factor of three or more, FCDA generates unique fits, independent of initial estimates. Two factors will, however, greatly affect the fits, regardless of the fitting procedure used. These two factors are discussed below.

- 1) The longest relaxation time, and thus, all the fractional amplitudes, are critically dependent on the baseline parameter. This dependency is clearly displayed in Table 2, where the baseline parameter is chosen to be fixed and is incremented by less than 0.5% of the total initial amplitude (~1 V) for five different fits. Once we understood this dependence

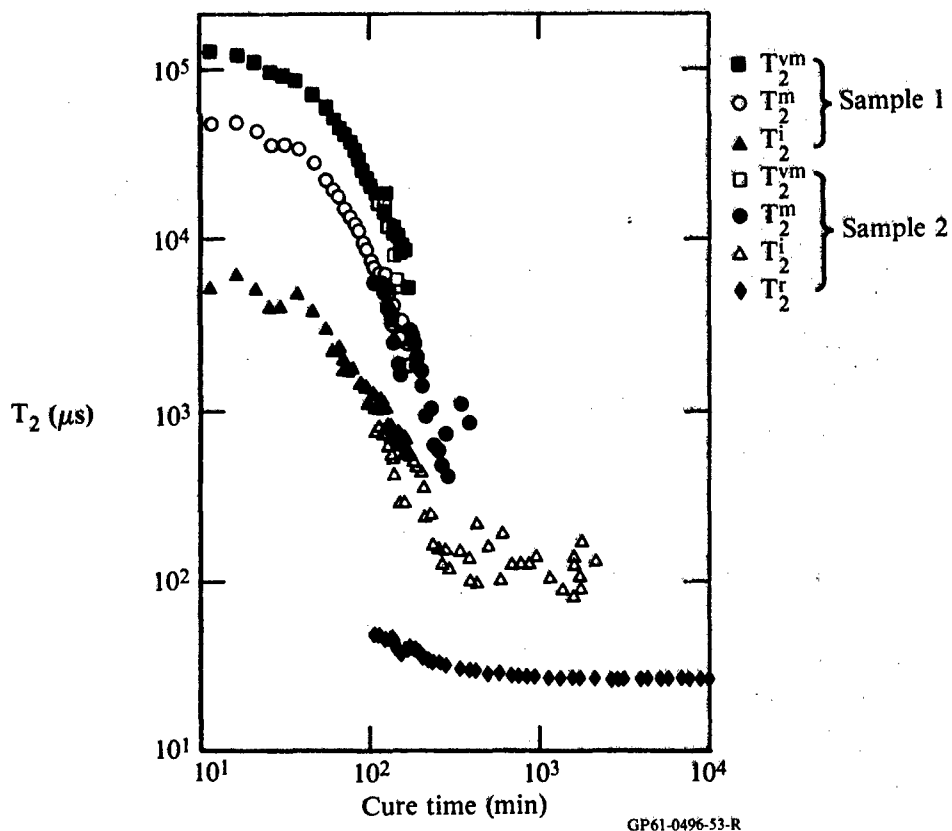
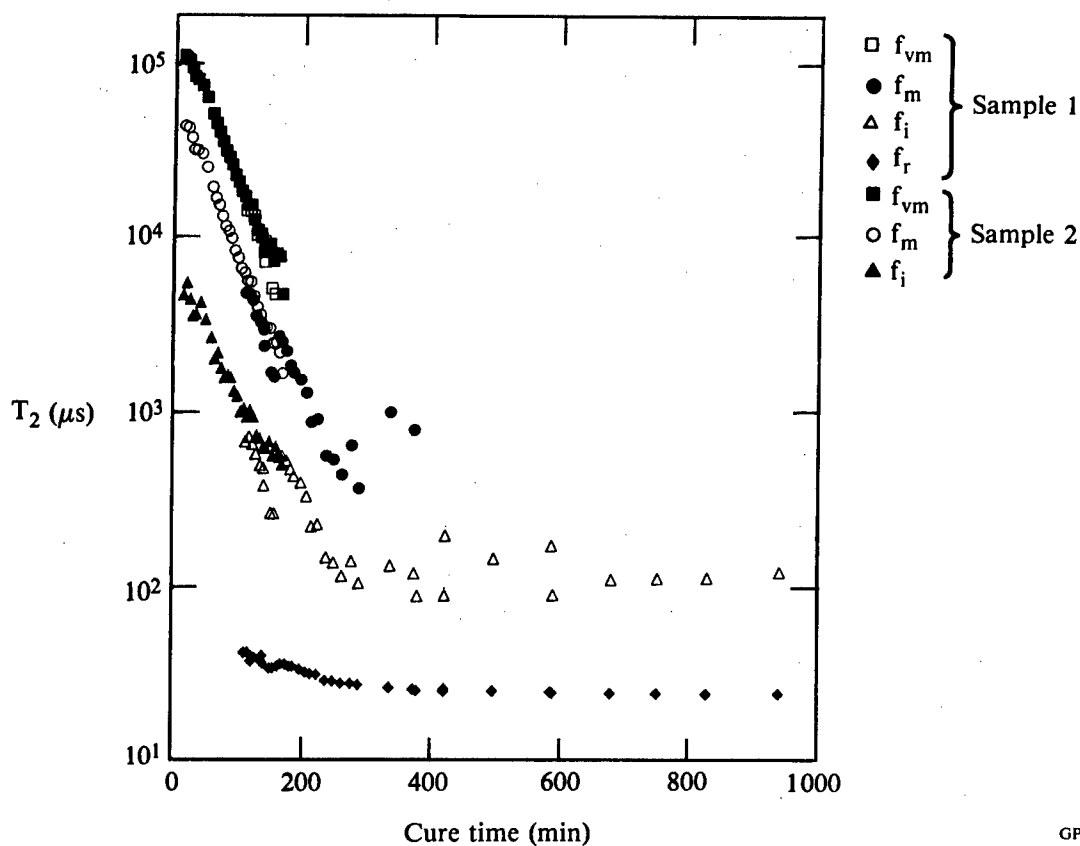


Figure 13. Spin-spin relaxation times of ATS during isothermal curing at 403 K (266°F) for two samples; all line shapes are Lorentzian except T_2^i which is Gaussian.

TABLE 2. CHANGES IN THE LONGEST RELAXATION TIME, T_2^{vm} , AND ITS CORRESPONDING FRACTIONAL AMPLITUDE, f_{vm} , DUE TO VARIOUS CHOICES OF THE BASELINE PARAMETER, C.

C (V)	T_2^{vm} (ms)	f_{vm}
-0.001	67	0.20
-0.002	85	0.12
-0.003	100	0.085
-0.004	120	0.067
-0.005	140	0.057

GP61-0496-2-R

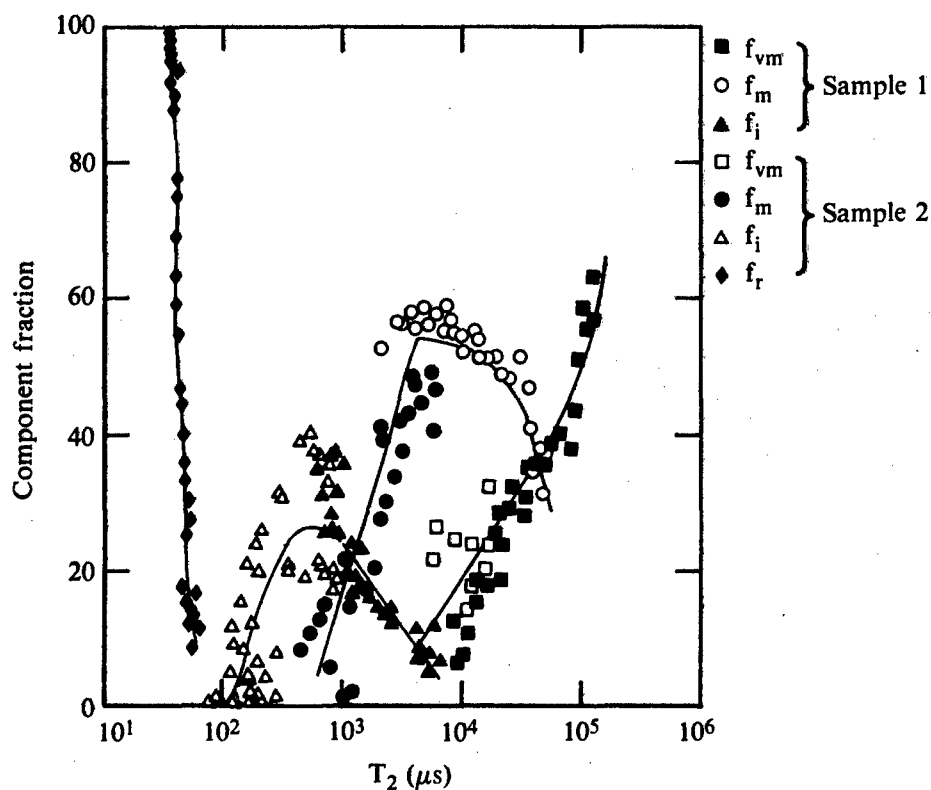


GP61-0496-54-R

Figure 14. Expanded view of Figure 13 with a linear scale for the cure time.

of T_2^{vm} ($vm \equiv$ very mobile, a new, fourth decay time) on the baseline parameter, we realized that our signal averager, a Nicolet 4094 digital oscilloscope, does not truly zero co-added spectra that are inverted to cancel baseline offset problems (the Nicolet has a digital round-off error). Spectra that were obtained by use of different numbers of co-added decays thus yield different baselines. For this reason, the data obtained at 403 K (266°F) had to be fit with a variable baseline parameter. This greatly reduced the scatter in the data, seen in Figures 11-15, in comparison to fits where the baseline was fixed at zero volts, as in Figures 9 and 10. Following this discovery of the problem with the Nicolet, the baseline on the Nicolet was carefully documented for all differing co-addition numbers. Calibrating the baseline reduced the fitting uncertainty even more this way.

- 2) Not surprisingly, the choice of line shape parameter, n_j , also greatly affects any fit. In theory, this parameter could be varied during the fit; however, for most practical cases, we would not obtain unique fits



GP61-0496-55-R

Figure 15. The spectrum of spin-spin relaxation times plotted against their respective fractional intensities for ATS cured isothermally at 403 K (266°F) for two samples. The solid lines are drawn in for visualization only.

this way. For example, the early cure data obtained at 403 K (266°F) can be fit quite well with only one decay having $n=0.8$. This makes no physical sense, and we therefore retain the usual assumptions that a decay curve having a long relaxation time ($>500 \mu\text{s}$) will be approximately Lorentzian ($n_j=1$), whereas a decay curve having a short relaxation time ($<50 \mu\text{s}$) will be approximately Gaussian in character ($n_j=2$). Although these assumptions are common in practice, caution must be applied in two areas:

- a) In the region where T_2 falls between 50 and 500 μs , the line-shape character will not necessarily transform smoothly from Lorentzian to Gaussian, nor can one assume a sudden transition in the line-shape character. If a decay relaxes with a T_2^j between 50 and 500 μs , then the fit will have additional uncertainty due to the choice of n_j .
- b) Additional complexity occurs whenever spin-spin relaxation decays of mobile, high-molecular-weight polymers are analyzed. It is well-

known that at a given temperature, there is a critical molecular weight, $M_c \sim 10^4$, of a polymer above which spin-spin relaxation behavior transforms from a single exponential (Lorentzian) to a multi- (usually two) component decay.¹⁵ It is understood that this phenomenon occurs because of the wide distribution of motional behavior present along a long, entangled or cross-linked polymer chain. When the motional frequencies fall within the NMR time scales ($\geq 10^5$ Hz), each motional frequency will result in a different spin-spin relaxation time. A distribution of frequencies often produces a decay having two distinct relaxation rates, one close to each end of the motional frequency (or spectral density) distribution curve.

Thus, we must cautiously interpret component decays in a spin-spin relaxation curve. If two decays are observed to be comparable to each other (\leq a factor of about three), as with T_2^{vm} and T_2^m in Figures 13 and 14, then these decays may result from

- (i) two molecules having different molecular weights (MW), both less than M_c , giving rise to two average motional frequencies $\geq 10^5$ Hz, or
- (ii) one molecule having a MW greater than M_c , or
- (iii) a mixture of molecules having a MW distribution producing a distribution of motional frequencies that are $\geq 10^5$ Hz.

For case (iii), if we assume that the various molecules have similar reaction rates during a cure, then the component fractions of the two spin-spin relaxation times observed should parallel each other. If, on the other hand, the reaction proceeds by consuming species of low MW to form oligomers of higher MW, then the component fractions would cross. For case (ii), the component fractions should parallel each other exactly. Case (i), on the other hand, could result in any behavior for the component fractions, depending on the reaction mechanism involved.

Spin-spin relaxation times, T_2^j , as shown in Figures 13, 14, and 15, reflect the motional behavior of the hydrogens being observed. Simply stated, as hydrogens move faster in a material, the T_2^j representing those hydrogens gets larger. This statement is not correct in general; fast restricted motions are not nearly as efficient at increasing T_2 as are fast isotropic motions. However, we use the general notion of faster motions increasing T_2^j

in the labeling; $j=vm$ for very mobile, $j=m$ for mobile, $j=i$ for intermediate, and $j=r$ for rigid.

Now consider the data shown in Figures 11-15. Keeping in mind that during the cure, the low-MW material reacts according to some mechanism, we point out the following important features of the data:

- 1) T_2^j and f_j vary smoothly during the cure (see Figures 11-15). These data illustrate the uniqueness of the fits (the initial estimates were changed considerably from fit to fit) since the fits do not jump from one solution to another (as opposed to the fits shown in Figure 9). Qualitative information from the fits therefore are accurate.
- 2) The T_2^j 's parallel each other, as shown in Figures 13 and 14, whereas the f_j 's cross, as shown in Figures 11 and 12. This crossing clearly indicates that two T_2^j 's are not attributable to any one species during the cure (case ii). It is still possible, however, that two T_2^j 's result from either two separate species, or from a mixture of species having a distribution of molecular weights (case i or iii).
- 3) Values of f_{vm} and f_m are appreciable at the beginning of the cure, whereas f_r remains < 0.10 for more than 100 min. It is impossible to differentiate, from the data currently available, whether f_{vm} and f_m are attributable to a monomer and an oligomer having a specific MW, or to a distribution of monomer and low-MW oligomers. Size-exclusion chromatography experiments would help resolve this question. The ratio T_2^{vm}/T_2^m of ~ 2.55 can be used to estimate the MW differences. Low-MW polymers in solution follow the relationship¹⁶

$$T_2 \propto (MW)^{-0.5} \quad (4)$$

During the early stages of cure, Equation (4) should be approximately true. If we assume f_{vm} represents a monomer of MW=451, then f_m would arise from an oligomer of MW=2700, or containing ~ 6 monomer units.

- 4) T_2^m/T_2^i initially is > 7 . This large ratio, along with the observation of essentially zero f_r during the first 100 minutes of cure, indicates that f_i is most likely attributable to polymer species having a fairly narrow MW distribution. Extrapolation of Equation (4) for f_i yields an approximate average MW of 2×10^5 for this component. This MW is an order of magnitude greater than M_c for common polymers. It would be ex-

pected then that we should observe two T_2 's from this intermediate-MW polymer (case ii). One possible explanation for our observation of just one T_2 is the highly aromatic, unsaturated nature of ATS. The backbone motions involving any hydrogens in ATS will be relatively rigid in comparison to the aliphatic backbone segments in most common polymers. The motional distribution of the intermediate-MW polymer species in ATS would not include the higher frequencies of most high polymers. This lack of higher motional frequencies in ATS is intrinsically related to its high-temperature properties, and the narrower distribution of motional frequencies present in ATS might be expected to lead to the observation of just one T_2 for ATS polymer species.

A mechanism for the cure, which is consistent with the data shown in this report, is as follows:



The notation follows Flory;¹⁷ I is an initiator species which we will not attempt to define here; $R\cdot$ is the primary reactive radical species; M is the monomer. M_x , M_y , and M_z are polymers where x and z are less than 300, and y is about 300 (from the T_2 ratios); Equation (9) includes both bimolecular coupling or disproportionation terminations, M_α being symbolic only; and $P_{x+z}\cdot$ is the cross-linked polymer, which can continue to react.

The reaction scheme incorporates the notion that the intermediate component i is a single, fairly narrow MW-distributed polymer species (with $y \sim 300$). Once initiation occurs, polymerization proceeds rapidly until termination occurs, i.e., $k_d, k_a, k_t \ll k_p$. This reaction pathway continues until the viscosity of the mixture becomes high enough to force two effects: (i) cross-linking begins to occur, i.e., k_c increases substantially, and (ii) the termination mechanism(s) slows, i.e., k_t decreases. The increase in k_c is simply attributable to the gel point. The decrease in k_t in some ways resembles autoacceleration (or the Trommsdorff effect) in that normal termination of the free-radical polymerization is slowed dramatically by the viscosity increase. Although there may not be a direct one-to-one correspondence to termination and radical decay, the assumed decrease in k_t is consistent with the EPR measurements, in which substantial increase in the free-radical concentration is observed only following an induction period similar to the period of delay seen here in the appearance of f_r (see the discussion in Section IV). For the mechanism suggested here, we have not considered the two fractions f_{vm} and f_m as separate, since interpretation of these fractions is speculative.

If $k_d, k_a \ll k_p$, we should observe a first-order reaction of monomer. From Equations (5-9), we obtain

$$-d[M]/dt = k_p (\kappa/k_t)^{1/2} [M] \quad (11)$$

where κ depends on the initiation reactions, Equations (5) and (6), and is usually constant.¹⁷ This approximate first-order reaction of monomer is shown in Figure 16, where f_{vm} and f_m have been summed. Autoacceleration in common polymers occurs because of the decrease of k_t in Equation (11) with increasing viscosity. But for ATS, the cross-linking reaction involves k_c , which almost certainly will stay $\ll k_p$, but may increase as k_t decreases. This increase in k_c will cancel, to some extent, the decrease in k_t , and acceleration in the extent of reaction during the cure may not necessarily be observed.

High-resolution (HR) ^1H NMR spectra were obtained in situ on ATS at 423 K (302°F). The objective of this experiment was the following. If f_m is attributable to an oligomer containing 6 monomers as estimated from T_2 ratios, then we would expect to see a dramatic decrease in the fractional content of the acetylene peak, f_{acet} , in the HR ^1H spectra during the cure; see Figure

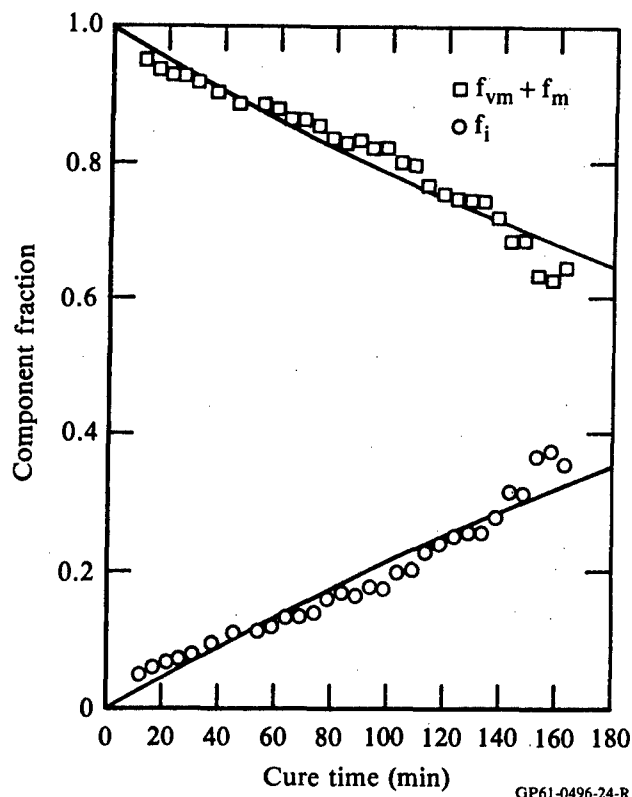
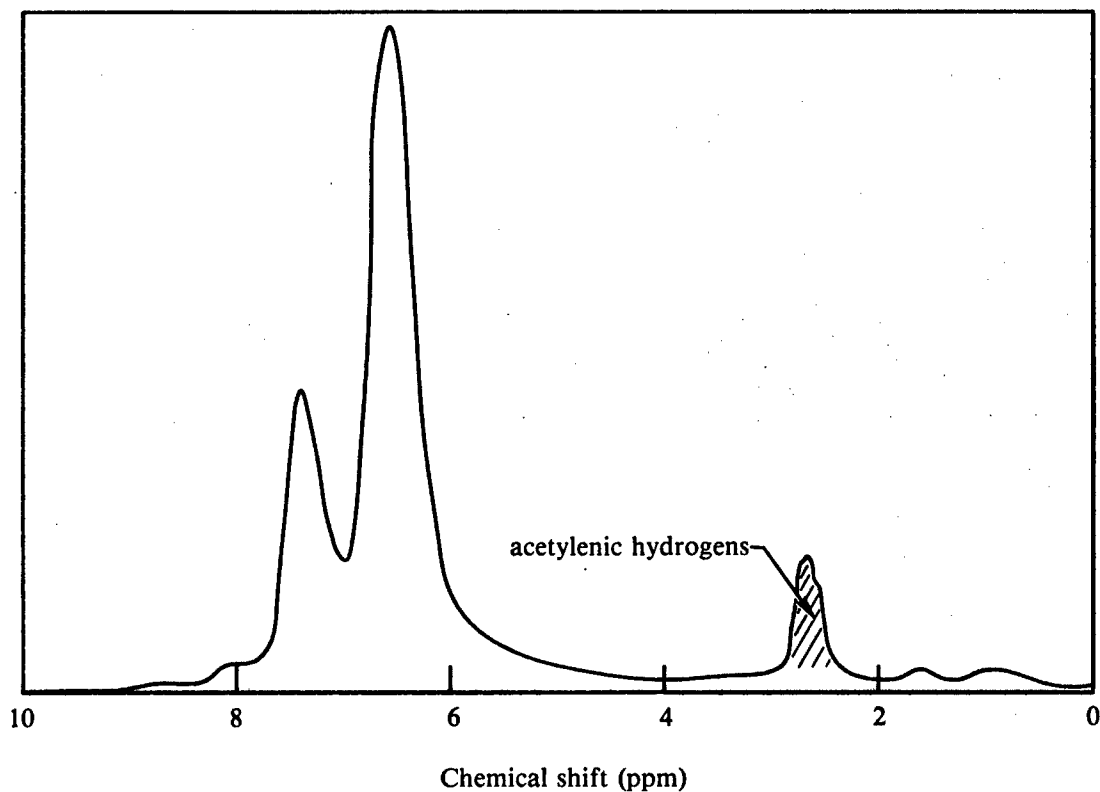


Figure 16. Approximate first-order uptake during early curing of ATS at 403 K (266°F). The component fractions f_{vm} and f_m from Figure 12 are summed to obtain the squares; f_i are the circles. The first-order rate constant is $k_1 \sim 4.0 \times 10^{-5} \text{ s}^{-1}$.

17. We would not expect to observe f_i or f_r in the HR ^1H spectra because of their dipolar broadness, and f_{acet} would therefore decrease as

$$f_{\text{acet}} \sim 0.11f_{vm} + 0.02f_m \quad (12)$$

The value 0.11 results from the ratio of 1 of 9 hydrogens on an ATS monomer being acetylenic; similarly, 1 of 51 or 0.02 hydrogens on an oligomer containing 6 monomers would be acetylenic. After heating ATS for 120 minutes at 403 K (266°F), see Figure 12, $f_{\text{acet}} \sim 0.11 \times 0.2 + 0.02 \times 0.55 = 0.033$, down from -0.09 at the beginning of the cure. If the curing reactions are simply accelerated at the higher temperature, then the results of the 423 K (302°F) cure would be the same, but would occur more rapidly. Curing at 403 K (266°F) in the HR spectrometer was not attempted because of problems in externally locking the magnetic field for a longer time than one hour. The results of the 423 K (266°F) cure experiment are shown in Table 3.



GP61-0496-77

Figure 17. High-resolution ^1H NMR spectrum of ATS cured 19 minutes *in situ* at 423 K (302°F). The fraction of acetylene hydrogens (f_{acet}) is the ratio of the acetylene peak to the total area.

TABLE 3. HIGH RESOLUTION ^1H NMR RESULTS ON ATS CURED AT 423 K (302°F).

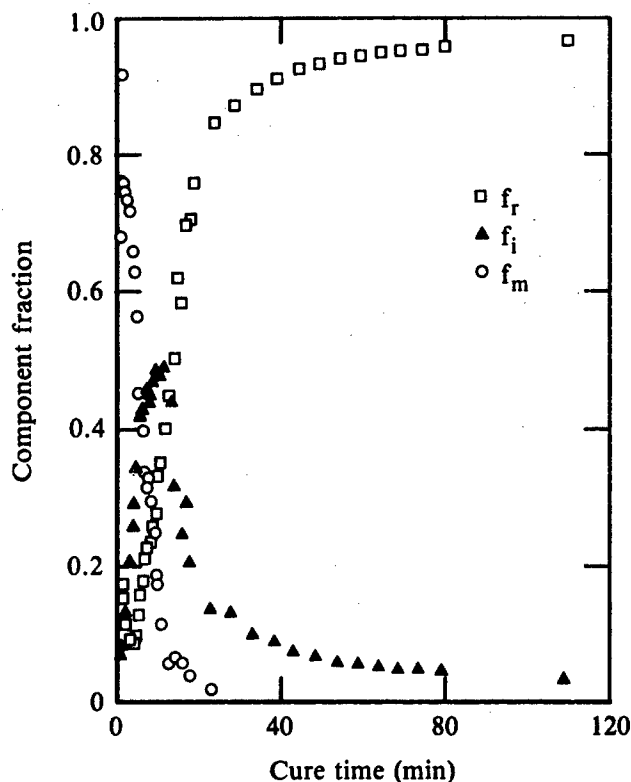
Cure time (min)	f_{acet}
14.5	9.1 ± 1
16.0	8.7
19.0	10.3
22.0	10.2
26.0	10.0
30.0	9.7
34.0	8.4
39.0	8.4
44.0	8.5
54.0	8.7
60.0	9.7
65.0	10.4
70.0	11.8
75.0	13.0 ± 4

GP61-0496-3-R

The initial impression from Table 3 is that only monomer species are being observed in the HR ^1H spectra; or, more likely, that the monomer:oligomer ratio remains fairly constant during the cure. The 423 K (302°F) spin-spin relaxation data, on the other hand, could be fit reasonably well with just three components; see Figures 9 and 10. This result suggests that f_m in the 403 K (266°F) cure spin-spin relaxation data (see Figures 11 and 12) might be an artifact of the lower temperature, which lowers M_c . On the other hand, we cannot eliminate the possibility that the monomer:oligomer ratio changes during the 403 K (266°F) cure according to $f_{vm}:f_m$, as shown in Figure 12, whereas the monomer:oligomer ratio does not change during the 423 K (302°F) cure. The 453 K (356°F) data, however, suggest that the cure mechanism is similar, irrespective of cure temperature. The HR ^1H NMR results, therefore, appear to contradict the ^1H spin-spin relaxation results. The experimental difficulties with broad signals being lost to the baseline in the HR ^1H NMR data make the data in Table 3 difficult to interpret.

Results of the generalized computer fitting of the ^1H NMR spin-spin relaxation data of ATS resin cured at 453 K (356°F) are presented in Figures 18-23. Again, the super-/subscripts used in the figures refer to the average motional characteristics of the species involved: vm =very mobile, m =mobile, i =intermediate and r =rigid. Figures 18-20 were obtained by assuming that the decay curves consisted of two Lorentzian plus one Gaussian (f_r and T_2^r) decays. The data could be fit slightly better by assuming three Lorentzian plus one Gaussian decays, and the results of analyzing the data by use of this assumption are shown in Figures 21-23. It is pointed out here that these data were affected by the introduction of the sample into the NMR probe. The sample was taken at room temperature, ~ 298 K (77°F), and was suddenly immersed in the probe at time $t=0$ at 453 K (356°F). The warming of the sample can be seen in Figures 18 and 21 from the initial increase of f_m, f_{vm} and corresponding decrease in f_r .

An important aspect of Figures 18-23 is the continued change of f_r, f_i and T_2^i at long cure times. This change does not occur for the 403 K (266°F) cure; see Figure 11. Because of the high sensitivity and quantitative in situ nature of the measurements, ^1H NMR could be considered as a long-cure monitor for selected materials.



GP61-0496-25-R

Figure 18. Component fractions of ATS during isothermal curing at 453 K (356°F). These data were fit using the 2+1 assumption; f_m and f_i are assumed Lorentzian in lineshape character, f_r is assumed Gaussian. The behavior of the data from 0 to 2 minutes does not conform to first-order kinetics because of sample heating from ~298 K (77°F) to 453 K (356°F).

Figure 24(a-d) displays the results of two fits to the same, representative, relaxation decay. Curve (a) displays the 2 Lorentzian plus 1 Gaussian (2+1) fit, whereas curve (d) shows results of fitting 3 Lorentzians plus 1 Gaussian (3+1) fit. Curves (b) and (c) were obtained by subtracting the 2+1 and 3+1 fitted curves, respectively, from the actual data. Curve (b) shows that the error of the 2+1 fit is >4% of the initial total intensity at $t=0$. Curve (c) shows that the 3+1 fits have no errors larger than the scatter intrinsic to the data: about $\pm 1\%$.

Comparison of the two different assumptions is shown most clearly in Figure 25, where f_{vm} and f_m from the 3+1 fits have been added together to simulate f_m from the 2+1 fits. The qualitative information is essentially the same between the two fitting procedures, except for the fact that the 3+1 fits contain more information than the 2+1 fits. In Figure 26, a comparison of the solid squares, obtained from the 2+1 fits, to the solid triangles, obtained

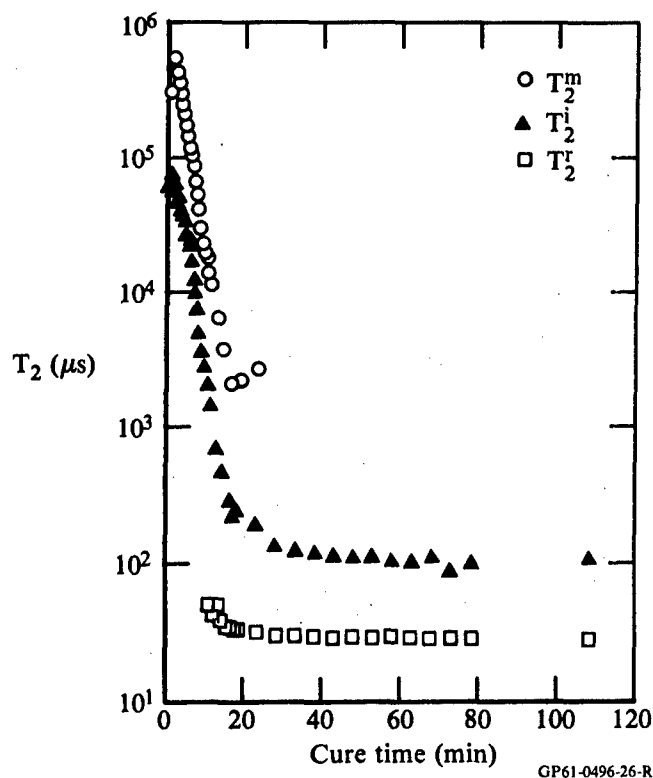


Figure 19. Spin-spin relaxation times of ATS during isothermal curing at 453 K (356°F). These data were fit using the 2 + 1 assumption; T_2^m and T_2^i are Lorentzian, T_2^r is Gaussian.

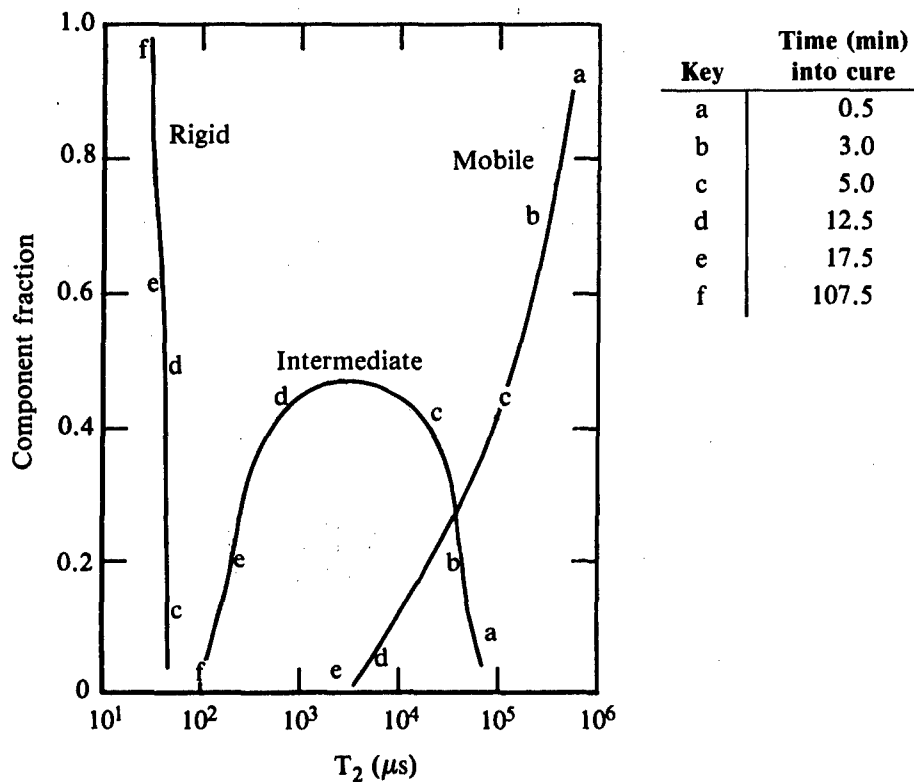
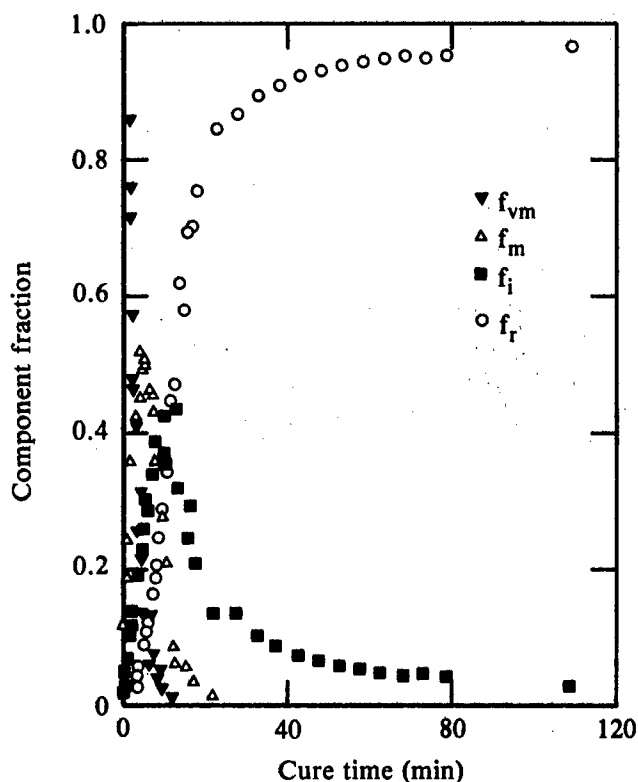


Figure 20. The spectrum of spin-spin relaxation times, T_2 , plotted against their respective fractional intensities for ATS cured isothermally at 453 K (356°F). These data were fit using the 2 + 1 assumption.



GP61-0496-28-R

Figure 21. Component fractions of ATS during isothermal curing at 453 K (356°F). These data were fit using the 3+1 assumption (compare with Figure 18); f_{vm} , f_m and f_i are Lorentzian, f_r is Gaussian. The behavior of the data from 0 to 2 minutes does not conform to first-order kinetics because of sample heating from ~ 298 K (77°F) to 453 K (356°F).

from the 3+1 fits, shows that even the quantitative information from the two fitting assumptions is nearly identical.

The data in Figures 18 and 21 closely resemble consecutive first-order reactions behavior, at least during the early cures. Figure 27 shows fits of the early cure analysis of Figure 18 to the standard equations derived from two consecutive first-order reactions.¹⁸ Similarly, Figure 28 shows fits to the early cure analysis of Figure 21 to the equations

$$[A] = [A]_0 \exp(-k_a t) \quad (13)$$

$$[B] = [A]_0 k_a \left\{ \frac{\exp(-k_a t) - \exp(-k_b t)}{k_b - k_a} \right\} \quad (14)$$

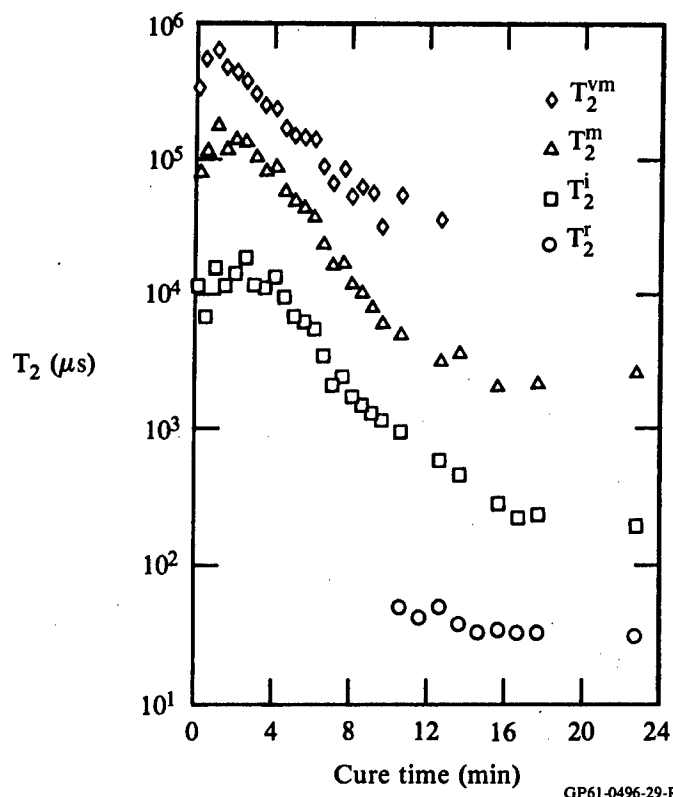


Figure 22. Spin-spin relaxation times, T_2 , of ATS during isothermal curing at 453 K (356°F). These data were fit using the 3+1 assumption (compare with Figure 19); T_2^{vm} , T_2^m and T_2^i are Lorentzian, T_2^r is Gaussian.

$$[C] = [A]_0 \frac{k_a k_b}{k_b - k_a} \left\{ \frac{\exp(-k_a t)}{k_c - k_a} - \frac{\exp(-k_b t)}{k_c - k_b} + \frac{(k_b - k_a) \exp(-k_c t)}{(k_c - k_a)(k_c - k_b)} \right\} \quad (15)$$

$$[D] = [A]_0 \left\{ 1 - \frac{1}{k_b - k_a} \left[\exp(-k_a t) \left(k_b + \frac{k_a k_b}{k_c - k_a} \right) - \exp(-k_b t) \left(k_a + \frac{k_a k_b}{k_c - k_b} \right) - \exp(-k_c t) \left(\frac{k_a k_b (k_b - k_a)}{(k_c - k_a)(k_c - k_b)} \right) \right] \right\} \quad (16)$$

which derive directly from the reaction scheme



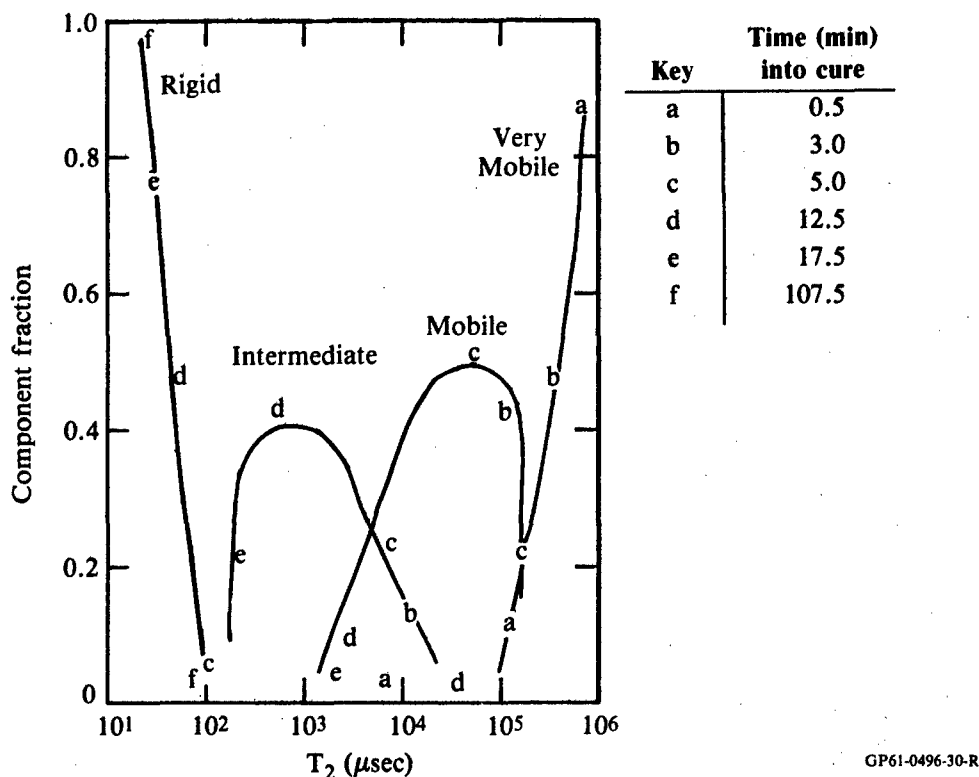
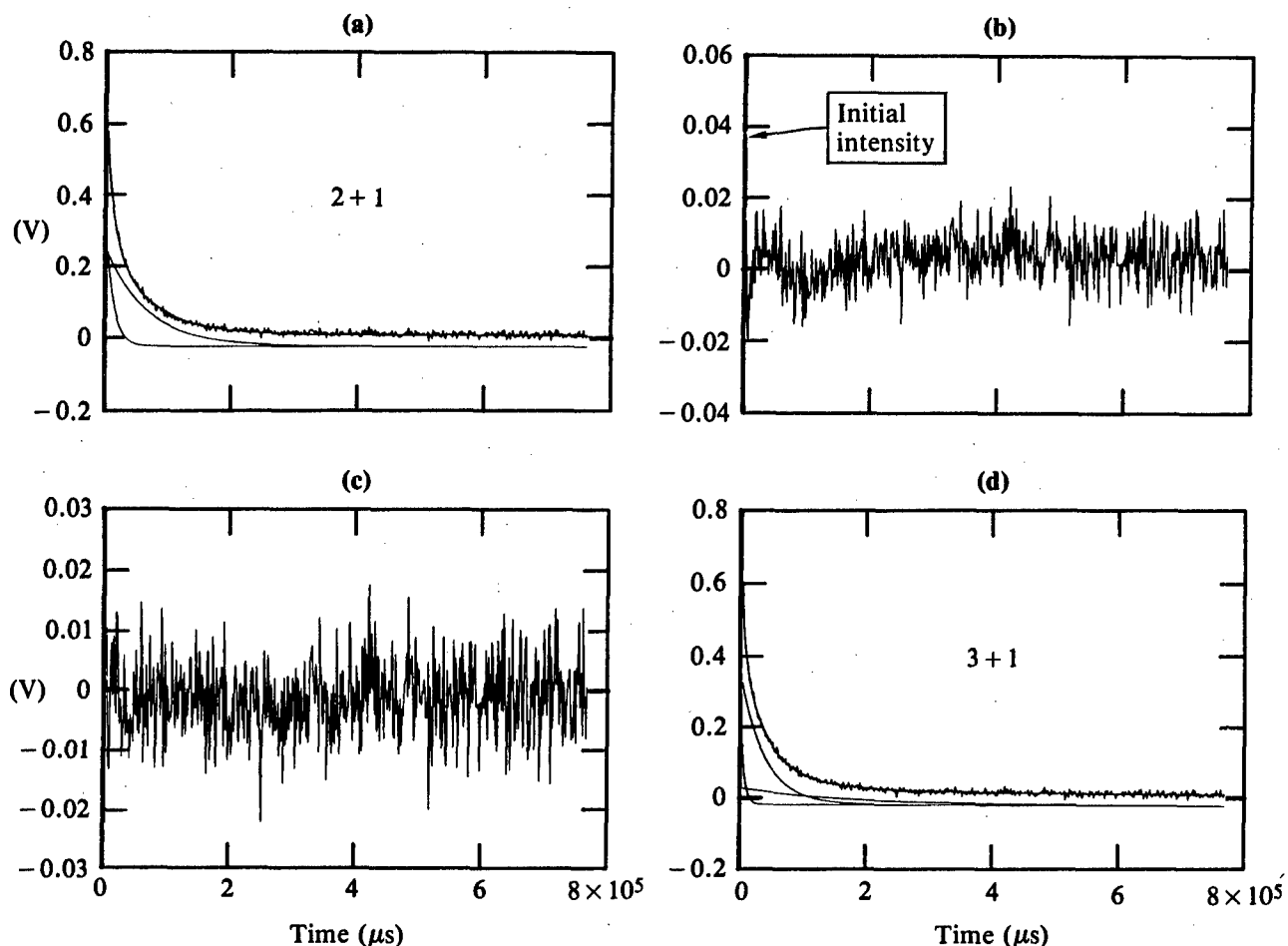


Figure 23. The spectrum of spin-spin relaxation times, T_2 , plotted against their respective fractional intensities for ATS cured isothermally at 453 K (356°F). These data were fit using the 3+1 assumption.

with the assumption that only A is present at $t=0$. The one-to-one correspondence used for the fits was $f_{vm} \rightarrow [A]$, $f_m \rightarrow [B]$, $f_i \rightarrow [C]$ and $f_r \rightarrow [D]$.

Although it appears implausible that ATS reacts according to Equation (17), the relatively good fit of Equations (13)-(16) to the data shown in Figure 28 requires further analysis. Any consideration of free-radical polymerization of ATS should include cyclization, as proposed by Pickard, et al.,² and/or the phenyl-naphthalene-forming intramolecular cyclization reaction (IMC) as proposed by Reinhardt and Arnold.¹⁹ As shown in Figure 29, IMC will be favored over continued free-radical addition if the third ATS monomer attacks a **cis-trans** biradical, and if the benzene rings have π -bonding overlap which favors planar geometry with the conjugated diene. If the biradical (a true biradical is not necessary for this discussion; we refrain from speculating on the exact nature of the intermediate radical) is **trans-trans**, as shown in Figure 30, one of two mechanisms can occur: (1) the benzene rings

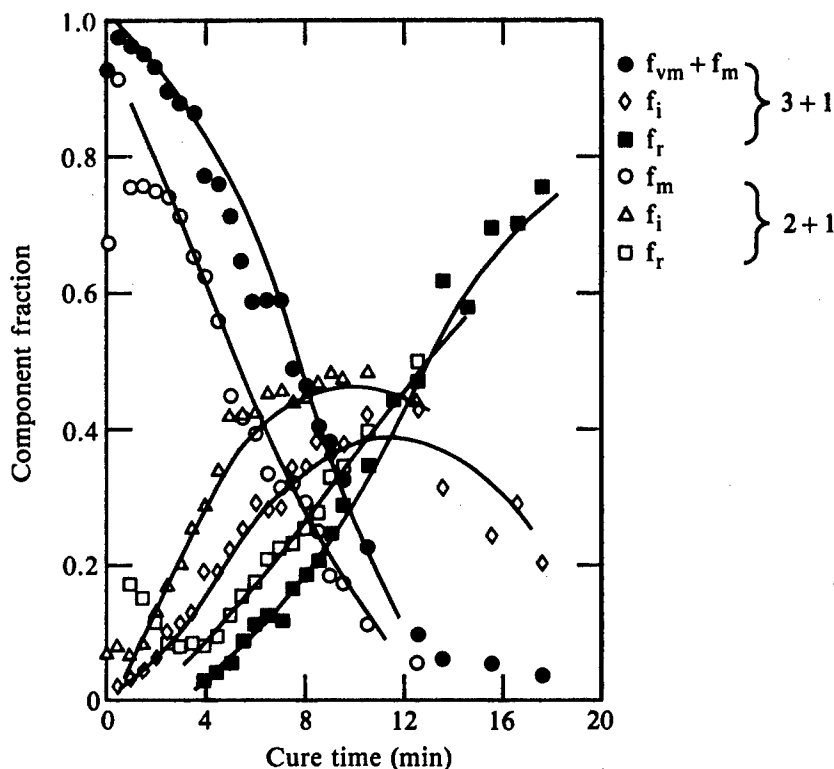


GP61-0496-31-R

Figure 24. Comparisons of 2+1 to 3+1 assumptions fitted to the raw data obtained *in situ* on ATS cured at 453 K (356°F) for 6.0 min (no rigid component is observable yet); (a) shows the 2+1 fit with components (offset -5%) and the raw data; (b) shows the difference plot of the fit in (a) to the raw data; (c) shows the difference plot of the fit in (d) to the raw data; (d) shows the 3+1 fit with components and the raw data. Note that the 3+1 fit, (c), displays no error greater than the signal-to-noise, whereas the 2+1 fit, (b), is > 4% from fitting the beginning of the decay.

rotate out of the plane of the diene and free-radical addition continues, or (2) IMC or cyclization occurs (Figures 29 and 30 show a slightly modified mechanism for the IMC from Reference 19). The relative stability of these reactions will be affected by the energy necessary to rotate the benzene rings out of the plane of the butadiene moiety. It is possible that this energy is significant, since, in the planar arrangement, π overlap between the conjugated diene and the benzene ring might occur.

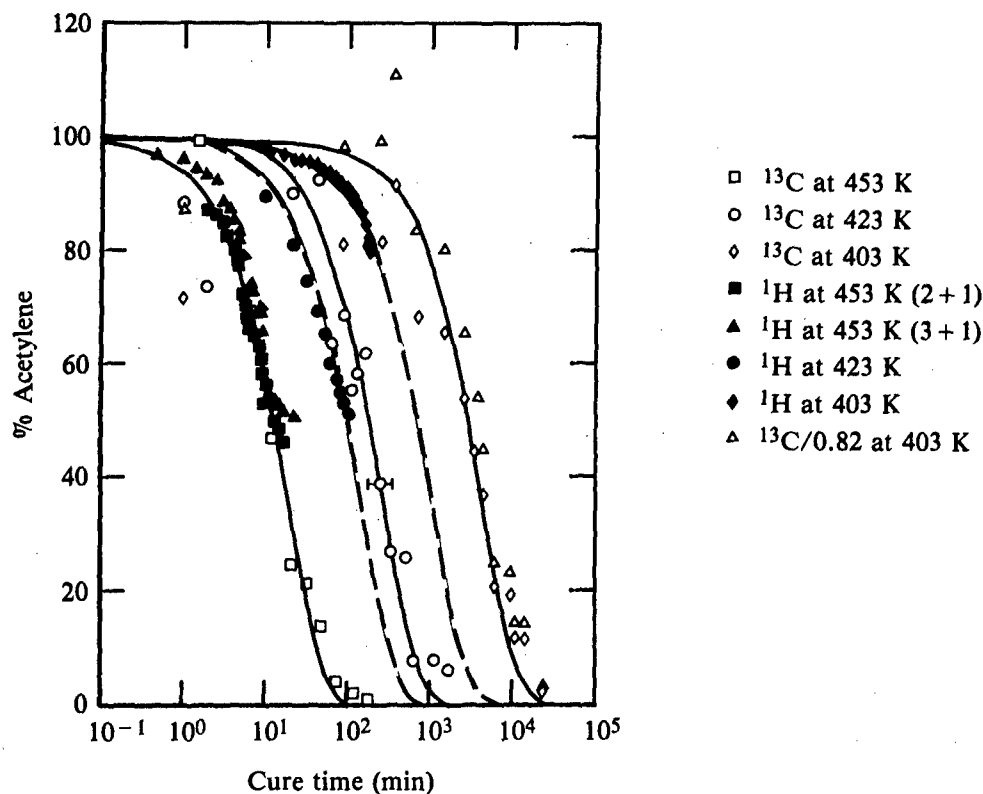
Studies of the rotational barriers in substituted styrenes should give some indication of the similar rotational barriers in ATS. Meta- and para-



GP61-0496-32-R

Figure 25. Direct comparison of the 2+1 and 3+1 fitting assumptions; the open symbols are the 2+1 data obtained directly from Figure 18, whereas the filled symbols are from Figure 21. f_{vm} and f_m of Figure 21 are summed to obtain the filled circles. The solid lines are drawn for visualization only.

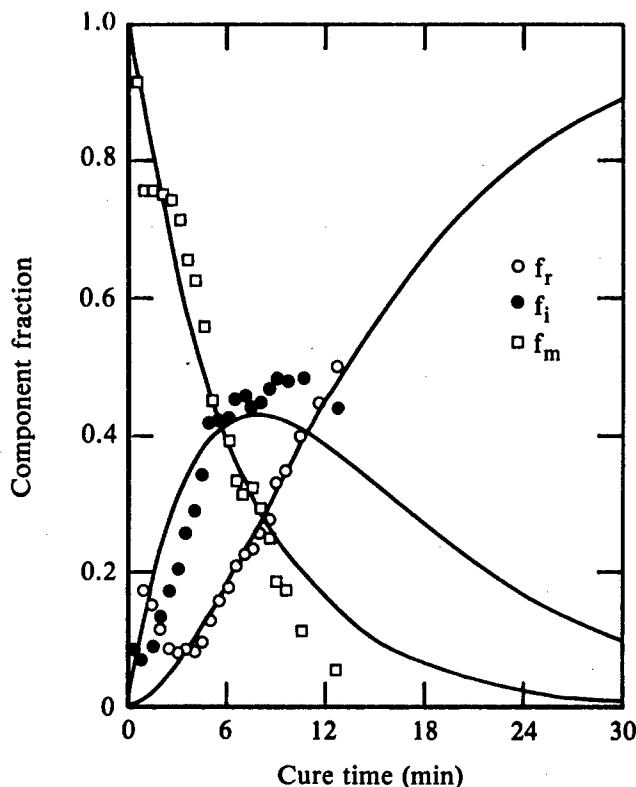
substituted styrenes are often found to have $10-13 \text{ kJ mol}^{-1}$ barriers to rotation of the ethenyl moiety away from the phenyl plane.²⁰ Styrene is found to have a slightly larger barrier to rotation of 13.5 kJ mol^{-1} .²¹⁻²³ If the styrene is α,β -substituted, on the other hand, steric effects predominate, and the minimum energy conformation is often skewed away from planar, with the barrier to rotation having its maximum for rotation through the phenyl plane.²⁴ Thus, we see that the π -overlap or hyperconjugation energies which favor planar conformations compete against steric effects because of side chains. Ab initio calculations²¹ have given considerable insight to the conformations of styrene, and might possibly be extended to studies of larger systems. Carreira and Towns point out that only the ground state of styrene and substituted-styrene molecules have been studied.²⁰ During reactions, the transition-state styrene moiety appears to favor the planar conformations much more than studies on the ground state have indicated.²⁰



GP61-0496-33-R

Figure 26. Comparison of the fraction acetylene obtained from ^{13}C and ^1H NMR measurements. The solid triangles, obtained from $f_{vm} + f_m$ of Figure 21, and solid squares, obtained from f_m of Figure 18 show that the 2+1, 3+1 assumptions are not qualitatively important for deriving f_{acet} . The open triangles are shifted by 20% from the open diamonds, and show that the ^{13}C and ^1H NMR results at 403 K (266°F) disagree more than experimental error. The solid lines are exponential best fits to the ^{13}C data with $k = 1 \times 10^{-3}$, 7×10^{-5} and $4.5 \times 10^{-6} \text{ s}^{-1}$ for the 453 K, 423 K, and 403 K cure temperatures, respectively. The dashed lines are exponential best fits to the ^1H data with $k = 2 \times 10^{-5}$ and $1.3 \times 10^{-4} \text{ s}^{-1}$ for 403 K and 423 K cure temperatures, respectively.

Since a simple resonance structure between the butadiene and the benzene ring is not possible with the meta substitution (it is, however, likely for the para substitution), free-radical polymerization is most likely a stable reaction pathway, at least for moderate degrees of polymerization. Moreover, the ^1H NMR spin-spin relaxation data imply that trimerization (or higher-order cyclization) is not the major reaction pathway. A broad distribution of molecular weights, consisting of 3, 5, 7, ... monomer units, would be expected in a scheme wherein trimerization is predominant. In this case, ^1H spin-spin relaxation would show at most two relaxation decays, not the three or four observed. Thus, a mechanism consisting of simple consecutive first-order reactions as shown in Equation (17) appears to be improbable. Still, the data



GP61-0496-34-R

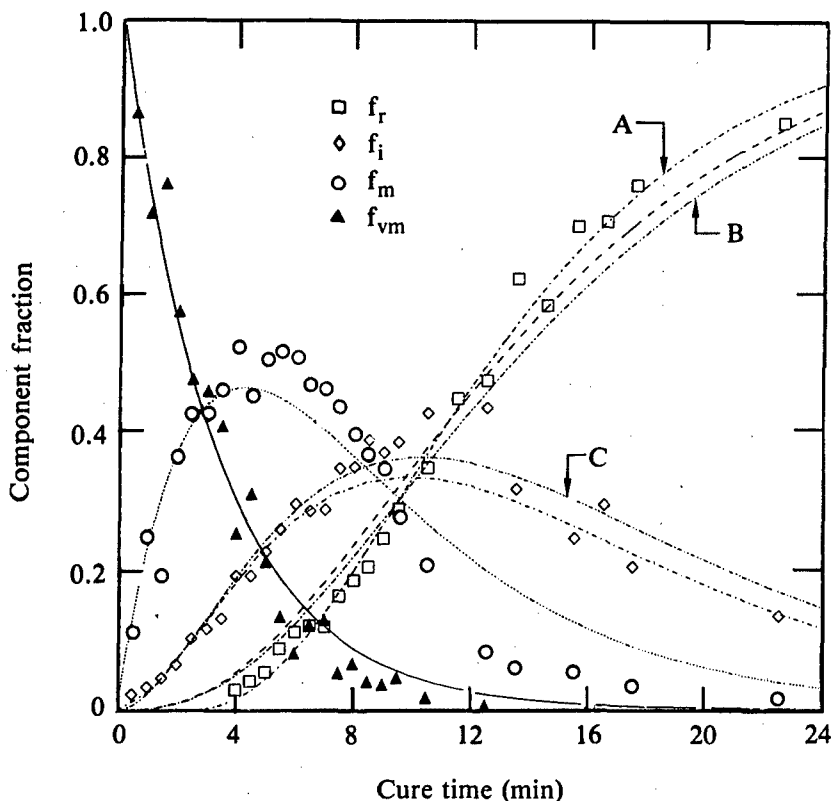
Figure 27. Successive first-order reactions fitted to the early cure data shown in Figure 18. The rate constants are $k_1 = 0.0026 \text{ s}^{-1}$ and $k_2 = 0.0018 \text{ s}^{-1}$. The non-first-order behavior of the data in the first 2 minutes (at least) is due to sample heating.

shown in Figure 28, specifically f_m , suggest that cyclization (but not necessarily trimerization) and/or IMC may be important reaction pathways; more experimental evidence is needed to substantiate this speculation.

Referring to Equation (4), we reintroduce the use of T_2 ratios to determine approximate average molecular weights (MW) of the various fractions during the cures. Earlier, we used the ratio

$$\frac{T_2^1}{T_2^2} \approx \left(\frac{MW_2}{MW_1} \right)^{0.5} \quad (18)$$

to estimate the MW, and suggested that the MW ratio of f_m to f_{vm} is ~6. If, on the other hand, trimerization is responsible for f_m , then the ratio would be 3. Instead of $T_2 \propto (MW)^{-0.5}$, we would have $T_2 \propto (MW)^{-1}$. The MW of f_i in the case of inverse proportionality would then be ~30 monomer units instead of 300 (this could be lower still; in fact, the exponential dependent of T_2 on the MW

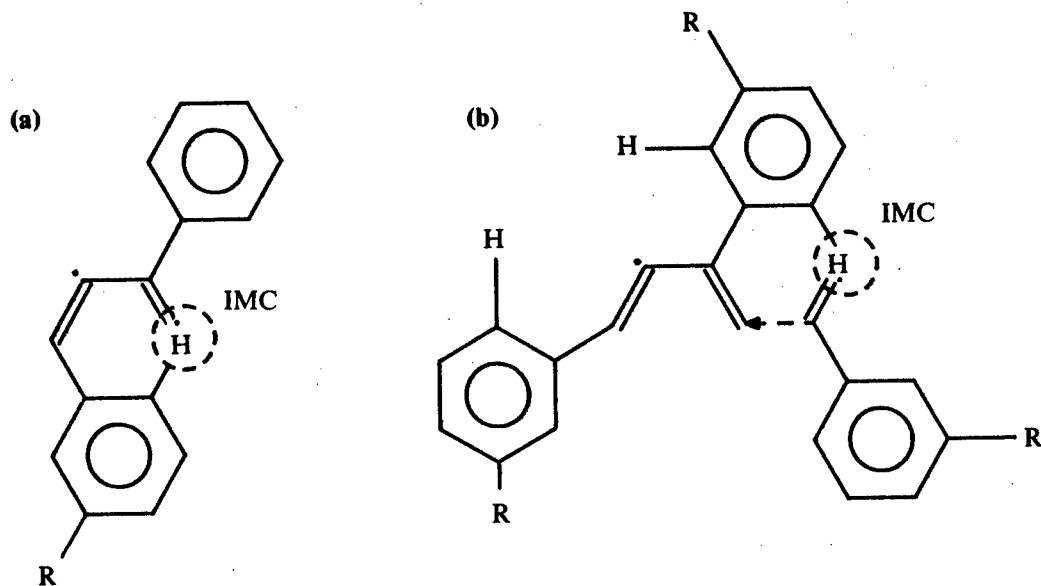


GP61-0496-35-R

Figure 28. Successive first-order reactions fitted to the early cure data shown in Figure 21. A fairly good set of rate constants to fit the data is $k_1 = 0.005 \text{ s}^{-1}$, $k_2 = 0.003 \text{ s}^{-1}$, and $k_3 = 0.0027 \text{ s}^{-1}$. Curve A has $k_3 = 0.0054 \text{ s}^{-1}$ and a time displacement of ~ 2 minutes, curve B has $k_3 = 0.00297 \text{ s}^{-1}$, and curve C has $k_3 = 0.0023 \text{ s}^{-1}$. The relatively good fit to first-order kinetics displayed here in the first 2 minutes, as opposed to Figure 27, is not understood. It should be noted, however, that the 1.5 minute point displays much more than the average error for the rest of the data.

must go to infinity as the $MW \rightarrow \infty$). This shows the extremely rough nature of this approximation. Without some additional evidence, we can say with conviction only that there are at least three distinct components due to polymers of fairly well-resolved MW in the ATS system during cure. In addition, f_i appears to be due to a polymer of fairly narrowly distributed MW, and whose average molecular weight is $>10^4$ but less than 1.5×10^5 .

Figure 26, presented earlier, compares ^{13}C CP/MAS NMR studies, as presented in Section III 1a, with the ^1H NMR spin-spin relaxation results. The open symbols in Figure 26 represent the fractional intensity of the acetylenic carbons, f_{acet} , observed in the ^{13}C solid-state NMR spectra. The solid lines resulted from least-squares fitting of the ^{13}C results to simple exponential decays (i.e., first-order reaction of acetylene moiety). The



GP61-0496-56-R

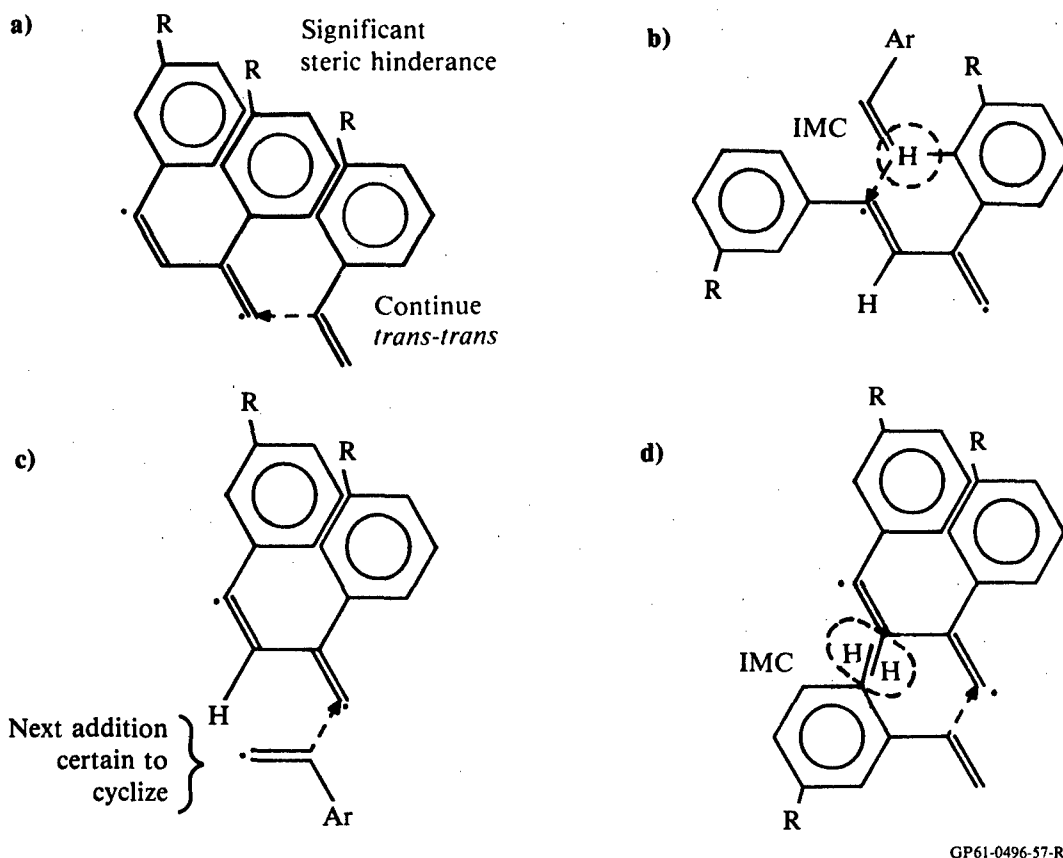
Figure 29. Suggested reaction pathways for *cis-trans* free-radical polymerization of ATS assuming head-to-tail addition throughout. *Cis-trans* polymerization can avoid intramolecular cyclization (IMC) only if the aromatic rings rotate considerably out of the diene plane. Since para-substituted ATS may contain an $\sim 40\text{kJ mol}^{-1}$ barrier to this rotation, termination may occur with each para-ATS (comprising $\sim 5\%$ of the original monomer mix) addition.

solid squares, circles, and diamonds are the estimated f'_{acet} from ^1H spin-spin relaxation data fitted with the 2+1 assumption (results shown in Figure 18) obtained at 453, 423 and 403 K (356, 306, and 266°F) cure temperatures, respectively.

f'_{acet} is estimated from the ^1H spin-spin relaxation data in the following way. First we assume that f_m in Figure 18 represents all the monomer in the system at any time during the early cure. Each monomer that disappears represents the consumption of one acetylene group (of the two on any monomer). During the early cure, this observed reaction of monomer constitutes the major decrease in acetylene moiety. From these assumptions, we estimate

$$\begin{aligned}
 f'_{\text{acet}} &\cong 1 - 0.5(1-f_m) = 0.5 + 0.5f_m \\
 &\cong 0.5 + 0.5\exp[-k_p(\kappa/k_t)^{1/2}t] \quad (19)
 \end{aligned}$$

The exponential dependence arises from the first-order reaction, as discussed in reference to Equation (11). During the early cure, Equation (19) should be



GP61-0496-57-R

Figure 30. Suggested reaction pathways for *trans-trans* free-radical polymerization of ATS assuming head-to-tail addition throughout. (a) *trans-trans* polymerization is seen to be sterically unfavored; the aromatic rings must necessarily rotate 90° out of the diene plane. (b) and (d) are additions resulting in *cis-trans* moieties, and will produce IMC unless significant rotation of the aromatic rings away from the diene plane occurs. (c) shows a route which is neither *cis-trans* nor *trans-trans*; this route will almost certainly cyclize, however, with the next addition.

fairly accurate. To check how far into the cure this is true, we make the assumption that any increase in f_r decreases f_{acet} exponentially in time as

$$(f_{acet})_{monomer} [1 - \exp(-k_c t)]$$

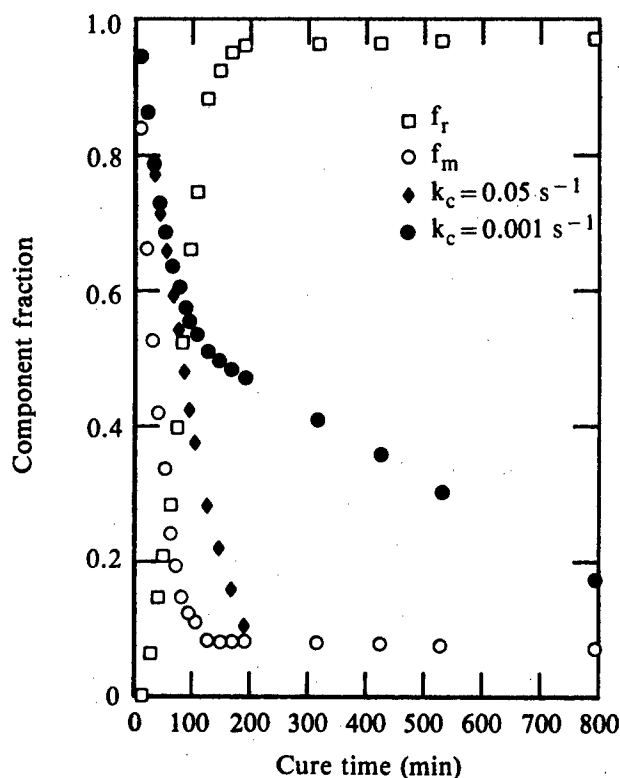
where k_c is a new reaction constant, according to the rate of crosslinking late in the cure, and $(f_{acet})_{monomer}$ is the fractional intensity of acetylene from monomer species. This assumption provides an approximation of

$$f_{acet} \approx [0.5 + 0.5f_m][1 - f_r]$$

$$= \{0.5 + 0.5 \exp[-k_p (\kappa/k_t)^{1/2} t]\} \exp(-k_c t) \quad (20)$$

The assumptions which are most serious in Equation (20) are that k_c and k_t are constants; in reality, they change with cure time. A reasonable approach to adjusting for changing k_c and k_t is to define a transition in the two rate constants at the gel point; i.e., define one set of constants before the gel point, and another set, k_c larger and k_t smaller, after the gel point. We shall not proceed along this line of reasoning. Figure 31 shows the results of Equation (20) for $k_c \sim 0.05 \text{ s}^{-1}$ (solid diamonds) and $k_c \sim 0.001 \text{ s}^{-1}$ (solid circles). From these results, we can see that Equation (19) is a good approximation when $f_{\text{acet}} \geq 0.55$; the rate of crosslinking does not significantly affect the calculation in this region. Equation (19), then, was used to generate the f_{acet} values, shown in Figure 26, calculated by use of the ^1H spin-spin relaxation data.

The ^1H and ^{13}C data in Figure 26 agree quite well with the 453 K (356°F) curing data. The solid triangles represent f_{acet} calculated by summing f_{vm} and f_{m} in Figure 21 together, and using the sum in Equation (19). Again, the agreement is well within the experimental error. As stated previously, this clearly displays the relative unimportance of the 2+1 and 3+1 assumptions for



GP61-0496-36-R

Figure 31. Acetylene consumption in ATS cured isothermally at 423 K (306°F) predicted from ^1H spin-spin relaxation data.

interpretation of the ^1H spin-spin relaxation data for information on the degree of cure.

The agreement between the ^1H and ^{13}C data begins to suffer in the 423 K (306°F) curing runs. The two sets of data are, however, within the error of the experiment because of the uncertainty of the temperature, ± 2 degrees. A horizontal error bar is drawn in Figure 26 to display the uncertainty. The 403 K (266°F) data, on the other hand, suggest that something other than experimental uncertainty is causing the differences between the ^1H and ^{13}C data for this cure temperature. In this case, the data are separated much more than the experimental error would allow. One possibility for the difference is the in situ versus room-temperature methods by which the ^1H and ^{13}C spectra were obtained, respectively. This difference should affect all the data, however, not just the 403 K (266°F) cure. Because of the large scatter in the ^{13}C data, the open triangles were obtained by dividing the data represented by the open diamonds (the original data) by the estimated largest random error possible in the data, 0.82, thus proving that the deviation in the ^1H and ^{13}C data is not the result of random errors in the analysis of the data. There is no special reason, however, for assuming first-order kinetics throughout the cure, as the fitted lines imply; as we shall show, systems such as ATS behave differently.

Since the ^1H and ^{13}C provide useful information in different cure regimes, i.e., in the early and later cures, respectively, non-first-order kinetics may yet allow that both sets of data are accurate. Final confirmation that the ^{13}C results for a cure temperature of 403K (266°F) are in error comes when these results are compared to differential scanning calorimetry (DSC) and Fourier transform infrared (FT-IR) results. This discussion is deferred to Section IV.

The proton-deuterium chemical exchange reaction between ATS and deuterated ethanol (EtOD) was examined by liquid ^1H NMR. This measurement was performed to determine if deuterated samples could be made for FT-IR studies. To an $\approx 10\%$ solution of ATS in toluene was added $\approx 20\%$ EtOD, and the NMR spectrum was recorded. At this point no significant exchange had taken place, as indicated by the fact that the terminal-acetylene proton resonance remained in the spectrum. We then added ≤ 5 mg of Na metal to the solution, which was subsequently re-examined. At this point, the near absence of the resonance line of the terminal acetylene protons verified that exchange had taken place.

Thus, a slightly alkaline environment catalyzed the exchange reaction. A preparative scale exchange reaction was not conducted due to limited time.

3. EPR Results

a. EPR Isothermal Cure Studies

Baseline data were collected on the uncured AT resins. It was determined that some radicals were present in the uncured resins and that the concentrations were about 1% of those obtained after ~90% cure. The signal observed from the uncured ATS resin was similar to that observed after curing, but had some subtle differences in line shape and linewidth. When the ATS resin was dissolved in toluene, a single EPR line having a width of ~ 1.0 mT was obtained. No resolvable hyperfine components could be distinguished; however, the presence of unresolved hyperfine components could be inferred from the overall broadness of the spectral line. It is likely that the radicals observed both before and after curing the ATS are delocalized into a conjugated double-bond system; this can explain the radical stability and the unresolved spectrum.

The m-ATB resin was not successfully monitored by EPR in toluene solution; however, data were obtained at low viscosity by monitoring of the EPR signals while the samples were at the cure temperature. Samples of m-ATB and PPPA were cured at 413-423 K (284°-302°F) and monitored at the cure temperature by EPR.

Both samples produced similar spectra, as shown in Figure 32. Instead of the single, broad (1.0-1.5 mT peak-to-peak) resonance line typically observed at room temperature, the spectra observed at 413 K (284°F) show partially resolved hyperfine structure. Thus, eight resonance lines separated by 0.15 mT are clearly seen. The enhanced resolution at 413 K (284°F) is apparently the result of thermally activated motional averaging of the anisotropic magnetic interactions that would otherwise broaden the spectral lines.

The observed first-derivative EPR spectrum for PPPA in Figure 32 is qualitatively similar to what would be a less-resolved version of the spectrum reported by Whitte et al.²⁵ for polyphenylacetylene. Thus, some of the free radical species suggested by these authors may be relevant to our m-ATB and PPPA studies.

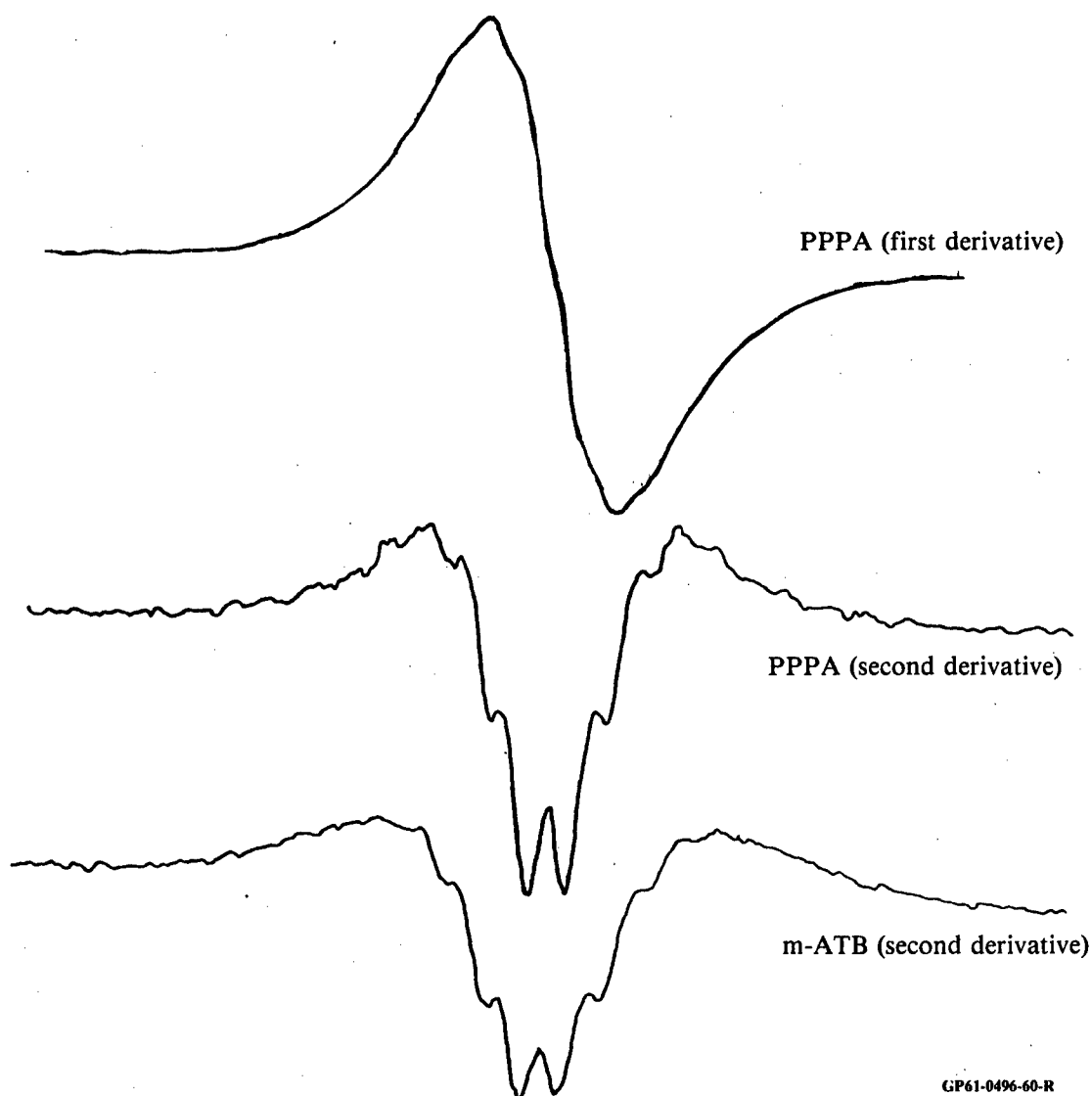


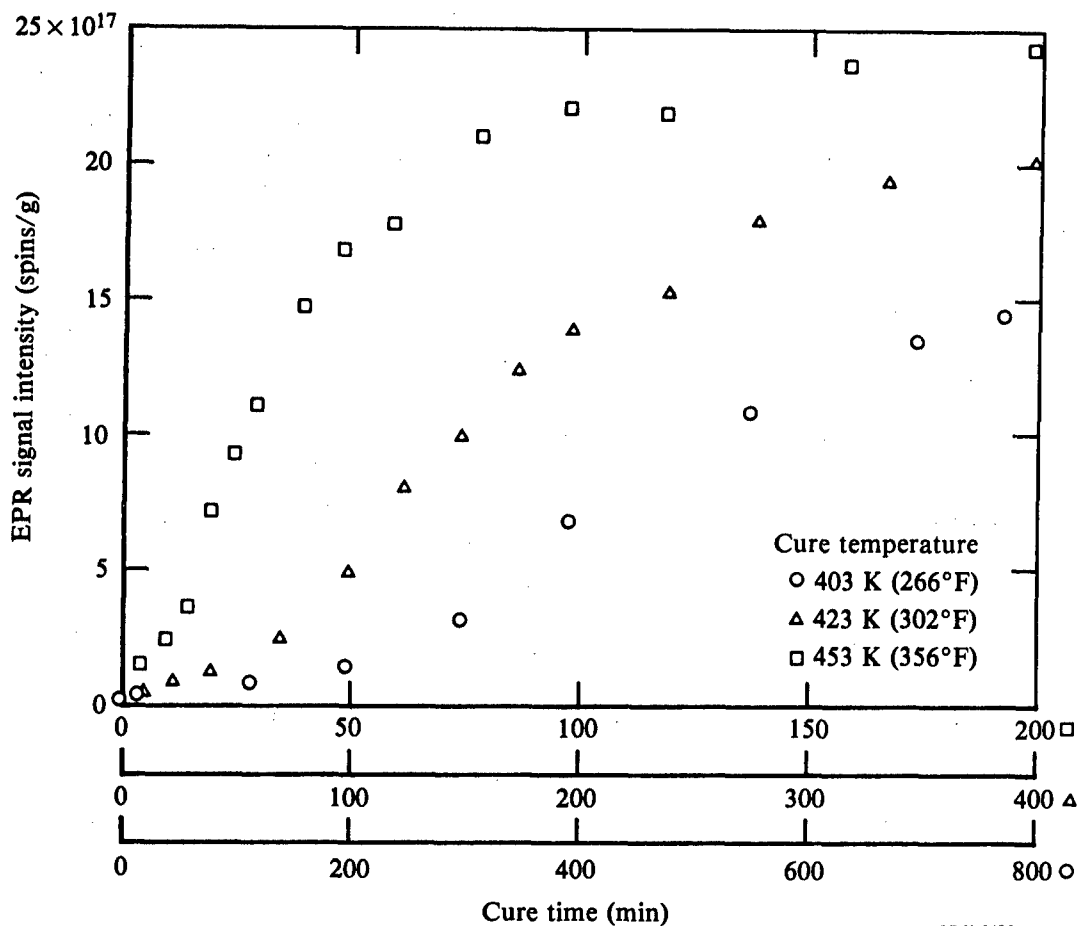
Figure 32. First- and second-derivative spectra of partially cured PPPA and m-ATB. Electron-nuclear hyperfine structure is partially resolved.

The behavior of the m-ATB and PPPA samples was similar in that upon heating at 413-423 K (284°-302°F) for ≈ 10 h, both samples lost their resolved spectral structure. This change may have been due to decreasing mobility as curing progressed. On the other hand, these samples behaved differently from each other in that m-ATB showed significant net radical production following a ≈ 400 min induction period, whereas PPPA showed an induction period only, which lasted longer than 800 min.

A sample of m-ATB was cured at 413 K (248°F) for ≈2 h, and was then examined by use of electron-nuclear double resonance (ENDOR) in the hope that resolved ENDOR spectra could help determine the structure of the radical observed during curing of ATS and m-ATB. Although the sample had shown partially resolved hyperfine splitting in the normal electron paramagnetic resonance (EPR) spectrum (Figure 32), no resolved spectral lines were found with ENDOR.

Following the baseline and qualitative line shape measurements discussed above, we collected EPR spectra from the AT resins at selected times during isothermal curing. A typical spectrum consisted of a single EPR line having a near-Gaussian shape and a width of about 1.0 to 1.5 mT. The growth in the signal intensity occurred on the same or slightly longer time scale as that of the curing process, as determined by changes in NMR and FT-IR spectra, sample viscosity, and DSC measurements. Thus, production of radicals is assumed to be associated with the curing process.

In the earlier portion of this study,³ EPR spectra were obtained from ATS samples at room temperature after they had been cured at three different elevated temperatures for selected times. The free-radical concentrations were determined and plotted as a function of cure time. These plots are shown in Figures 33 and 34. There are three distinct regions of interest in these curves. First, at early stages of cure, there is an induction period during which net radical production is low. Second, there is a region in which radical concentration increases linearly with $\log(t)$, where t is the cure time. Finally, after the curve maxima is a third region in which the radical concentration decreases with time. Samples cured at the highest temperature produced radicals at the highest rate, but had the smallest concentration of free radicals at the maximum. Conversely, samples cured at the lowest temperature produced radicals at the lowest rate but had the largest concentrations of free radicals at the maximum. The fact that samples cured at different temperatures have different radical concentrations at comparable degrees of cure (as determined by FT-IR, DSC or ^{13}C NMR) makes EPR signal intensity an independent parameter for determining the cure state of a given sample. Relevant EPR cure parameters for isothermally cured ATS are listed in Table 4.

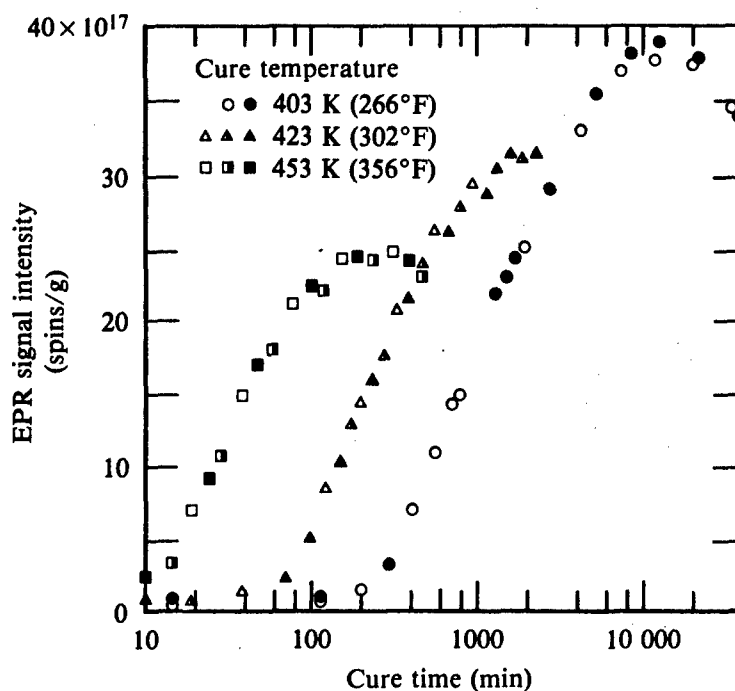


GP61-0496-40-R

Figure 33. EPR signal intensities for ATS as a function of cure time at early stages of cure. The presence of an induction period at short cure times indicates inhibited net radical production.

The reaction kinetics for EPR data from ATS samples cured isothermally at 403 K (266°F) and at 453 K (356°F) have been analyzed in terms of successive first-order reactions. The model employed is not necessarily unique, and it does not include the effects of viscosity; however, it is simple and produces curves that fit the data fairly well.

In this model it is assumed that ATS (species A) reacts to form a non-paramagnetic intermediate (species B) which then reacts to form the free radical (species R•). For example, the ¹H NMR spin-spin relaxation data presented in the previous section suggest that species B could be a non-crosslinked polymer, which could be formed by free-radical polymerization and then be rapidly terminated to become diamagnetic. Radical R• could then be produced during crosslinking and be protected by the resulting immobile network.



GP61-0496-72-R

Figure 34. EPR signal intensities in ATS as a function of cure time.

TABLE 4. EPR CURING PARAMETERS FOR ATS.

Cure temperature [K (F°)]	Peak radical concentration $\times 10^{-17}$ (spins/g)	Cure time at peak radical concentration (min)
403 (266)	38	12,000
423 (302)	32	1,700
453 (356)	25	240

Finally, the radical ($R\cdot$) gradually decomposes to another nonparamagnetic species (species C). This sequence is expressed by the following equations:



where k_1 , k_2 , and k_3 are the rate constants and all reactions are first order.

Equation (21a) is introduced to explain the initial induction period observed in the EPR data. $R\cdot$ does not significantly increase until enough time has elapsed for the concentration of its precursor, species B, to build up. Equation (21b) describes the production of radical $R\cdot$ after the induction period, and Equation (21c) describes the gradual decay in radical concentration observed at long times.

Integration of the first-order differential equations corresponding to Equations (21) yields the following equation, identical in form to Equation (15), for the concentration of radical as a function of time, t :

$$[R\cdot] = A_0 k_1 k_2 \left(\frac{\exp(-k_1 t)}{(k_3 - k_1)(k_2 - k_1)} - \frac{\exp(-k_2 t)}{(k_3 - k_2)(k_2 - k_1)} + \frac{\exp(-k_3 t)}{(k_3 - k_2)(k_3 - k_1)} \right) \quad (22)$$

At the limit $k_1 \gg k_2$, and $k_2 \gg k_3 \approx 0$, this expression reduces to a simple exponential growth in radical concentration as expected:

$$[R\cdot] = A_0 [1 - \exp(-k_2 t)] \quad (23)$$

where A_0 is the value of $[R\cdot]$ at long times.

The 403 K (266°F) and 453 K (356°F) curing data were analyzed by use of a nonlinear least-squares routine to fit Equation (22) to the experimental data. The values for parameters A_0 , k_1 , k_2 , and k_3 were obtained and are shown in Table 5. The 423 K (302°F) data could not be analyzed by this fitting procedure because no data points were collected after the maximum radical concentration was reached. However, approximate values of A_0 and k_2 were obtained by comparison of the 423 K data with the data taken at 403 K and 453 K. These results are included in Table 5.

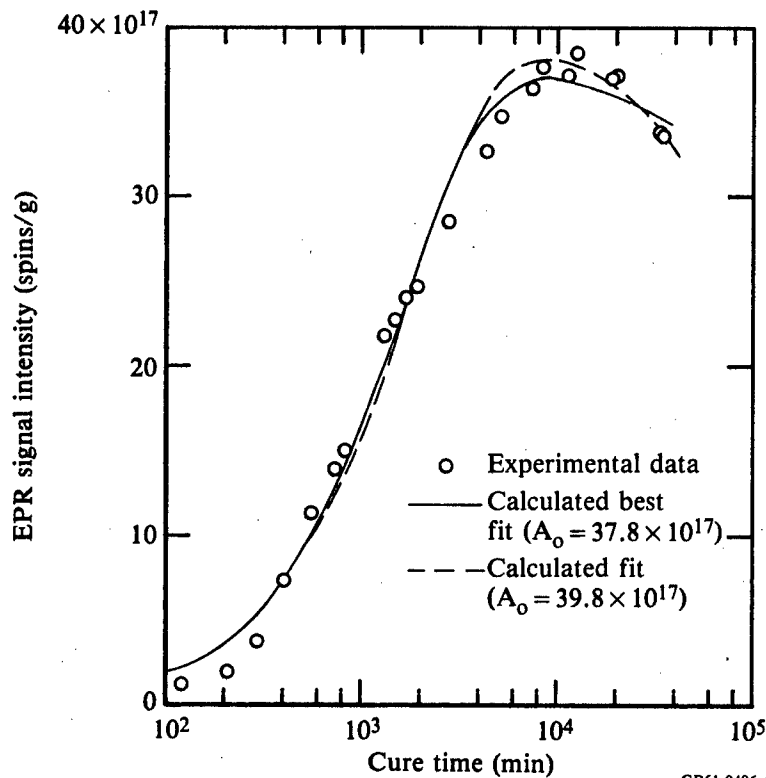
The curves calculated for the 403 K (266°F) and 453 K (356°F) data are shown as solid lines in Figures 35 and 36. The fits are generally good, although at long times (i.e., where the radical concentration is decaying), the fits are poorer because the calculated values of k_3 are so small. By forcing the values of A_0 to be 39.8 and 25.2×10^{17} for the 403 K (266°F) and 453 K (356°F) data, respectively, we obtained values of k_3 that resulted in a better fit of the theoretical curve to the experimental data at long times; however, the quality of the overall fit was somewhat reduced. These new values of the

TABLE 5. PARAMETERS DETERMINED FROM LEAST-SQUARES FIT OF EPR DATA.

Cure temperature	403 K (266°F)	423 K (302°F)	453 K (356°F)
A_0 (spins/g):	37.8×10^{17}	32×10^{17} *	23.7×10^{17}
k_1 (s^{-1}):	2.3×10^{-4}	—	1.8×10^{-3}
k_2 (s^{-1}):	1.0×10^{-5}	6.1×10^{-5} *	4.8×10^{-4}
k_3 (s^{-1}):	4.4×10^{-8}	—	1.2×10^{-6}

*These parameters are estimates, not from least squares analysis.

GP61-0496-5-R



GP61-0496-42-R

Figure 35. Fits of Equation 22 to ATS curing data collected by EPR. Curing temperature is 403 K (266°F).

calculated parameters are shown in Table 6. Plots of the theoretical curves made with these parameters are shown as dashed curves in Figures 35 and 36.

One additional fit of Equation (22) to the 453 K (356°F) data was made. In this case a large value of A_0 (32.8×10^{17}) was used to test the hypothesis

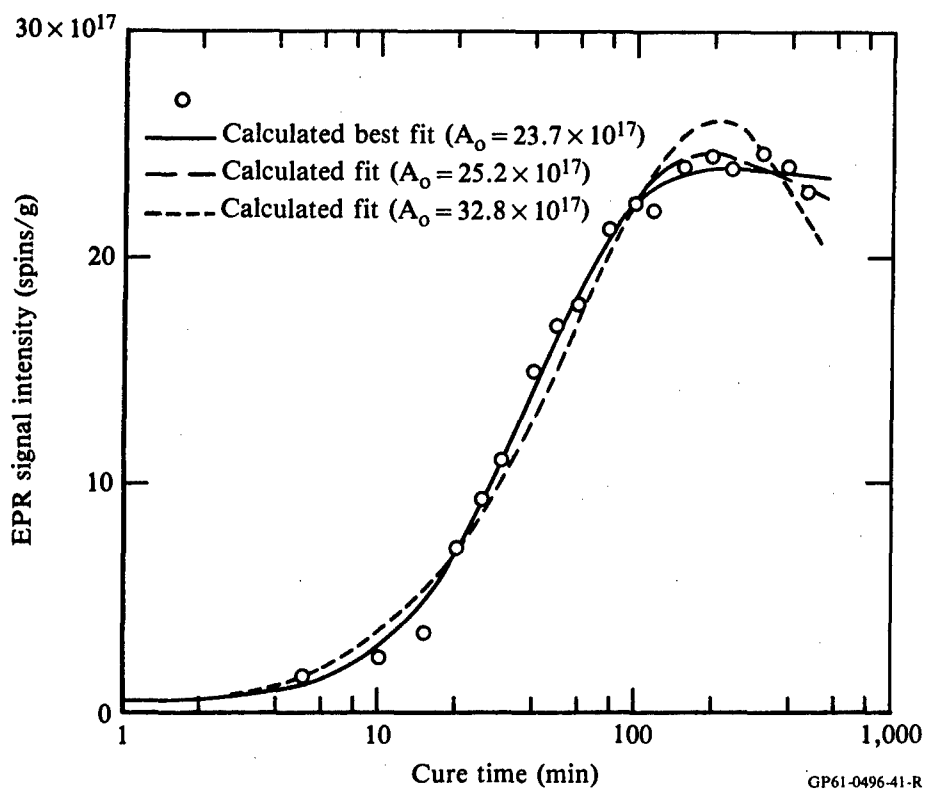


Figure 36. Fits of Equation 22 to ATS curing data collected by EPR. Curing temperature is 453 K (356°F).

TABLE 6. PARAMETERS DETERMINED FROM FORCED LEAST-SQUARES FIT OF EPR DATA.

Cure temperature	403 K (266°F)	453 K (356°F)
A_0 (spins/g) ^a :	39.8×10^{17}	25.2×10^{17}
k_1 (s ⁻¹):	3.5×10^{-4}	2.3×10^{-3}
k_2 (s ⁻¹):	8.9×10^{-6}	4.0×10^{-4}
k_3 (s ⁻¹):	8.2×10^{-8}	4.5×10^{-6}

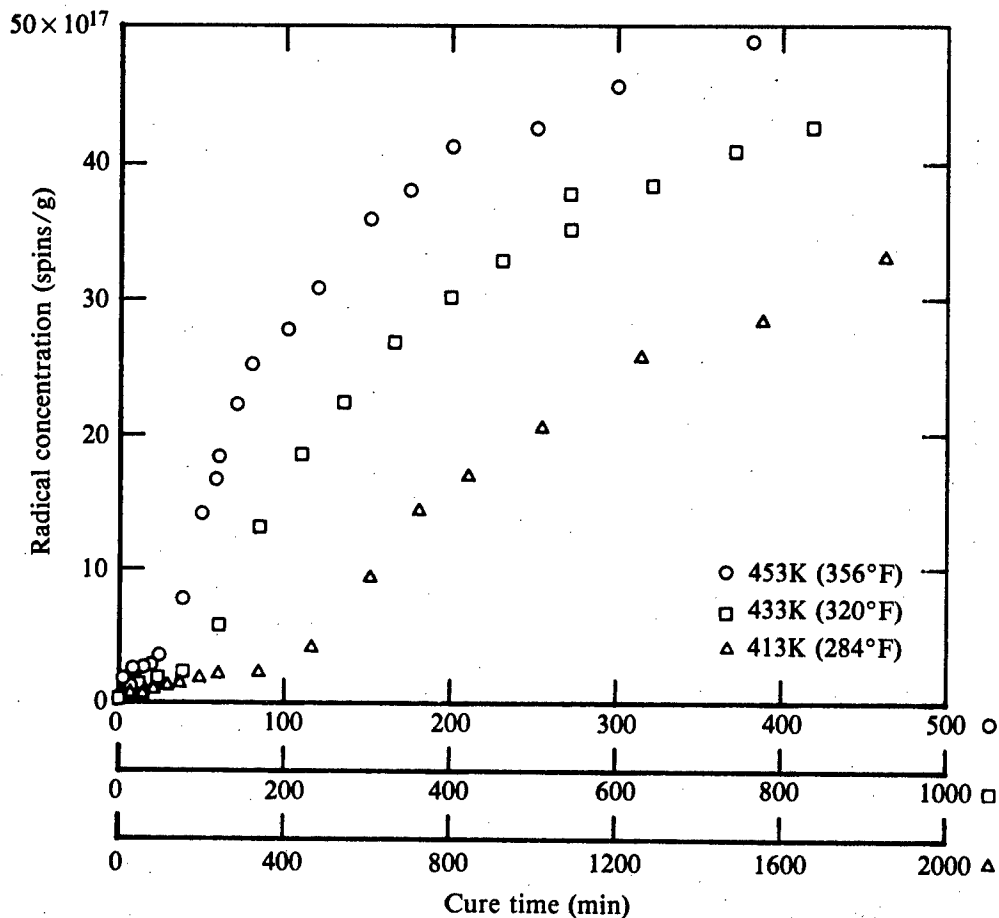
^aNot calculated, but forced to equal this value.

GP61-0496-6-R

that the A_0 values for the 403 K (266°F) and 453 K (356°F) data should be nearly equal. (Equal A_0 values might indicate that equal numbers of radicals were produced at both reaction temperatures.) The dotted line in Figure 36 results from this calculation. The fit obtained with $A_0 = 32.8 \times 10^{17}$ is clearly much poorer than the fits obtained with A_0 in the range of $23\text{--}25 \times 10^{17}$.

Thus, the samples cured at different temperatures have different A_0 values, which could indicate that 1) the radicals observed by EPR are the net result of radical generation reactions and radical decay reactions that occur together during ATS curing, or 2) the radicals produce polymer chains of different lengths at different temperatures.

The EPR techniques developed for isothermal studies of ATS were applied to m-ATB. The m-ATB samples were isothermally cured in a nitrogen atmosphere at three different temperatures, 413 K (284°F), 433 K (320°F), and 453 K (356°F). The EPR intensity-vs-time results are shown in Figures 37 and 38. The radical concentration values at the curve maxima were originally inconsistent with the results for ATS shown in Figure 34. For ATS, the intensity at the maximum increased with decreasing cure temperature, but for the original m-ATB data, the maximum intensity for the 413 K (284°F) cure was less than the maximum for the 433 K (320°F) cure.



GP61-0496-59-R

Figure 37. Free radical concentration as a function of cure time for m-ATB.

Cure temperature K (°F)	Original data	New data
413 (284)	△	▲
433 (320)	○	●
453 (356)	□	■

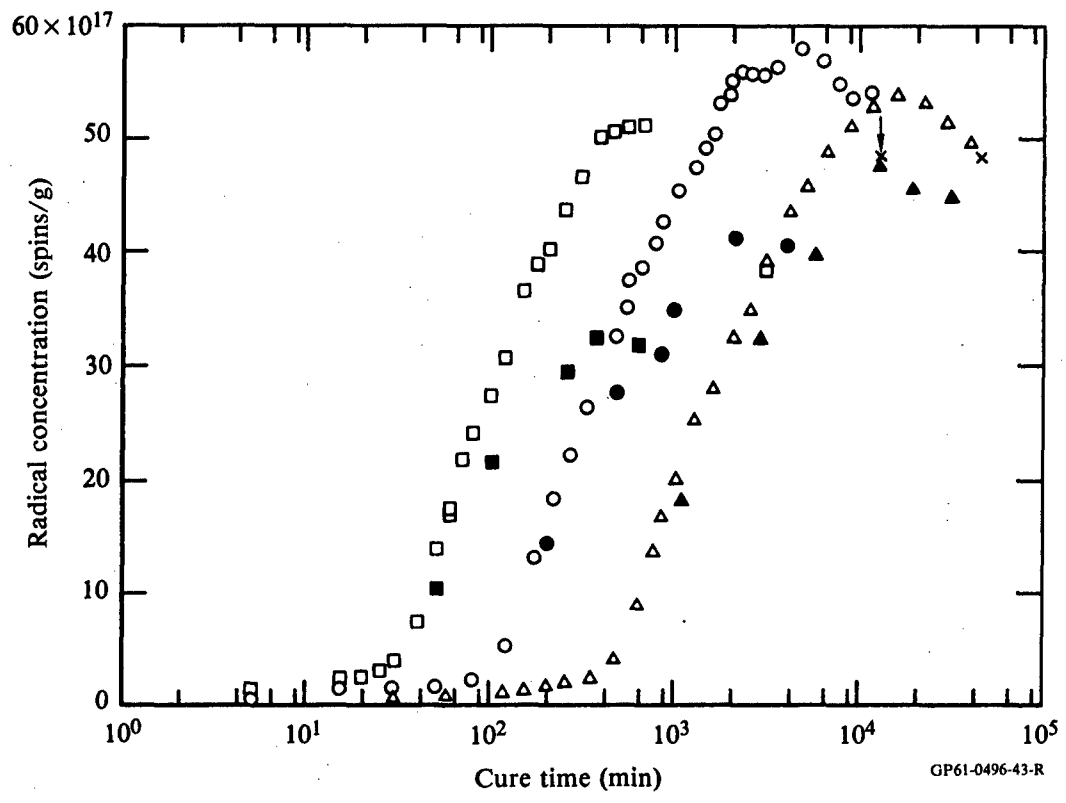


Figure 38. EPR signal intensity for m-ATB as a function of cure time. Points (x) correspond to postcuring of 413 K and 433 K samples at 453 K.

Because of this unexpected result, new m-ATB samples were prepared and the curing experiments were repeated for each cure temperature with only 5-6 data points being collected at each temperature. These new results, shown in Figure 38, are consistent with the ATS results. In addition, the signal intensities are significantly lower than those observed in the first m-ATB curing studies. Repetition of the intensity-vs-time experiment for another new sample at 453 K (356°F) indicated that the more recent set of m-ATB curing data was correct and that the original set was anomalous.

A possible explanation for these results is that oxygen was not completely eliminated from the original set of m-ATB samples because, following degassing, the samples were backfilled with nitrogen gas from a central

supply that may have been contaminated. The more recent set of samples was backfilled with nitrogen gas from a local cylinder so that curing occurred in an oxygen-free atmosphere. Maximum signal intensities and corresponding cure times for the ATB samples are listed in Table 7.

The EPR results for m-ATB are similar to those for ATS. Thus, an initial induction period during which the rate of net radical production was low was observed for the m-ATB, as shown in Figure 37. Following this, the m-ATB produced radicals approximately linearly with respect to $\log(t)$, where t is cure time (Figure 38). Eventually, a maximum radical concentration was reached, after which the concentration gradually decreased with time. Although the curves are qualitatively similar to those for ATS, the reaction times for the m-ATB at a given temperature were generally slightly longer. No significance is attached to this observation at present.

In order to examine AT curing in a non-crosslinking resin, we examined phenoxyphenoxyphenylacetylene (PPPA) received from AFWAL/ML. The EPR intensity and line shape of PPPA were monitored as a function of cure time at 413-423 K (284°-302°F). The total cure time accumulated by the sample was 797 min. It was anticipated that, consistent with the above m-ATB data, an induction period of about 400 min might be observed, and that this would be followed by a linear increase in radical concentration with $\log(t)$; however, this was not observed. Instead, the radical concentration remained low over the entire 797 min of curing, indicating either that the induction period was longer or that no period of increased radical production would follow at all. The latter possibility makes sense if a network structure were required for net radical production to be significant. Unlike the m-ATB samples, the PPPA is not expected to form a significant network structure upon curing because of the mono-acetylene functionality of the monomer. The PPPA results thus suggest that the increase of radicals in ATS and m-ATB following the initial in-

TABLE 7. EPR CURING PARAMETERS FOR m-ATB.

Cure temperature [K (°F)]	Peak radical concentration $\times 10^{-17}$ (spins/g)	Cure time at peak radical concentration (min)
413 (284)	47	16 000
433 (320)	42	2 800
453 (356)	32	500

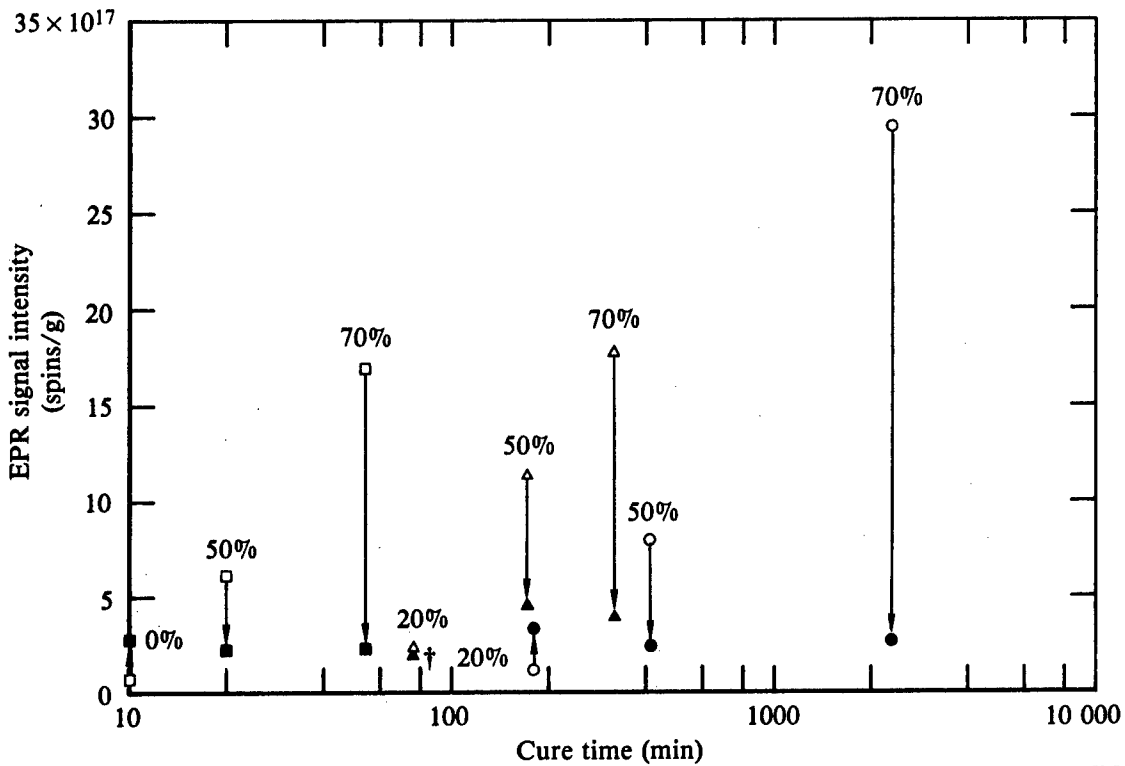
GP61-0496-7-R

duction period is associated with crosslinking at the later stages of curing. This increase will be addressed more fully in Section IV of this report.

b. EPR Postcure Studies

EPR studies of ATS samples postcured at 573 K (572°F) for 2 h were performed. Spectral intensities were recorded both before and after postcuring. The results for these samples and the samples previously postcured³ at 523 K (482°F) and 543 K (518°F) are shown in Figures 39-41.

Cure temperature [K (°F)]	Before postcure	After postcure
403 (266)	○	●
423 (302)	△	▲
453 (356)	□	■



GP61-0496-73-R

Figure 39. Radical concentrations of cured ATS samples before and after postcuring at 523 K (482°F). Cure temperatures and percents of cure (as determined by IR) are as indicated. The samples cured to 50% or above lose intensity upon postcuring. The uncured sample (0%) should have a higher value for radical concentration following postcure; however, it could be determined because much of the sample was outside the EPR cavity. (The † sample broke open during postcuring.)

Prior to postcuring, the EPR spectral intensities were consistent with the data obtained during isothermal curing studies, i.e., the data fell on or near the curves shown in Figures 33 and 34. The spectral intensities of samples cured to > 50% of full cure decreased in intensity upon postcuring to a spin concentration value of $\sim 5 \times 10^{17}$ spins/g. In contrast to this, EPR signals from the samples cured to < 20% of full cure generally increased in intensity following postcuring; moreover, the samples having the lowest radical concentration prior to postcuring generally had the greatest radical concentration following postcuring (6×10^{17} spins/g).

It appears, therefore, that there is a complicated process involving competition between radical production and destruction at the postcure tempera-

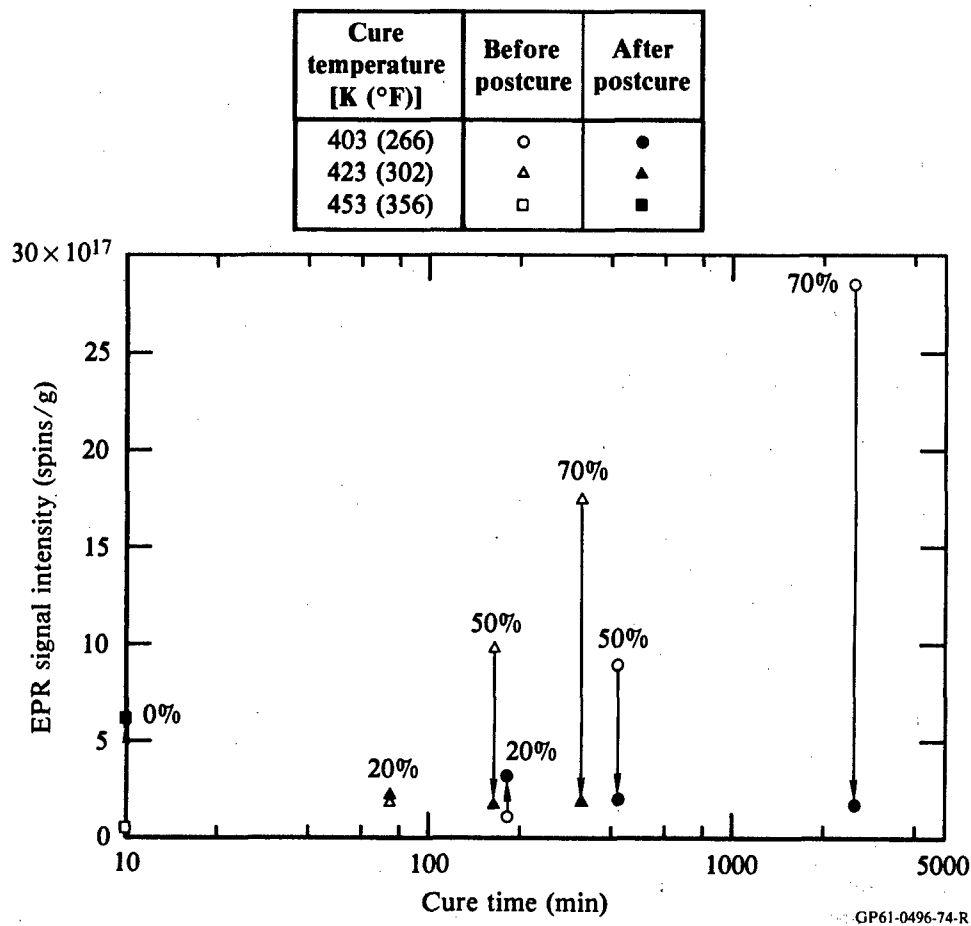
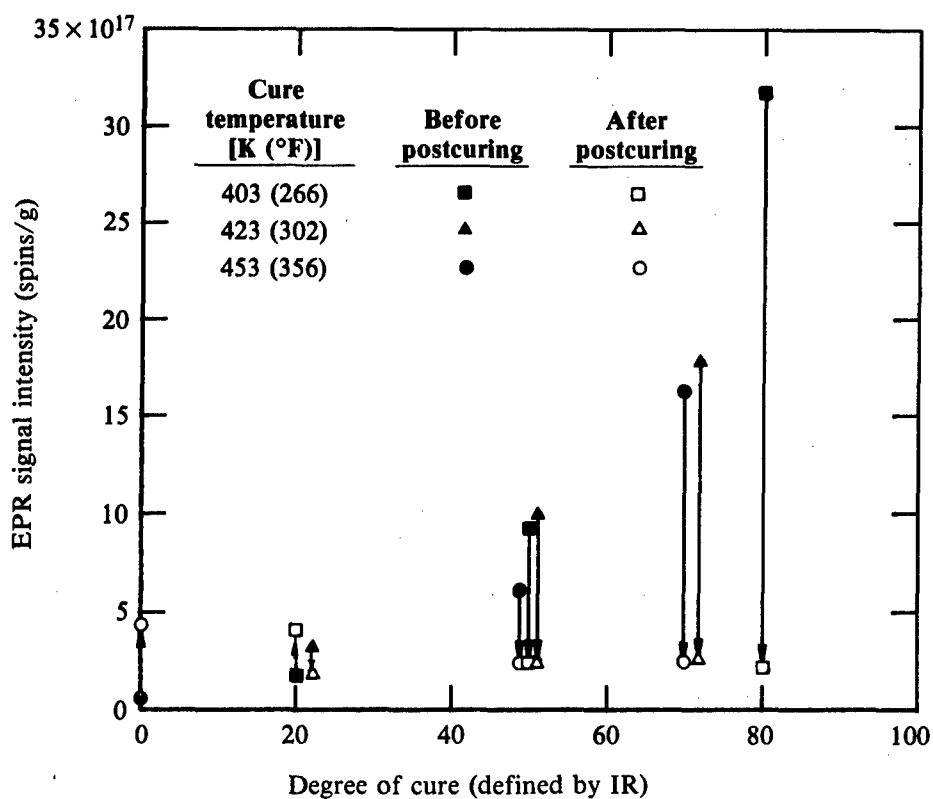


Figure 40. Radical concentrations of cured ATS samples before and after postcuring at 543 K (518°F). Cure temperatures and percents of cure (as determined by IR) are as indicated. The samples cured to 50% or above lose intensity upon postcuring, whereas the samples cured to 20% or below gain intensity. In particular, the uncured sample (0%) showed a significant increase in intensity (to over $\sim 6 \times 10^{17}$ spins/g) upon postcuring.



GP61-0496-45-R

Figure 41. EPR signal intensity, both before and after postcuring at 573 K (572°F), as a function of degree of cure.

tures, and that the number of radicals remaining in a sample following postcuring may depend on the extent of network development prior to postcuring.

The EPR linewidths of all samples decreased as a result of the postcuring process, and some samples produced spectra that appeared to be superpositions of two separate component spectra having different linewidths (see Figure 42). Thus, for example, the linewidths of samples that had attained at least 50% cure at 403 K (266°F) or 453 K (356°F) were typically 1.2-1.4 mT prior to postcuring and about 1 mT following postcuring at 523 K (482°F). An uncured sample subjected to postcuring at 523 K (482°F) produced an EPR spectrum having a linewidth of 0.69 mT, down from the initial 1.05 mT linewidth, and a sample cured 20% at 403 K (266°F) changed in linewidth from 1.16 mT to 0.81 mT upon postcuring at 523 K (482°F). The latter spectrum appears to be a superposition of two separate component spectra, one having a linewidth on the order of 0.7 mT and the other on the order of 1.0-1.2 mT.

Therefore, some of the postcured samples produced both the broad spectrum that is normally observed upon postcuring, and an additional narrow line. Two

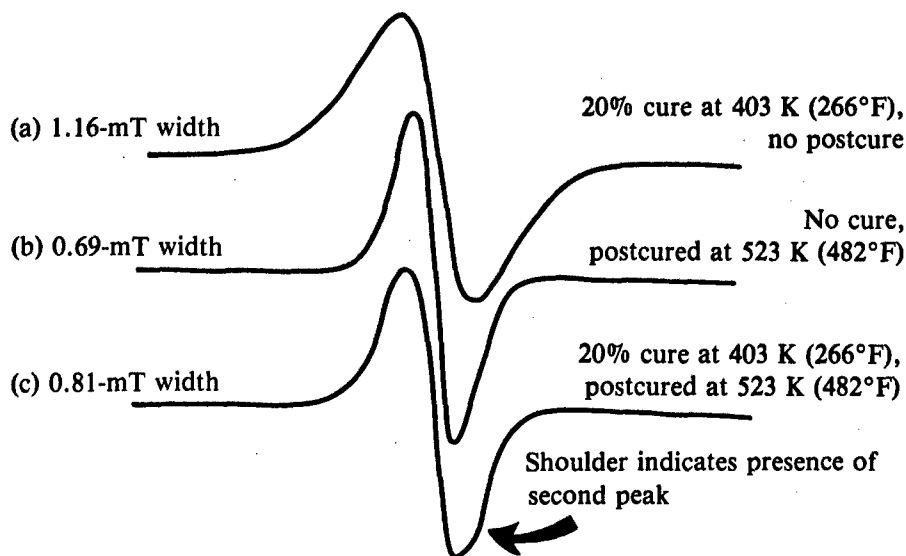


Figure 42. EPR spectra observed during curing/postcuring of selected ATS samples. Uncured and unpostcured samples have a background signal with a linewidth of ~ 1.05 -mT. Curing causes the linewidth to increase with increasing radical concentration: (a) 20% cure at 403 K (266°F) produces a 1.16-mT line, (b) high-temperature curing (523 K, 482°F) produces a much narrower line (~ 0.69 -mT), and (c) spectra from samples cured to $\sim 20\%$ at low temperature and subsequently postcured at high temperatures show the presence of two superimposed spectral components of different linewidth.

types of radical species thus seem to be present in some postcured samples. The above results imply that those radicals producing the broad line in the postcured spectrum could be a remnant of the radicals originally present subsequent to curing but prior to postcuring. On the other hand, those radicals producing the narrow line in the postcured spectrum may be newly generated by the postcuring process. The anomalous narrow line 0.7 mT (~ 7 G) cannot be explained exclusively in terms of reduced electron-electron dipolar interactions resulting from reduced overall radical concentrations in the samples in question; ATS samples having even lower radical concentrations can produce EPR spectra with linewidths of over 1 mT. Possible sources of differences among linewidths in samples having the same radical concentration include radical clustering, differences in electron delocalization, and/or the number of magnetic nuclei encountered by electrons for a given delocalization.

m-ATB samples that had been cured at 433 K (320°F) for 11,500 min or at 413 K (284°F) for 40,000 min were examined by EPR before and after additional curing at 453 K (356°F) for 261 and 120 min, respectively. Table 8 shows EPR intensity data for the two samples. The 433 K sample showed a small ($\approx 10\%$)

**TABLE 8. EFFECTS OF POSTCURING m-ATB SAMPLES
AT 453 K (356°F).**

Sample cure temperature [K (°F)]	Cure time (min)	Postcure time (min)	EPR intensity $\times 10^{-17}$ (spins/g)	
			Prior to postcure	Following postcure
413 (284)	40 000	120	49	48
433 (320)	11 500	261	53	48

GP61-0496-8-R

decrease in signal intensity and the 413 K sample showed an even smaller decrease ($\approx 2\%$).

These results demonstrated that no net production of radicals occurred as a result of this "postcuring" process. It had been expected that added mobility might allow some further curing and net radical production at 453 K. These samples, however, had been cured for times beyond the maximum EPR signal intensity; net radical production might have been observed if the samples had been cured for somewhat shorter times before postcuring.

4. FT-IR Results

IR parameters suitable for characterization of the cure states were derived from three distinctly different sets of spectral changes which were monitored as a function of the degree of cure: (1) changes in band intensities (or band areas) of the acetylene bands, (2) changes in ratios of bands representing various nonreactive moieties, and (3) cure-induced frequency shifts.

a. FT-IR Isothermal Cure Studies

Relevant generalizations for infrared changes observed during polymer curing are as follows:²⁶

- 1) The infrared bands that decrease at the fastest rate are usually attributed to the reactive groups consumed during polymerization. In cross-linked networks derived from polyfunctional monomers, these bands will not go to zero absorbance even in stoichiometrically balanced systems because of incorporation of monomer units in positions which inhibit further reaction. Absorption of low-molecular-

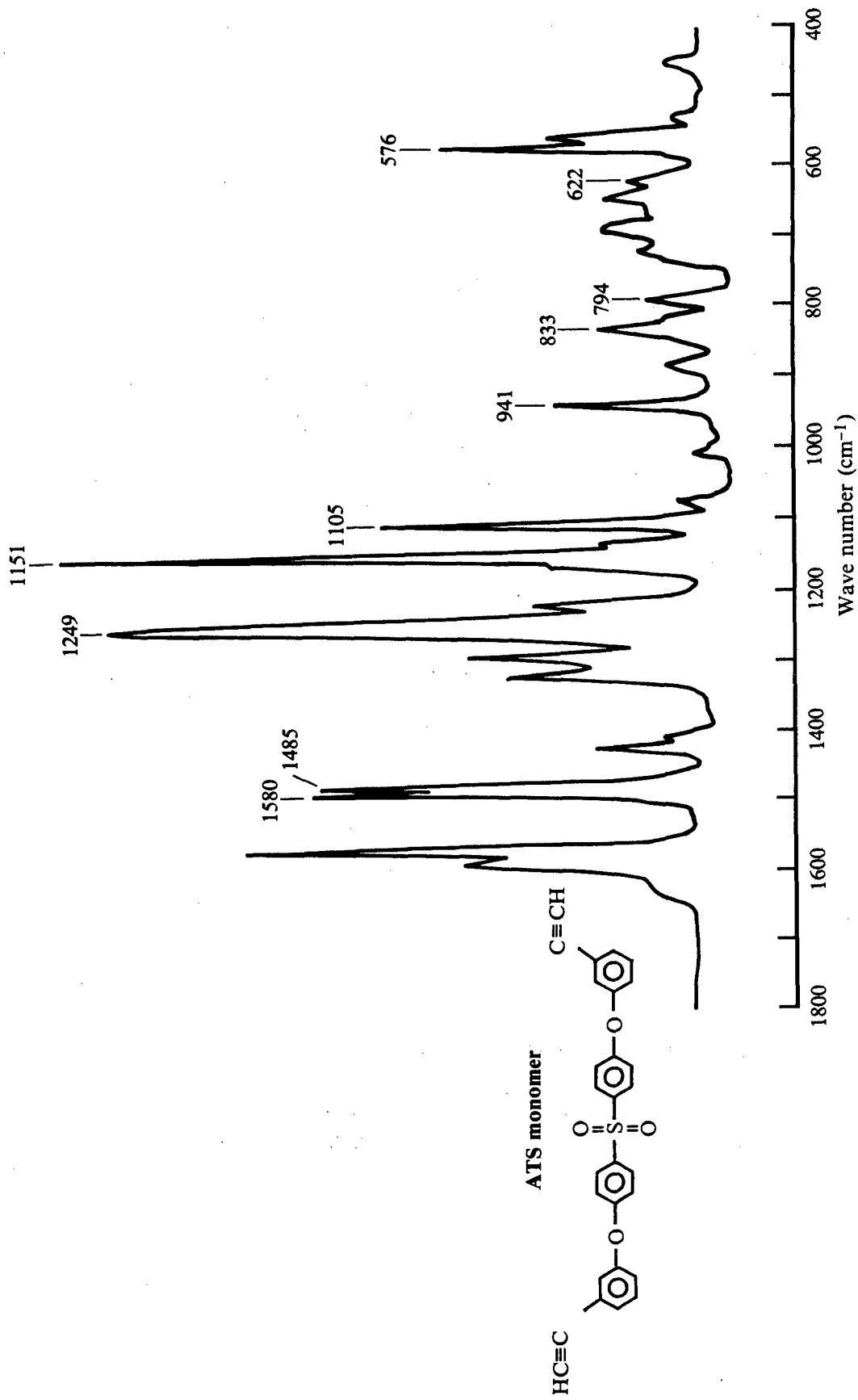
weight solvents or atmospheric moisture plasticize or swell the rigid network, thus permitting further reactions. These reactions embrittle the polymer and can cause internal stresses accompanied by bond rupture when the plasticizing agent is removed by drying. Thus, a spectrum of a sample obtained after elimination of the plasticizing conditions, or after post-curing, may still show that reactive functional groups were reduced while indicating other spectral changes which point to bond rupture.

- 2) Bands that are highly sensitive to the mass of the substituents would be expected to decrease at a faster rate than bands that are reduced by the general broadening that accompanies polymerization.
- 3) Most bands that represent unreactive portions of the molecule not participating in the reaction show broadening and decrease in intensity.
- 4) Bands representing functional groups which enter into intermolecular interactions restricting their normal vibrations change at a rate faster than the bands considered in 3).
- 5) Infrared bands representing the newly formed bonds in the network should, in principle, show an increase at a rate similar to the rate of decrease of bands representing the reactive groups. However, because monomer units are incorporated in different network positions, certain new bonds give rise only to a broad absorption which cannot be defined as a band.

In the earlier portion of this study, FT-IR spectra were obtained on ATS samples at room temperature after they had been isothermally cured at three different elevated temperatures for selected times.³ The main functional groups of ATS and the corresponding FT-IR bands arising from their vibrations are the following (see Figures 43-45):

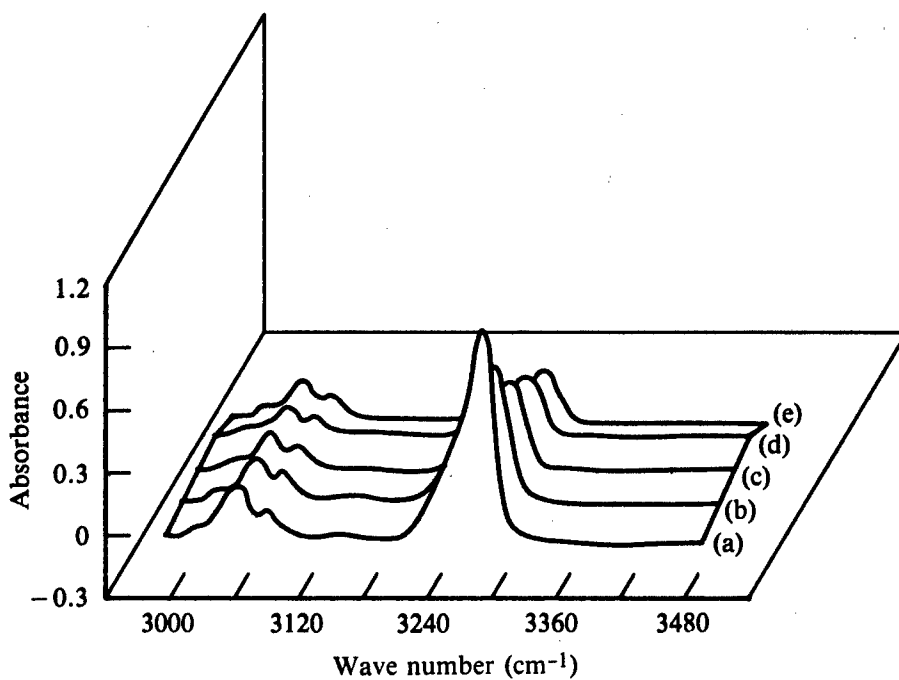
- (1) Acetylene group--622, 941, 2108, and 3295 cm^{-1} .
- (2) Sulfone group--576, 1105, and 1151 cm^{-1} .
- (3) Aryl ether link--1249, cm^{-1} .
- (4) Benzene rings (carbons)--1485 and 1580 cm^{-1}
- (5) Benzene rings (hydrogens)--794, 833, and 3040-3120 cm^{-1}

The two main acetylene bands at 941 and 3295 cm^{-1} can be assigned with confidence to the following vibrations: the 3295 cm^{-1} band to the C-H stretch of the acetylenic H atom, and the 941 cm^{-1} band to the bending of the entire



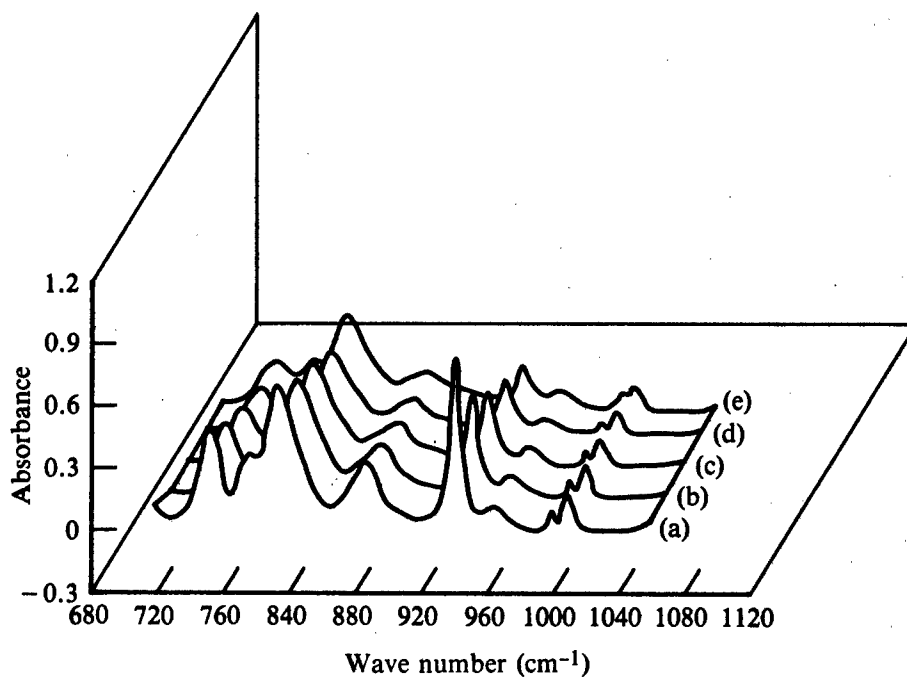
CP61-0496-70-R

Figure 43. FT-IR spectrum of ATS monomer.



GP61-0496-67-R

Figure 44. Superimposed FT-IR spectra of the 3295 cm⁻¹ acetylene-band region of ATS at different stages of cure at 423 K (302°F); (a) 0 min cure, (b) 40 min cure, (c) 70 min cure, (d) 100 min cure, and (e) 150 min cure.



GP61-0496-68-R

Figure 45. Superimposed FT-IR spectra of the 941 cm⁻¹ acetylene-band region of ATS oligomer in different stages of cure at 423 K (302°F); (a) 0 min cure, (b) 40 min cure, (c) 70 min cure, (d) 100 min cure, and (e) 150 min cure.

acetylene group relative to the benzene ring, based on the assignment made by Bloor et al.²⁷

The weak acetylene band at 622 cm⁻¹ can be assigned to bending vibrations of the acetylenic H, whereas the very weak band at 2108 cm⁻¹ originates in the stretch vibrations of the acetylene carbons. Cure-state parameters were derived only from measurement of the changes in the two main acetylene bands, while a very weak band at 2334 cm⁻¹ was used to detect formation of enyne linkages.³

The strong FT-IR band at 1249 cm⁻¹, which can be assigned to the stretch vibration of the aryl ether moiety, was used to study the utility of cure-induced frequency shifts as cure-state parameters. Some of the changes in the bands originating in the vibrations of the benzene ring hydrogens (mainly the aromatic C-H stretch) were used as evidence to support the intramolecular cyclization (IMC) mechanism.¹⁹

Acetylene Band Intensity Changes

The absorbance decreases of the FT-IR bands at 3295 cm⁻¹ and 941 cm⁻¹, which originate in the vibrations of the acetylene group, are the most pronounced spectral changes observed in the early stages of ATS cure, as shown in Figures 44 and 45.

The terminal acetylene groups of the ATS monomer react simultaneously during cure via a number of routes.² Thus, consumption of the terminal acetylene groups, which is directly reflected in the absorbance decreases of the acetylene bands at 3295 cm⁻¹ and 941 cm⁻¹, was used as basis for determining the degree of cure. The two primary methods for calculating DOC from FT-IR absorbances are

- (1) from normalized band areas of the acetylene band at 3295 cm⁻¹ using $R_t = (A_o - A_t)/A_o \times 100$, where R_t is the degree of isothermal cure after curing for a given period (t), A_o is the band-area before curing normalized to the 833 cm⁻¹ band area, and A_t is the band area after curing for the given period similarly normalized to the 833 cm⁻¹ band area, and
- (2) from normalized band areas of the acetylene band at 941 cm⁻¹ plus the same expression for R_t .

The FT-IR-derived DOC values determined for isothermal curing by the two different methods were compared with the DOC values derived by differential scanning calorimetry (DSC);²⁸ the results are given in Tables 9-11.

The two different FT-IR values for DOC are in good agreement. The considerably higher DOC values derived by DSC could possibly be attributed to secondary curing reactions other than those that involved the acetylene groups, i.e., the intramolecular cycloaddition (IMC) reaction¹⁹ (see also the discussion in Section IV).

TABLE 9. COMPARISON OF THE DEGREE OF CURE (DOC) VALUES FOR ATS DERIVED BY DIFFERENT METHODS AT 403 K (266°F).

Cure time (min)	DOC derived by DSC ²⁸ (%)	DOC derived by 3295 cm ⁻¹ band area (%)	DOC from IR 941 cm ⁻¹ band area (%)
0	0	0	0
90	5.5	11.3	13.4
185	17.5	20.4	22.8
420	41.9	48.2	51.0
1300	78.0	62.1	64.9
2680	86.3	68.5	69.8

GP61-0496-9-R

TABLE 10. COMPARISON OF THE DEGREE OF CURE (DOC) VALUES FOR ATS DERIVED BY DIFFERENT METHODS AT 423 K (302°F).

Cure time (min)	DOC derived by DSC ²⁸ (%)	DOC from IR 3295 cm ⁻¹ band area (%)	DOC from IR 942 cm ⁻¹ band area (%)
0	0	0	0
25	6.0	6.7	9.4
51	23.0	11.1	18.9
100	47.0	31.8	35.4
200	70.0	58.0	62.7
508	89.0	70.2	72.6
600	91.0	73.2	74.7
990	93.0	76.8	78.6

GP61-0496-10-R

TABLE 11. COMPARISON OF THE DEGREE OF CURÉ (DOC) VALUES FOR ATS DERIVED BY DIFFERENT METHODS AT 453 K (356°F).

Cure time (min)	DOC derived by DSC ²⁸ (%)	DOC from IR 941 cm ⁻¹ band area (%)	DOC from IR 3295 cm ⁻¹ band area (%)
0	0	0	0
5	11.2	17.7	26.4
10	33.7	31.1	33.9
20	65.5	47.0	49.4
30	82.3	59.7	62.1
40	89.1	66.2	66.6
60	91.2	72.3	71.4

GP61-0496-11-R

A comparison of DOC values for cure at 453 K (Table 11) shows a discrepancy between the DSC and the FT-IR values. The extent of discrepancy for the advanced stages of curing is significant; the differences are greater at higher cure temperatures, possibly reflecting the greater extent of IMC¹⁹ and other nonacetylenic reactions that can occur at elevated temperatures.

The degree of cure determined from the average of the DOC values derived from the 941 cm⁻¹ and the 3295 cm⁻¹ acetylene band areas is plotted as a function of the cure times for the three isothermal cures in Figure 46.

These FT-IR techniques for determining the degree of cure from the normalized band areas were applied to the isothermal cure studies of ATB. A specimen of p-ATB was cured at 443 K (338°F), and FT-IR spectra were recorded before and after curing for nine different time intervals, as given in Table 12. The degree of cure derived from the normalized 3295 cm⁻¹ band area is also presented in Table 12.

The acetylene band that appears in the IR spectrum of ATS at 941 cm⁻¹, which was extensively used as a parameter in characterizing ATS cure states, (see Figure 45 and Tables 9-11), does not appear in the spectrum of p-ATB (Figure 47b). This band also does not appear in the IR spectrum of 4,4-diethynyphenyl ether;²⁹ however, it appears in the IR spectrum of the pure meta-ATB monomer (Figure 47a). These observations of the presence of the 941 cm⁻¹ band in two different meta-AT monomers and its absence in two different para-AT monomers suggest that the acetylene deformation vibrations in

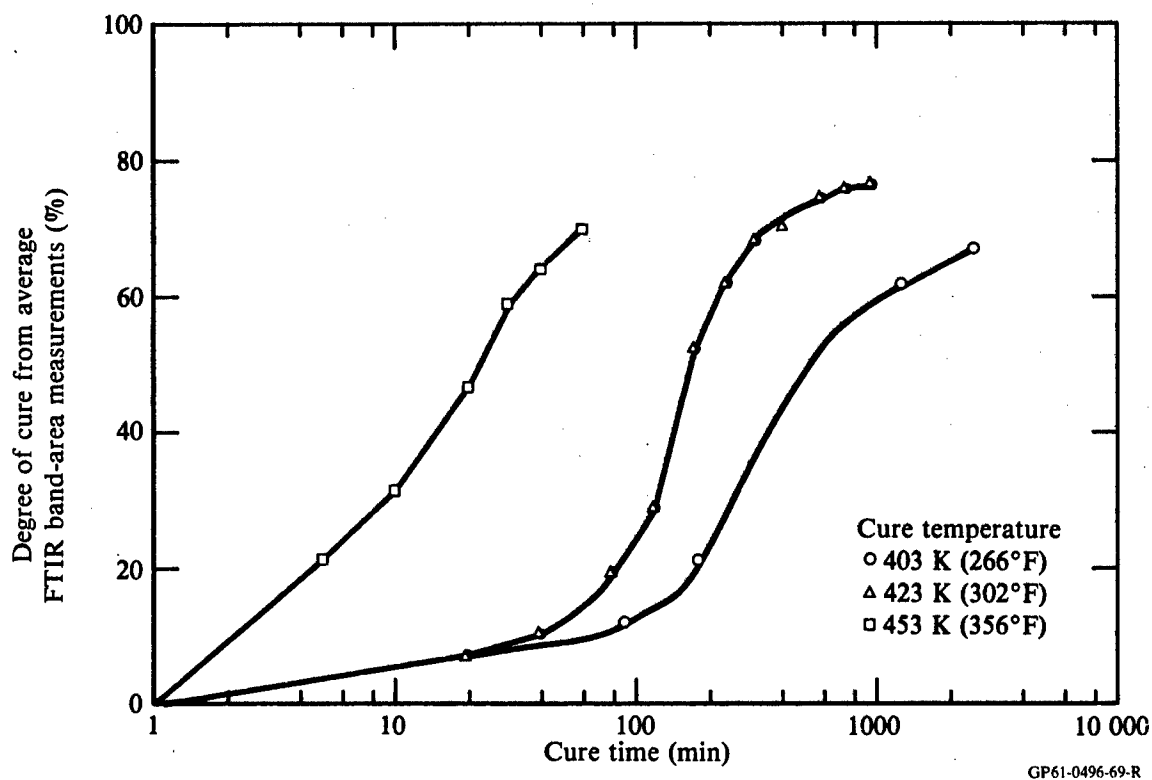


Figure 46. Degree of cure determined from the average of 941 cm^{-1} and 3295 cm^{-1} FT-IR band-area measurements for the three different isothermal cures of ATS samples.

TABLE 12. DEGREE OF CURE (DOC) OF p-ATB AS A FUNCTION OF CURE TIME AT 443 K (338°F).

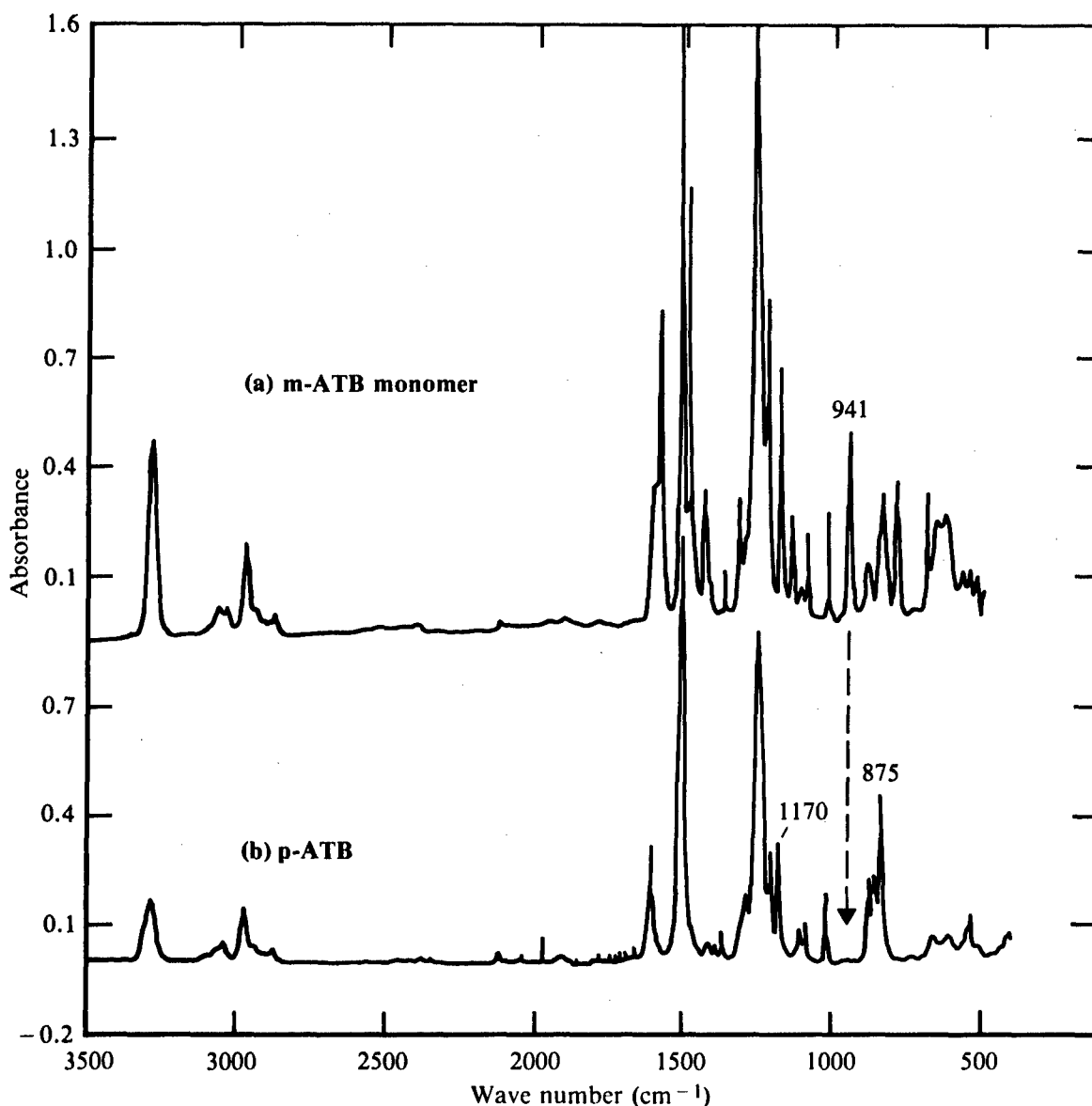
Cure time (min)	3295 cm^{-1} acetylene band area ^a	Degree of cure (%)
0	10.1	0
10	9.4	6.7
20	8.7	14.2
30	8.0	20.5
50	6.8	32.8
90	4.6	54.8
120	3.1	69.3
155	2.4	76.4
180	1.0	90.4
217	0.4	96.3

^aNormalized to the band area of the 830 cm^{-1} band.

GP61-0496-12-R

which this band originates are IR active in the meta configuration but not in the para configuration. The presence of the 941 cm^{-1} band in the pure meta-ATB monomer indicates that the assignment made by Shields and Koenig³⁰ is incorrect. IR spectra of additional aryl acetylene compounds will be required in order to assign this band conclusively to deformation vibrations of the aryl-acetylene moiety.

Purified monomeric m-ATB was cured at 433 K (320°F), and FT-IR spectra were recorded before and after curing for 12 time intervals for a total cure time of 420 min as shown in Table 13. The DOC, based on the rate of "consump-



GP61 0496 46 R

Figure 47. Superimposed FT-IR spectra: (a) m-ATB monomer and (b) p-ATB monomer.

TABLE 13. DEGREES OF CURE (DOC) OF m-ATB AS A FUNCTION OF CURE TIME AT 433 K (320°F).

Cure time (min)	DOC ^a from 3295 cm ⁻¹ (%)	DOC ^a from 941 cm ⁻¹ (%)	DOC ^b from 3295 cm ⁻¹ (%)	DOC ^b from 941 cm ⁻¹ (%)	Average DOC
5	3.2	2.8	4.0	3.7	3.4
15	8.7	7.9	10.0	9.2	8.9
30	18.1	19.0	17.0	17.8	18.0
60	31.3	32.4	29.6	30.6	30.9
91	44.9	46.5	41.7	43.3	44.1
120	60.5	60.0	57.5	57.0	58.7
150	71.7	70.8	68.4	67.4	69.6
180	76.4	74.3	73.8	72.0	74.1
255	81.0	80.0	77.7	76.5	78.8
300	82.7	81.4	79.5	78.0	80.4
360	84.3	83.3	81.4	80.2	82.3
420	85.4	84.3	82.5	81.3	83.4
Post cure 60 min at 523 K (482°F)	98.2	97.0	97.8	96.4	97.3

^aNormalized relative to band area of the 3840 - 3010 cm⁻¹ aromatic C-H bands.

^bNormalized relative band area of the 830 cm⁻¹ hydrogen wag band.

GP61-0496-13-R

tion" of two different acetylene bands, was determined for each cure interval. The band areas of the 941 cm⁻¹ and the 3295 cm⁻¹ acetylene bands used to determine DOC values were normalized relative to (1) the band area of a group of three relatively weak and only partially resolved aromatic C-H stretch bands appearing in the 2840-3010 cm⁻¹ region, and (2) the 830 cm⁻¹ band which originates in the out-of-plane hydrogen wag for two adjacent hydrogens of para-disubstituted benzene rings. The DOC values from the individual determinations, as well as the average values, are also given in Table 13.

A second specimen of purified monomeric m-ATB was cured at 453 K (356°F) and FT-IR spectra were recorded before and after curing for 14 intervals of time for a total cure time of 150 min. The DOCs reached after each cure interval are listed in Table 14 for the two acetylene bands and for the two different normalizations.

Plots representing DOC as a function of cure time for ATB curing at 433 K (320°F) and 453 K (356°F) are given in Figures 48-51. An interesting difference between the DOC values derived from the 941 cm⁻¹ and the 3295 cm⁻¹ bands

TABLE 14. DEGREES OF CURE (DOC) OF m-ATB AS A FUNCTION OF CURE TIME AT 453 K (356°F).

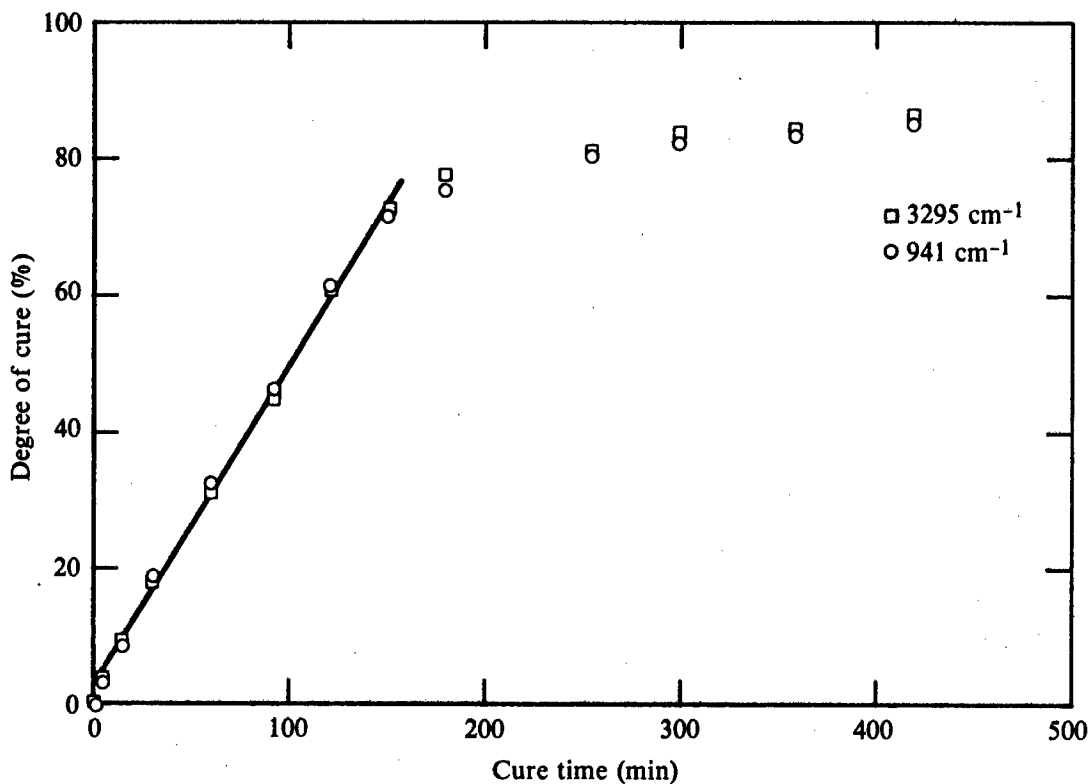
Cure time (min)	DOC ^a from 3295 cm ⁻¹ (%)	DOC ^a from 941 cm ⁻¹ (%)	DOC ^b from 3294 cm ⁻¹ (%)	DOC ^b from 941 cm ⁻¹ (%)	Average DOC
5	12.6	12.0	11.8	11.3	11.925
10	24.4	24.1	23.4	23.1	23.75
15	34.6	33.7	35.3	34.4	34.5
20	47.6	46.6	46.7	45.7	46.6
25	62.6	61.0	61.5	59.9	61.2
30	74.0	71.2	72.9	70.0	72.0
33	78.8	75.9	77.5	74.5	76.7
40	80.9	78.2	79.7	76.9	78.9
45	82.3	79.5	81.1	78.1	80.3
50	83.4	80.5	82.2	79.0	81.3
60	84.3	81.9	82.9	80.2	82.3
70	85.1	82.6	84.0	81.2	83.2
85	86.4	83.3	85.4	82.0	84.3
120	87.9	85.2	86.7	83.8	85.9
150	89.0	86.3	87.9	84.9	87.0

^aNormalized against band area of the 3840 - 3010 cm⁻¹ aromatic C-H bands.

^bNormalized against band area of the 830 cm⁻¹ hydrogen wag band.

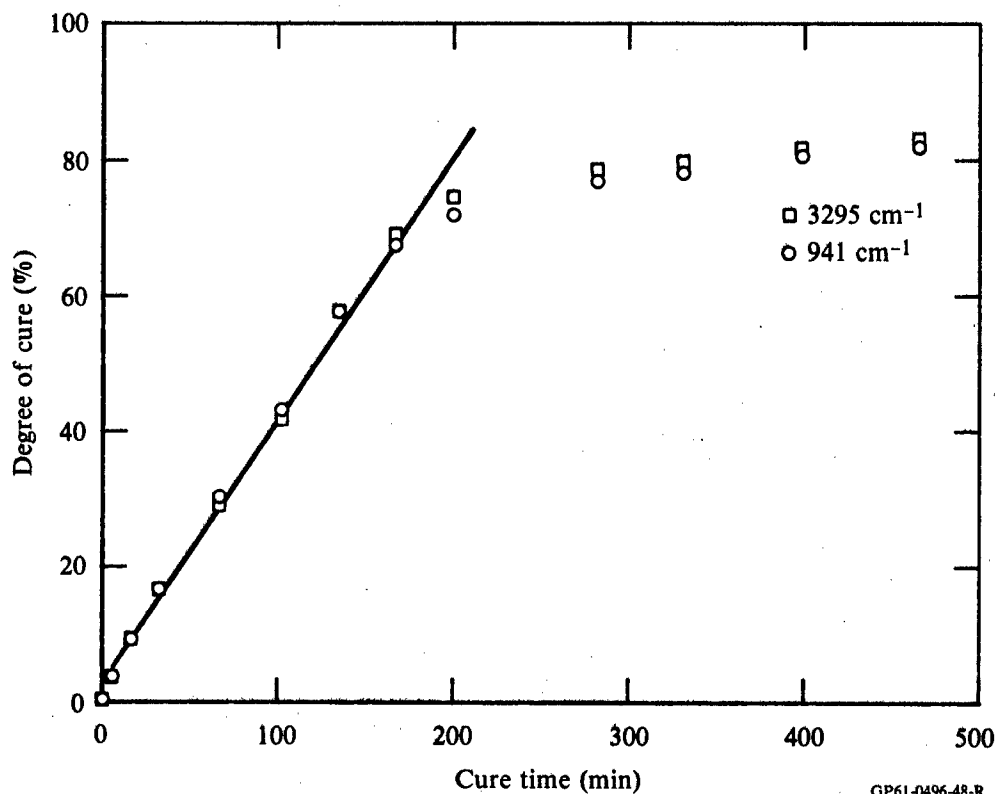
GP61-0496-14-R

is observed when the 433 K (320°F) cure is compared with the 453 K (356°F) cure. For the 433 K (320°F) cure of m-ATB, the points that correspond to the DOC values derived from the 941 cm⁻¹ band coincide fairly closely with the points derived from the 3295 cm⁻¹ band throughout the entire cure cycle for both normalization schemes, as shown in Figures 48 and 49. For the 453 K (356°F) cure, however, (Figures 50 and 51) the DOC values derived from the 941 cm⁻¹ are consistently lower than the DOC values derived from the 3295 cm⁻¹ band cure for times longer than 30 min. This period corresponds to the time at which the slope of the curve changes and suggests that the T_g of the resin has reached the cure temperature, i.e., the sample has vitrified. The origin of this difference in the two DOC values between cure at 433 K (320°F) and 453 K (350°F) is not clear; however, the different values quite possibly reflect differences in the network rigidity which would affect the vibrations of the 941 cm⁻¹ band but not the C-H stretch vibrations of the 3295 cm⁻¹ band.



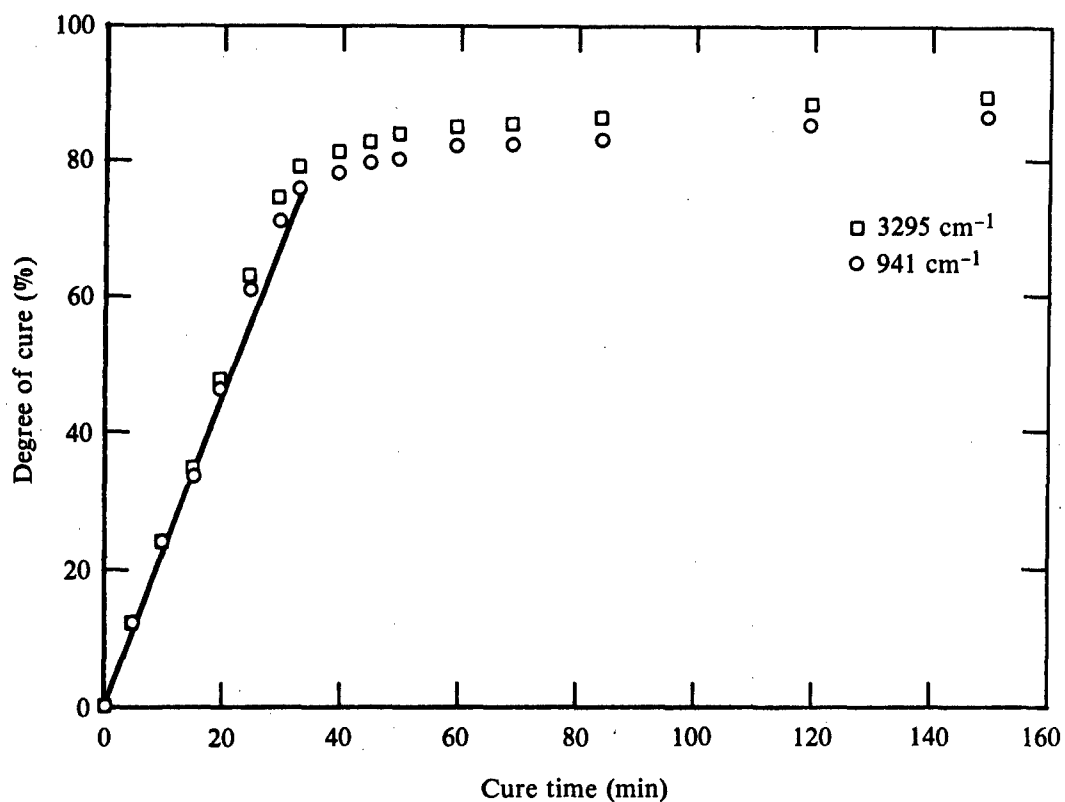
GP61-0496-47-R

Figure 48. Degree of cure in m-ATB isothermally cured at 433 K (320°F) determined with FT-IR. Normalized against 3010 - 2840 cm^{-1} band.



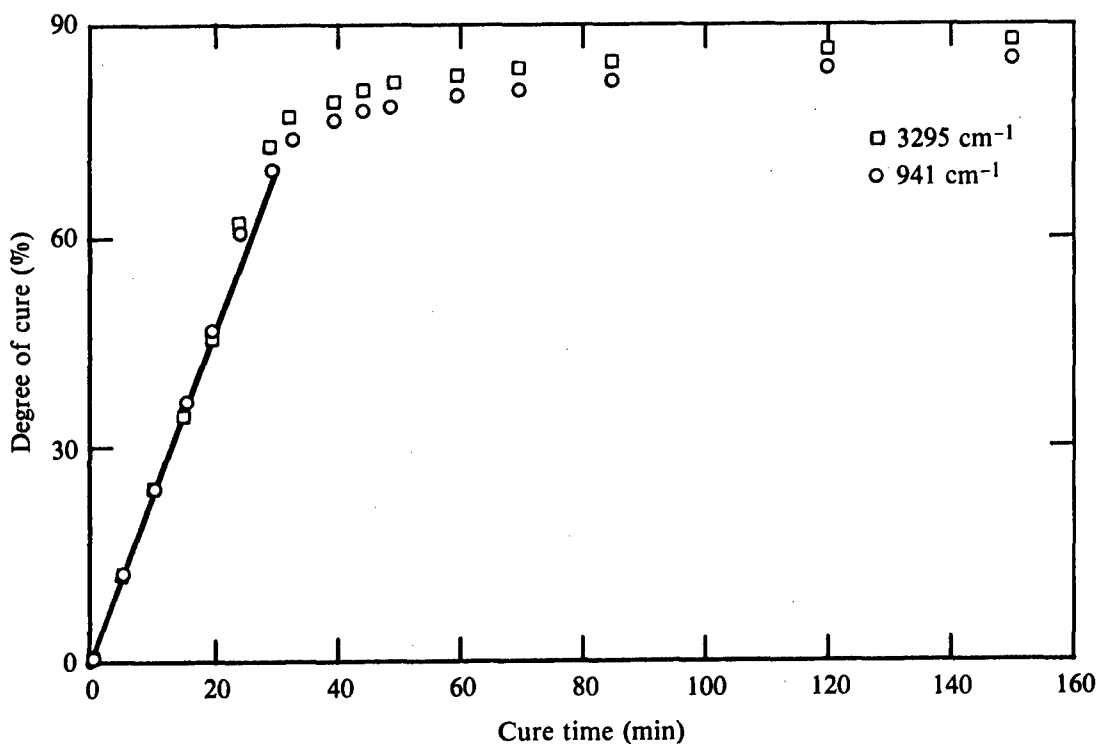
GP61-0496-48-R

Figure 49. Degree of cure in m-ATB isothermally cured at 433 K (320°F) determined with FT-IR. Normalized against 822 - 805 cm^{-1} band.



GP61-0496-49-R

Figure 50. Degree of cure in m-ATB isothermally cured at 453 K (356° F) determined with FT-IR. Normalized against 3010 - 2840 cm⁻¹ band.



GP61-0496-50-R

Figure 51. Degree of cure in m-ATB isothermally cured at 453 K (356° F) determined with FT-IR. Normalized against 882 - 805 cm⁻¹ band.

Frequency Shifts

Difference spectroscopy is a powerful method for detecting minor spectral changes in polymers. Difference spectra representing the net cure-induced changes between two consecutive stages of ATS cure are shown in Figure 52. In addition to exhibiting the expected negative acetylenic band at 941 cm^{-1} , which reflects the consumption of acetylene groups, these difference spectra exhibit spectral profiles that are indicative of frequency shifts for some of the bands. A typical difference spectrum intensity profile for a frequency-shifted FT-IR band is shown in Figure 53. Such a profile provides a greatly amplified record for small and otherwise difficult-to-measure frequency shifts.³¹ The peak-to-peak intensity, μ , is related to $\Delta\nu$ and can thus be used to measure small frequency shifts.³¹

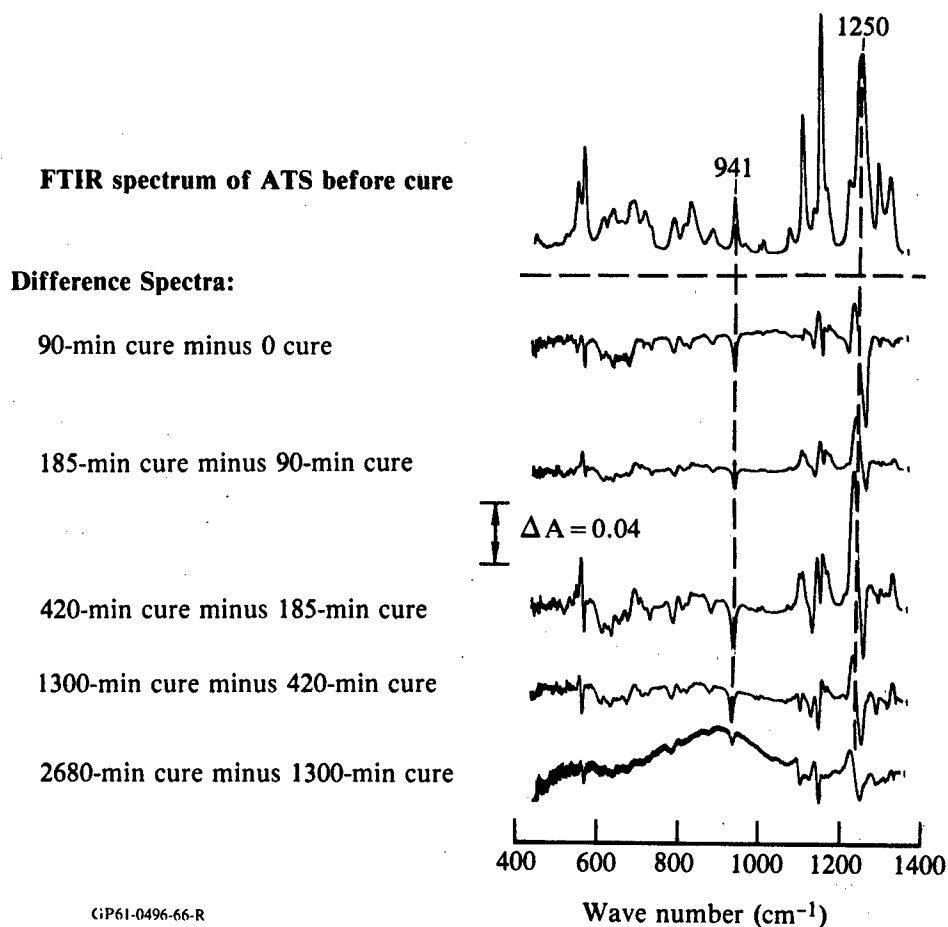
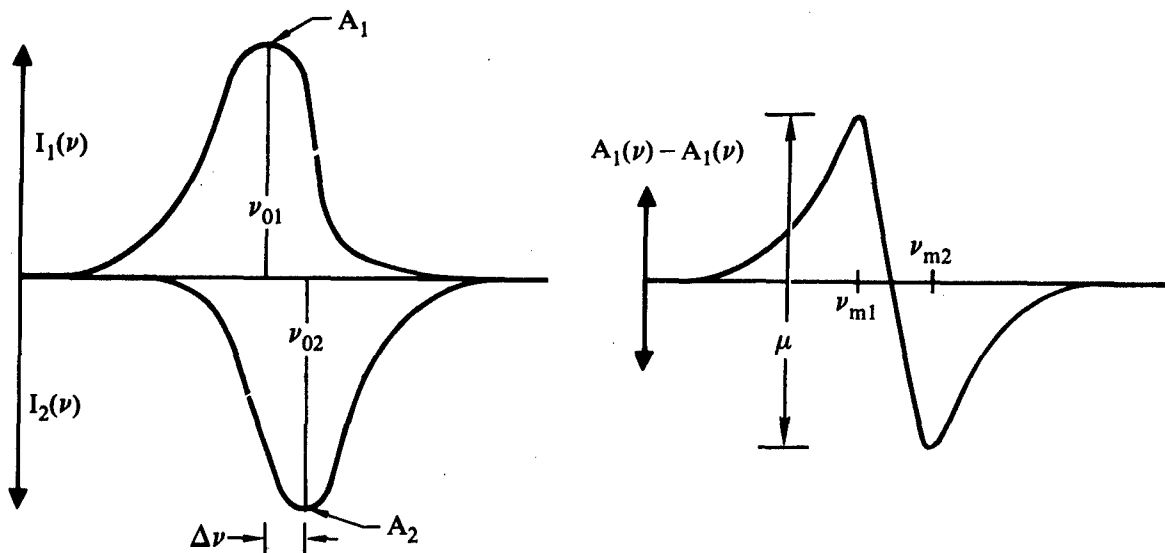


Figure 52. Superimposed difference FT-IR spectra of the $400 - 1400\text{ cm}^{-1}$ region. These spectra represent the net spectral differences between consecutive stages of ATS cure at 403 K (266°F), showing that the pronounced changes in later stages of cure are a result of band frequency shifts.



GP61-0496-65-R

Figure 53. Schematic illustration of a frequency-shifted band; $I_1(\nu)$, $I_2(\nu)$, and the resulting spectral profile observed in its difference spectrum, $D(\nu)$.

The difference FT-IR spectra between consecutive stages of curing ATS (Figure 52) show that the frequency shifts of the 1250 cm^{-1} band, which originates in the aryl-ether C-O stretch vibration, are the most pronounced of spectral changes observed during the later stages of cure. Cure-induced molecular strain is one possible mechanism that contributes to the frequency shift of the 1250 cm^{-1} band.

A specimen of p-ATB was cured at 433 K (338°F), and FT-IR spectra were recorded before and after curing for several different time intervals. The main reason for conducting this series of experiments was to search for cure-induced frequency shifts in a specific IR band which originates in coordinated vibrations of the para-diphenylether (DPE) moiety and appears in the $875\text{--}885\text{ cm}^{-1}$ region. In an earlier study of stress-induced molecular phenomena in polyimide films (Kapton 50H), we observed unique frequency shifts in this particular band,^{32,33} and assumed that if similar frequency shifts appeared in p-ATB, they could be correlated with the cure state, thus providing a new cure-state parameter.

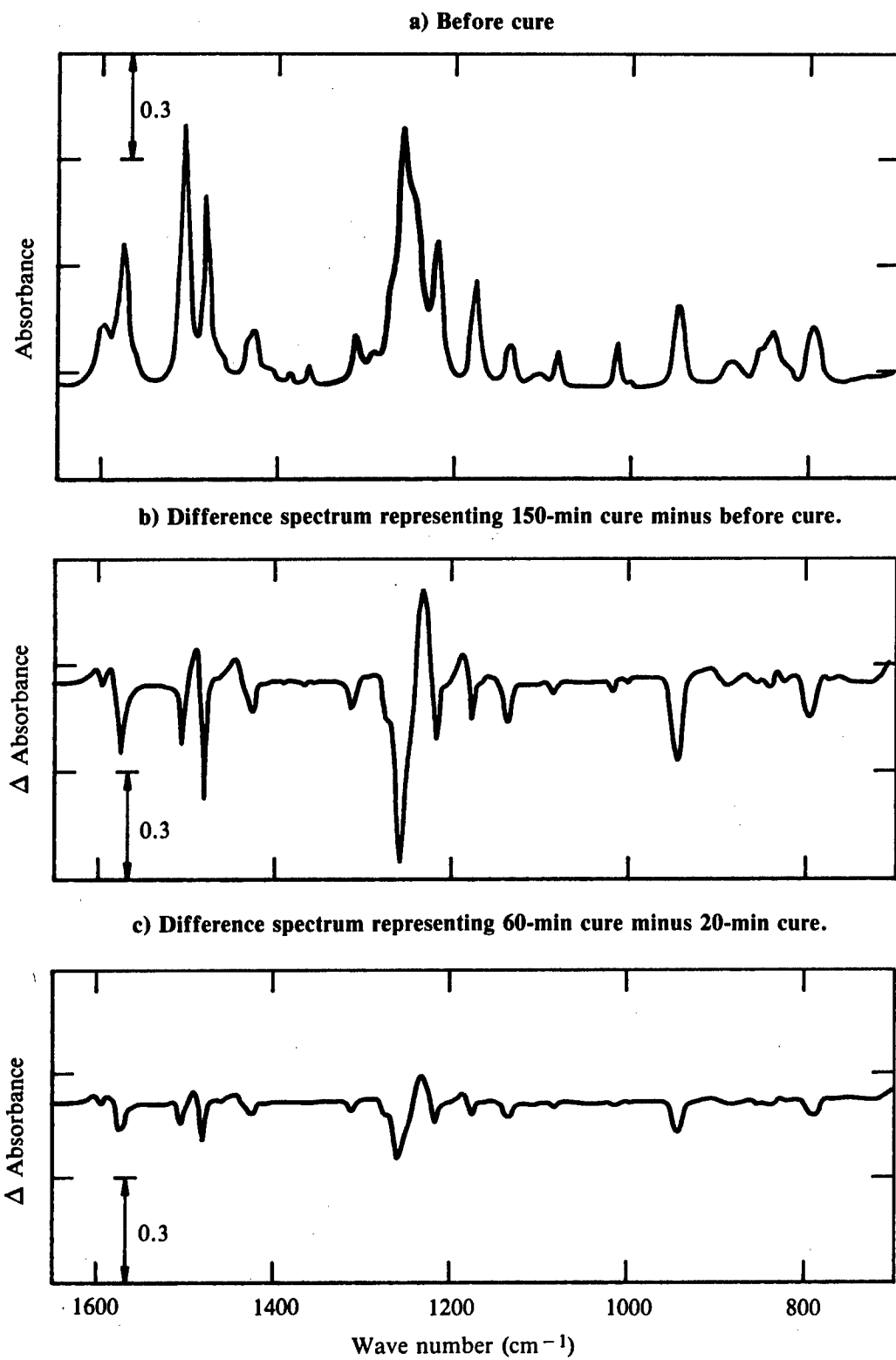
The p-DPE band at 875 cm^{-1} and its companion band at 1170 cm^{-1} are both present in the FT-IR spectrum of para-ATB (Figure 47b); however, these bands do not exhibit detectable frequency shifts as a function of the degree of cure. The frequency shifts were expected based on the assumption that if the

intra-molecular cyclization (IMC) mechanism occurs it would induce a molecular strain which would give rise to frequency shifts. Since frequency shifts were not observed, one can speculate that this mechanism is probably absent in p-ATB.

Spectral differences observed between consecutive stages of cure for m-ATB were studied by difference FT-IR spectroscopy. The magnitude of the spectral features observed in a difference spectrum obtained by subtraction of the spectra of two consecutive stages of cure determines the extent to which AT resins of similar cure times can be characterized or differentiated. The individual FT-IR spectra of m-ATB recorded at 15 consecutive stages of cure at 453 K (356°F) were used to obtain the difference spectrum between any two stages of cure. Typical difference FT-IR spectra of m-ATB are shown in Figures 54 and 55, along with the FT-IR spectrum of m-ATB before cure. The most pronounced spectral feature observed in the difference spectra is in the 1249-cm⁻¹ band (Figure 54b and c) assigned with confidence to the stretch vibrations of the aryl-ether moiety. This absorbance peak was also observed in the FT-IR spectra of ATS.

It should be noted that the peak-to-peak magnitude of the largest spectral feature observed in the difference spectrum shown in Figure 54c (≈ 1250 cm⁻¹) has an absorbance of 0.270. The difference spectrum shown in Figure 54c results from subtraction of the spectrum recorded after 20 min cure from the spectrum recorded after 60 min cure. Therefore, assuming linear spectral changes with cure time and spectrometer absorbance resolution of 0.0001, and considering this parameter alone, we can say that 270 discrete ATB cure steps can be differentiated between the 20 min cure and the 60 min cure. Since the minor cure-induced network changes occurring during a relatively short increment of cure time (2-3 min) seem to be most pronounced in the 1250 cm⁻¹ range, it is desirable to determine the molecular origin of these spectral changes.

In general, spectral profiles such as the ones appearing in the difference FT-IR spectra (Figures 54b and c) in the 1250 cm⁻¹ range are characteristic of frequency shifts. To explain similar spectral features observed in the 1250 cm⁻¹ region in the difference spectra of consecutive cure stages of ATS,³ we proposed cure-induced molecular strain as a possible mechanism



GP61-0496-63-R

Figure 54. Superimposed FT-IR spectra m-ATB ($700 - 1650 \text{ cm}^{-1}$) for 453 K (356°F) cure.

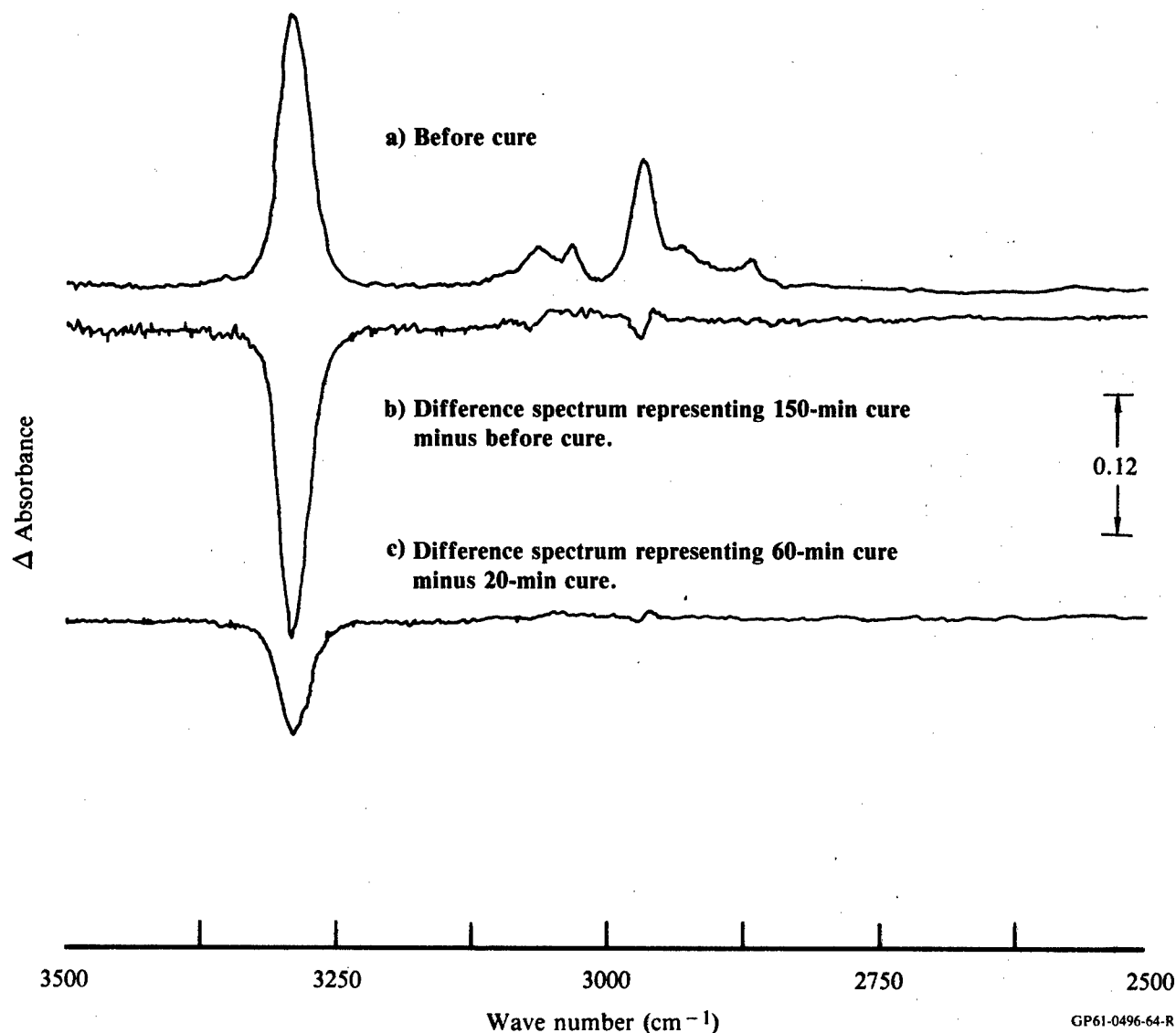


Figure 55. Superimposed FT-IR spectra m-ATB (2500 - 3500 cm^{-1}) for 453 K (356°F) cure.

causing frequency shifts in that band. However, other mechanisms which can develop such spectral features must also be considered, particularly since the 1250 cm^{-1} band appears to consist of several severely overlapped bands whose absorbances could change independently with cure.

Correct assignment of the origin of these overlapping bands would aid the interpretation of the observed results. We therefore concluded that an attempt to assign the overlapped bands to specific vibrations is the next step towards solution of the problem.

A search of the FT-IR group frequencies for the molecular moieties present in uncured m-ATB and the moieties expected in the cured m-ATB revealed

that only an overtone of the acetylene band at 622 cm^{-1} , which is assigned to the bending vibrations of the acetylenic H atom, can contribute to absorbances in the 1250 cm^{-1} region. Availability of FT-IR spectra of m-ATB with deuterated acetylenic groups ($\text{DC} \equiv \text{C} - \text{R} - \text{C} \equiv \text{CD}$) as a function of cure would conclusively determine if the differences spectral feature at 1250 cm^{-1} is the result of the changes in the overtone of acetylenic H bending vibrations.

Regardless of the origin, the difference spectrum profile in the 1250 cm^{-1} region and changes in its peak-to-peak ΔA values can be effectively exploited to characterize the cure states with a considerable degree of resolution.

b. FT-IR Postcure Studies

Postcure studies of ATS samples incompletely cured at 403 K (266°F) were performed. These results, along with results obtained earlier for postcure studies of samples incompletely cured at 423 K (302°F) and 453 K (356°F),³ are summarized in Tables 15-17. These measurements show that postcure heating leads to an almost total consumption of the acetylenic moieties, which yields apparent degrees of cure close to or greater than 98.5%.

TABLE 15. FT-IR RESULTS OF INCOMPLETE CURE OF ATS AT 403 K (266°F) FOLLOWED BY 120 MIN POSTCURE AT 523 K (482°F), 543 K (518°F), AND 573 K (572°F).

Sample number	Cure time at 403 K (min)	Postcure temperature (K)	Acetylene band area 3295 cm^{-1}	Degree of cure (%)	Aromatic C-H stretch band area $3040 - 3120\text{ cm}^{-1}$
36	180	—	8.7	56.5	2.4
37	180	523	^a 0.2	^a 98.5	3.1
38	180	543	^a 0.2	^a 98.5	2.6
39	180	573	^a 0.2	^a 98.5	2.8
40	420	—	5.4	73.1	2.1
41	420	523	^a 0.2	^a 98.5	2.6
42	420	543	^a 0.2	^a 98.5	2.6
43	420	573	^a 0.2	^a 98.5	2.3
44	2700	—	2.2	89.0	2.3
45	2700	523	^a 0.2	^a 98.5	2.8
46	2700	543	^a 0.2	^a 98.5	2.6
47	2700	573	^a 0.2	^a 98.5	2.8

^aBand area less than 0.2 units and DOC greater than 98.5%.

GP61-0496 15-R

TABLE 16. FT-IR RESULTS OF 423 K (302°F) CURE OF ATS FOLLOWED BY A 120 MIN POSTCURE AT 523 K (482°F), 543 K (518°F), AND 573 K (572°F).

Sample number	Cure time (min)	Postcure temperature [K (°F)]	Acetylene band area 3295 cm ⁻¹	DOC % derived from 3295 cm ⁻¹	Band area ratios			
					Sulfone Aromatic 1495 cm ⁻¹	Sulfone aryl ether	Aromatic 1495 cm ⁻¹	aryl ether Aromatic 1595 cm ⁻¹
12	75	None	6.2	19.5	1.3	0.64	1.07	2.62
13	75	523 (482)	0.3	96.2	1.2	0.80	1.17	2.34
14	75	543 (518)	0.1	98.6	1.3	0.77	1.14	1.96
15	75	573 (572)	0.2	97.8	1.4	0.78	1.06	2.53
16	170	None	2.8	56.6	1.3	0.81	1.21	2.27
17	170	523 (482)	0.2	97.8	1.3	0.81	1.17	2.30
18	170	543 (518)	0	100.0	1.3	0.80	1.14	2.26
19	170	573 (572)	0	100.0	1.3	0.79	1.11	2.50
20	320	None	1.7	76.2	1.3	0.81	1.19	2.55
21	320	523 (482)	1.2	84.0	1.4	0.83	1.11	2.74
22	320	543 (518)	0	100.0	1.3	0.82	1.17	2.30
23	320	573 (572)	0	100.0	1.4	0.81	1.17	2.58

GP61-0496-16-R

TABLE 17. FT-IR OF INCOMPLETE CURE OF ATS AT 453 K (356°F) FOLLOWED BY 120 MIN POSTCURE AT 523 K (482°F), 543 K (518°F), AND 573 K (572°F).

Sample number	Cure time at 453 K (356°F) (min)	Postcure temperature [K (°F)]	Acetylene band area 3295 cm ⁻¹	Degree of cure (%)	Aromatic C-H stretch 3040 - 3120 cm ⁻¹
25	0	523 (482)	^a 0.20	^a 98.5	2.2
26	0	543 (518)	^a 0.20	^a 98.5	2.2
27	0	573 (572)	^a 0.20	^a 98.5	2.2
28	20	—	3.41	55.5	1.9
29	20	523 (482)	0.30	97.0	1.9
30	20	543 (518)	^a 0.20	^a 98.5	2.2
31	20	573 (572)	^a 0.20	^a 98.5	2.1
32	55	—	1.80	76.5	2.1
33	55	523 (482)	^a 0.20	^a 98.5	2.0
34	55	543 (518)	^a 0.20	^a 98.5	2.2
35	55	573 (572)	^a 0.20	^a 98.5	1.9

^aBand area < 0.2; DOC > 98.5%.

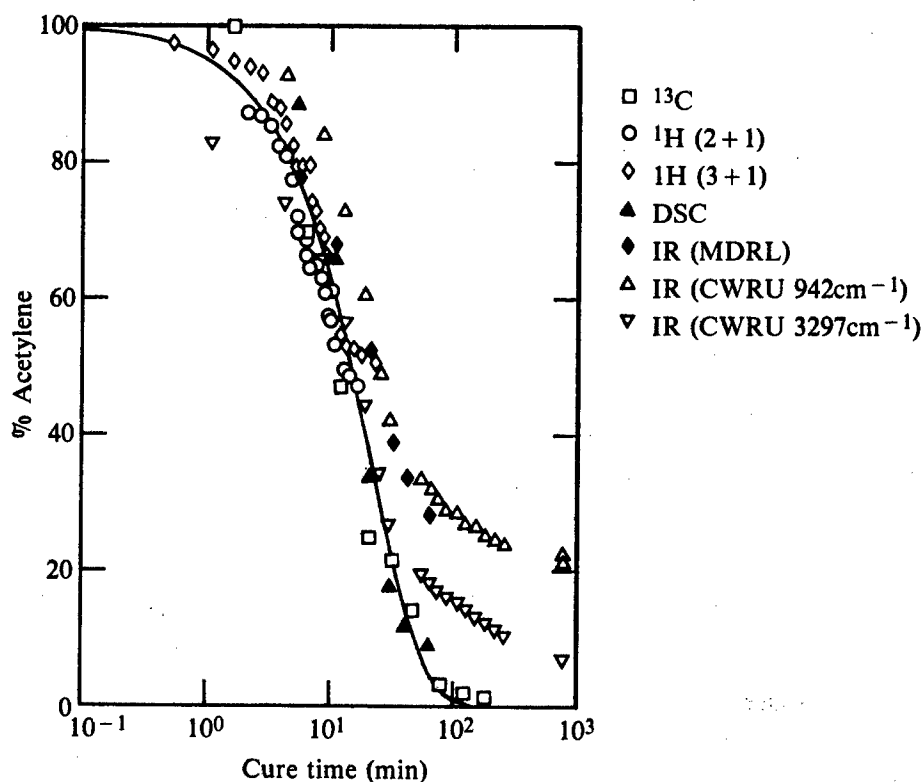
GP61-0496-17-R

Similar postcure results were obtained for m-ATB. For example, an m-ATB sample that had been cured at 433 K (320°F) for 420 min to achieve an 85.4% degree of cure was postcured at 523 K (482°F) for 60 min. The only significant change brought about by this postcure was a decrease in the areas of 3295 cm^{-1} and 941 cm^{-1} bands. After this postcure, the degree of cure derived from these band areas was 97.3%.

In a search for other parameters more sensitive to postcuring, we examined the band area ratios as a function of postcuring. These ratios show that no significant changes occur in the relative band intensities of the aromatic, aryl-ether, and sulfone moieties as a result of postcure heating.

IV. DISCUSSION OF RESULTS

Comparison of the NMR data with DSC and FT-IR determinations of the degree of cure (DOC) is most useful. Figures 56-58 display all the results gathered from MDRL - the ^1H NMR, ^{13}C NMR and FT-IR results as discussed in Sections III 2, III 1a, and III 4a, respectively - DSC results from Rockwell,²⁸ and FT-IR results from Case Western Reserve University,³⁰ (all three laboratories working under contract with the AFWAL/ML). The quantity % acetylene is obtained from the DOC by subtracting one hundred. In Figures 56-58, the MDRL FT-IR results have been determined by averaging the band areas of the 942 and 3297 cm^{-1} absorbance bands. Koenig and Shields, however, do not give credence to their 942 cm^{-1} band.³⁰ They observe a substantially higher DOC for the 942 cm^{-1} band than for the 3297 cm^{-1} band, an effect not observed, at least to such an extent, at MDRL. We thus show their 3297 cm^{-1} data in Figures 56 and 57, and their 942 cm^{-1} data separately in Figure 56 for com-



GP61-0496-37-R

Figure 56. Comparison of ^{13}C and ^1H NMR results to DSC and FT-IR results for acetylene uptake in ATS cured isothermally at 453 K (356°F). The exponential has a rate constant of $k = 8 \times 10^{-4} \text{ s}^{-1}$.

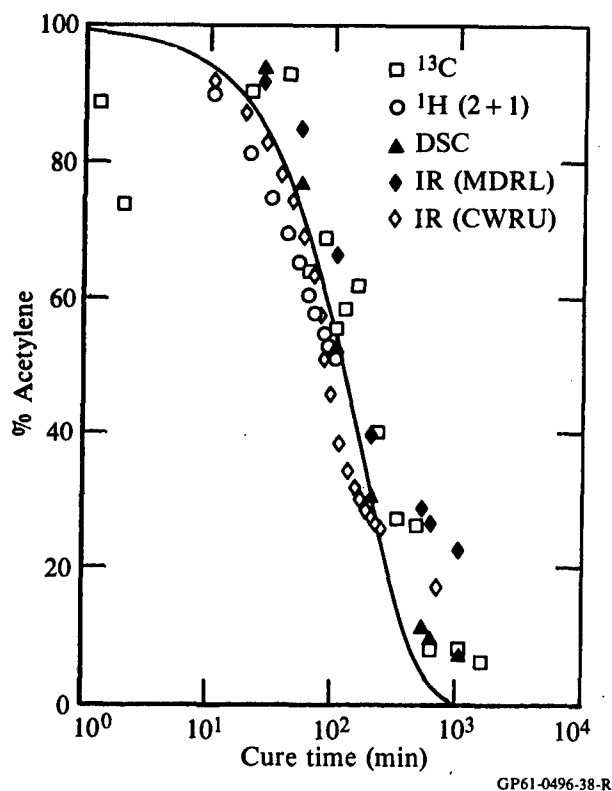
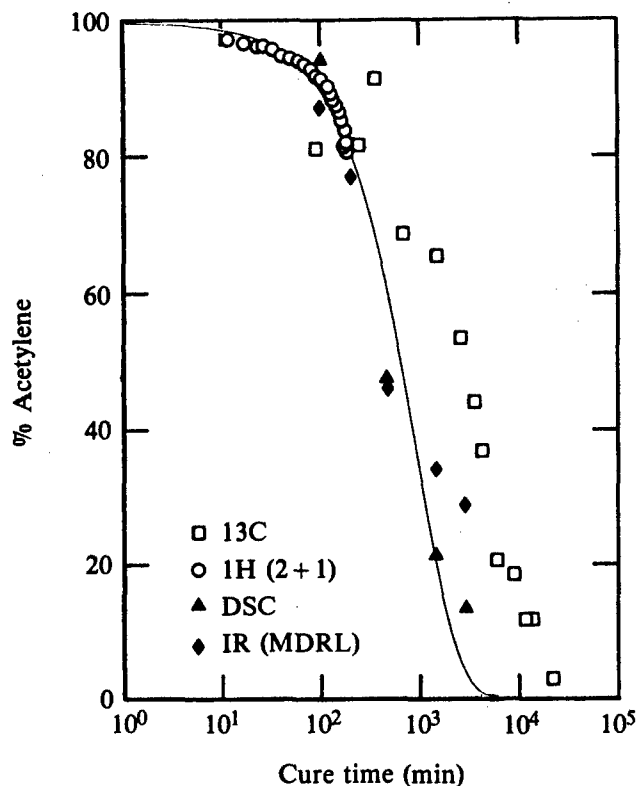


Figure 57. Comparison of ^{13}C and ^1H NMR results to DSC and FT-IR results for acetylene uptake in ATS cured isothermally at 423 K (306°F). The exponential has a rate constant of $k = 1 \times 10^{-4} \text{ s}^{-1}$.

parison purposes only. It should be noted that Koenig and Shields used purified ATS, whereas the rest of the data were obtained from a common stock of ATS. The exponential decay curves shown in Figures 56-58 are for comparison purposes only; no special significance is attached to them. First-order decrease of monomer is observed during the early cure, but as discussed below, the apparent continuation of first-order kinetics into the later cure, as suggested by DSC and ^{13}C NMR, is likely to be misleading.

As Figures 56-58 show, all the data are in fairly good agreement for % acetylene > 40. Minor variations could easily occur from differences in samples or small differences in the cure temperature. The FT-IR data clearly show, however, that the DOC slows significantly away from first-order kinetics when % acetylene < 35. The FT-IR results in these later stages of cure are at variance with the ^{13}C NMR and DSC results. The DSC results have been shown to be suspect.³⁴ The ^{13}C results, on the other hand, present some problems in interpreting the differences with the FT-IR results. It is possible that the cross-polarization contact time was not optimized for the later stages of



GP61-0496-39-R

Figure 58. Comparison of ^{13}C and ^1H NMR results to DSC and FT-IR results for acetylene uptake in ATS cured isothermally at 403 K (266°F). The exponential has a rate constant of $k = 2 \times 10^{-5} \text{ s}^{-1}$.

cure. This is a common problem with ^{13}C solid-state NMR, where differences in hydrogen $T_{1\rho}$ relaxation times can adversely affect quantitative results if the contact time is not carefully chosen. The contact time was optimized for the ATS samples at the beginning of the cure, but it is possible that the hydrogen $T_{1\rho}$'s changed enough during the cure to decrease the relative acetylenic peak in the ^{13}C spectra. A longer than normal contact time of 4 ms was chosen to ensure adequate cross-polarization to non-protonated carbons. If a problem occurred because of the contact time, it was more likely to occur at an enyne acetylene than at a normal protonated acetylene. Enyne moiety, indicated to occur in ATS from the 2334 cm^{-1} absorbance band observed at MDRL,³ may not be quantitatively identified in the ^{13}C CP/MAS spectra. Postcure studies show that the FT-IR results display, at least qualitatively, the true behavior of the DOC.

More information is available from the data obtained so far. A "gel point," defined as the point at which the reacting system is no longer completely soluble in some normal solvent,³⁵ is suggested by the EPR results, as

discussed below, and by the ^1H NMR results. The time at which f_r appears in the ^1H data (see Figures 10, 12, 18, and 21) appears to be a precursor to the gel point. The time at which f_r appears is defined as the extrapolation of the tangent to the maximum slope of f_r to the abscissa. In addition, the time at which f_i maximizes is probably close to the gel point. The "induction period" observed by EPR, similarly defined as the maximum slope extrapolation to the abscissa (see Figures 33 and 37), is nearly identical to the time of the maximum in f_i , and therefore also is indicative of the gel point. These times are listed in Table 18.

Vitrification of the resin during cure is observed in both the ^1H NMR results, and in the FT-IR results. The transition in f_r (see Figures 10, 12, 18 and 21), defined as the intersection of the tangent of the long time asymptote to the tangent to the maximum slope, is close to the vitrification

TABLE 18. SELECTED CURE TIMES MEASURED BY EPR, ^1H NMR, AND FT-IR.

	Resin type	453 K (356°F)	423 K (306°F) time (min)	403 K (266°F)
The gel point				
^1H NMR - Increase in rigid component concentration	ATS	4	40	110
^1H NMR - Peak concentration of intermediate species	ATS	9	50	200
EPR - Increase in free radical concentration	m-ATB	25	90*	400†
	ATS	10	60	200
Vitrification				
^1H NMR - Rigid component transition	ATS	21	110	320
^1H NMR - Mobile component spin-spin relaxation time transition	ATS	25	120	260
FT-IR - 3297 cm^{-1} transition	m-ATB	24	180*	
	ATS	32	118	500
Radical decay				
EPR - Free radical content levels off	m-ATB	500	2800*	$\sim 10^4$ †
	ATS	250	1700	$\sim 10^4$

*Cure temperature was 433 K (320°F).

† Cure temperature was 413 K (284°).

GP61-0496-76-R

point. A better indication of vitrification is given by the mobile spin-spin relaxation times, T_2^m , observed by ^1H NMR (see Figures 9, 14, 19 and 22). The time at which this relaxation time reaches its asymptotic value indicates vitrification. The transition in the FT-IR DOC values (see Figures 48-51 and 56-58) also indicates vitrification. These times are also listed in Table 18.

The induction period shown by the EPR data for both the ATS and m-ATB (Table 18) seems to be a general feature of the crosslinkable AT resins. This effect can be attributed to one of the following possibilities: (1) enhanced radical decay resulting from the presence of a limited number of reactive impurity molecules in the resin, (2) enhanced radical decay prior to matrix vitrification, or (3) delayed net radical production following the prerequisite buildup of a diamagnetic intermediate. Since the m-ATB is purer than the ATS, one would expect the m-ATB to have a shorter induction period than the ATS if possibility (1) were important. Actually, the induction periods of ATS and m-ATB are similar, indicating that possibility (1) probably does not contribute to the induction period in these polymers.

The fact that the non-crosslinkable PPPA resin never exhibited a significant increase in radical concentration with curing implies that either crosslinking of diamagnetic oligomeric intermediates [possibility (3) above] or some means of matrix vitrification [possibility (2) above] is essential for the accumulation of stable radicals in the AT polymers. Prior to such radical stabilization, the radicals produced during curing are decomposed rapidly enough to keep the steady-state concentrations low.

The results of Pickard et al.² are consistent with this hypothesis. Their results indicate that a typical oligomeric chain formed during curing of phenoxyphenylacetylene is on the order of ≈ 10 monomeric units long, whereas the current EPR data indicate that only one radical is observed for every few hundred acetylene groups initially present in the ATS or m-ATB resins. If the data of Pickard et al.² are applicable to the present AT resins, it can be inferred that only one radical is observed by EPR for every 20-50 polyene chains in the fully cured ATS or m-ATB matrix. The ^1H NMR spin-spin relaxation measurements imply, however, that monomer reacts to form an oligomer having $n \approx 6$, and that an intermediate-MW polymer forms having $30 < n < 300$. In this case, there would be one radical for every 1 to 17 intermediate-MW chains. The observed increase in radical concentration begins approximately where the peak concentration in f_1 occurs. Thus, the production of the

intermediate-MW polymers is not accompanied by net radical production. If chain transfer reactions and polymerization pathways that do not involve free radicals are considered not to dominate the curing process, then the above results imply that most of the radicals produced during early polymerization decay instead of accumulating.

The ^1H NMR data presented in Figures 9, 14, 19, 22 and Table 18 indicate that vitrification of ATS (as defined by T_2 of the mobile component reaching its asymptotic value) occurs much later than the inflection point in the EPR data. Thus, complete vitrification of the matrix [possibility (2) above] is not essential for an increase in net radical concentration. The ^1H NMR data in Figures 10, 12, 18, 21, 27, and 28 indicate that ATS curing occurs in at least two major steps. In the first step, the most mobile component reacts to form a semi-rigid intermediate, and in the second step, the intermediate reacts to form the rigid product. The most rigid component forms at its maximum rate only after the concentration of intermediate component has reached its maximum value.

From the ^1H NMR data in Figures 10, 12, 18, 21, 27, and 28 and Tables 18 and 19, it appears that the most rigid component of the curing resin begins to be produced somewhat prior to the EPR induction period. This time delay indicates that stable radicals cannot be associated with the regions of initial local crosslinking appearing in an otherwise non-crosslinked matrix. It seems that radicals become stabilized only after significant crosslinking has taken

TABLE 19. ATS RESIN RATE CONSTANTS FOR RADICAL PRODUCTION (EPR) AND RIGID COMPONENT PRODUCTION (NMR).

	403 K (266°F)	423 K (302°F)	453 K (356°F)
Radical Production (EPR)	$1.0 \times 10^{-5} \text{ s}^{-1}$	$6.1 \times 10^{-5} \text{ s}^{-1}$	$4.8 \times 10^{-4} \text{ s}^{-1}$
Rigid Component Production (^1H NMR)	$9 \times 10^{-5} \text{ s}^{-1}$	$2.4 \times 10^{-4} \text{ s}^{-1}$	$2.4 \times 10^{-3} \text{ s}^{-1}$
Rate Ratio (NMR: EPR)	9	4	5

GP61 0496 75 R

place, but prior to complete vitrification. This suggests that a point near gelation may be associated with the onset of significant net radical production. Therefore, an important implication of the EPR results is that a sudden decrease in terminations or radical decay occurs in the vicinity of the gel point. Gelation could prevent large-scale diffusion of the radicals and thus prevent them from encountering reactive sites that would lead to radical decay.

Activation energies for the decrease of monomer can be obtained from the rate constants shown in Figures 56-58. An approximate activation energy of 130 kJ mol^{-1} is found, comparing fairly well with other determinations.^{2,36}

For all the observations discussed in this report, most can be explained in terms of the mechanism described by Equations (5-10). One possible description of the curing process of AT resins is as follows. Initiation occurs (a process not investigated here). Polymerization follows, but most likely terminates, possibly by intramolecular cyclization reactions, producing low-MW oligomers having a degree of polymerization of about six. Enyne formation is also observed to occur during the early cure.

Polymerization continues, either from monomer initiators, or from low-MW oligomers, but as long as the viscosity remains low, termination reactions prevent formation of any significant amount of high-MW polymer. Conjugation of the phenoxyphenyl moiety, most likely of a para-substituted group, may contribute to termination of the free-radical polymerization. Perhaps more likely, steric hinderance prevents the free-radical addition from advancing to large degrees of polymerization. High-MW polymer would then form only from crosslinking reactions. The decay times of radicals produced during the early cure polymerization are short compared to the EPR experimental observation times, keeping the observed net radical production low. During this induction period, the decrease of monomer follows first-order kinetics. The intermediate-MW polymer formed is found to have a fairly narrow MW distribution and a degree of polymerization between 30 and 300.

At the "gel point," the resin viscosity becomes large and crosslinking becomes significant. Termination reaction rates might decrease because of the lower mobilities of reacting radicals, monomers, and oligomers. Radical concentration is observed to increase at this point. The only firm statement we can make about net radical production is that it is viscosity dependent; the high viscosities occurring near the gel point are necessary before large net

radical production will be observed. The increased rate of crosslinking most likely occurs because of the longer residence times of exterior acetylene moieties on adjacent, intermediate-MW polymers in close proximity to each other. In this way, the resin most likely has a true gel point; i.e., crosslinking does not occur until the intermediate-MW polymers have such a large concentration that they are forced into relatively long-time, close-proximity contact, and "gel" into an extended network.

Crosslinking slows down at vitrification of the AT resins due to both the very low mobility of the resin components and the remote location of the remaining acetylenic moieties from one another. Postcuring studies, performed mainly with FT-IR, reveal that either very long cure times past vitrification or high temperature postcures are necessary to consume all the acetylenic moieties, and hence, to complete the network formation of AT resins.

V. CONCLUSIONS

A. Early Cure

1. Average molecular weight of uncured AT resins may be obtained from ^{13}C CP/MAS NMR, or from solution NMR.
2. Some stable free radicals are present in the uncured m-ATB and ATS resins. These radicals probably exist in a conjugated system.
3. Monomer is consumed according to first-order kinetics during the early cure. The activation energy for this process is -130 kJ mol^{-1} .
4. A 2334 cm^{-1} band observed by FT-IR, the only band found to increase in intensity during the early cure, implies that enyne formation occurs in AT systems.
5. The formation of a low-MW oligomer having an average degree of polymerization of 5-6 is likely to occur during the early cure.
6. Radicals do not accumulate in the mono-acetylenic, non-crosslinkable system, PPPA.
7. EPR spectra from radicals produced in PPPA and in slightly cured m-ATB resemble each other and are similar to those observed in polyphenylacetylene by Whitte et al.²⁵
8. It appears that enyne formation, as suggested by FT-IR, and/or intramolecular cyclization (IMC) mechanisms are important in the curing process, irrespective of the cure temperature.
9. Conjugation and/or hyperconjugation of the phenoxyphenyl moiety into the conjugated polyene backbone may be important with regard to specific termination steps during polymerization.

B. Later Cure

1. An intermediate-MW polymer having a fairly narrow MW distribution and an average degree of polymerization not less than 30 but not more than 300 is observed. This result is in contradiction to the results of Koenig and Shields.³⁰
2. An induction period is observed, during which termination reactions prevent the formation of a high-MW polymer.

3. Results from PPPA compared to ATS or m-ATB confirm that net radical production is viscosity dependent and occurs either from crosslinking reactions producing stabilized radical structures or because termination/decay of the radicals is enhanced at low viscosity.
4. The higher radical concentrations observed in one series of cured m-ATB samples were probably the result of oxygen contamination during sample preparation. This indicates that oxygen may have an effect on curing since the steady-state radical concentration presumably affects the details of the polymerization process.
5. Viscosity-dependent termination and crosslinking reactions compete, and the crossover from the relatively low-MW termination region to high-MW crosslinking, occurring close to the gel point, can be monitored by use of ^1H NMR and EPR.
6. The radical concentration increases sharply following the sudden increase in the rigid ^1H NMR component concentration and before vitrification.
7. The gel point can be monitored with ^1H NMR and EPR.
8. The vitrification point can be monitored with ^1H NMR and FT-IR.
9. Vitrification of the resin system slows acetylene consumption and causes it to deviate from the initial first-order kinetics.
10. At the peak radical concentration, one radical is observed per every few hundred acetylene groups initially present in the uncured resin.

C. Postcure

1. Either very long cure times or high-temperature postcures are necessary to complete the crosslinking of an AT network.
2. The final uptake of acetylene moiety following high-temperature postcures as observed by FT-IR suggests that the FT-IR results at long cures are at least qualitatively correct.
3. Two different radicals appear to be present in some postcured (523 K) [482°F] ATS samples. One is probably the original curing-generated radical or a derivative of it, and the other may be a new radical generated by the postcuring.
4. m-ATB samples cured at 413 K (284°F) and 433 K (320°F) did not show additional radical formation during postcuring at 453 K (356°F).

D. General

1. The fractional components monitored with ^1H NMR bear similarity to either two or three consecutive first-order reactions.
2. ^1H spin-lattice relaxation times show an initial increase resulting from the decreasing mobility of the resin, and then a decrease as a result of the increase in free radicals.
3. Radical production during curing is qualitatively similar in m-ATB and ATS.
4. The net radical production observed by EPR is probably the result of both production and decay reactions occurring together in the curing resin.
5. The radicals are relatively stable and are therefore probably in π orbitals. They may be delocalized over several phenylacetylene-type monomer units.
6. Radical production bears qualitative resemblance to a process involving two successive first-order reactions.
7. At least three distinct species are observed with ^1H NMR during curing of ATS resin, and the formation of four or more distinct species during the cure is likely.
8. The highly aromatic, unsaturated character of AT resins is believed to lead to the observation of only one ^1H NMR spin-spin relaxation time for the high-MW AT polymers, as opposed to the two spin-spin relaxation times observed for common high polymers.
9. The rapid increase of rigid component observed by ^1H NMR in some ways resembles autoacceleration, although the decrease in termination reactions may be offset by the increase in crosslinking.
10. A detailed mechanism consisting of initiation; polymerization; viscosity and/or MW-dependent termination reactions, which may include enyne and IMC formation; and crosslinking is proposed to explain most of the observations discussed in this report.
11. DOC can be determined with ^1H NMR in situ during the early cure.
12. DOC can be determined with FT-IR during the complete cure process.
13. All the techniques used agree very well with regard to the DOC except for the long cure times. It would appear that FT-IR and EPR provide the most sensitive measurements in this later cure region.

14. The 942 cm^{-1} and 3297 cm^{-1} FT-IR bands are found to both be quantitative measures for the DOC in AT systems. This conclusion is in contradiction to the results of Koenig and Shields.³⁰
15. Various spectroscopic parameters can be used as cure-state monitors, including hydrogen spin-lattice and spin-spin relaxation times, fractional acetylene content from ^1H and ^{13}C NMR and FT-IR, and radical concentration from EPR.
16. In situ ^1H NMR is a better cure-state monitor, although FT-IR is perhaps easier for determining the DOC, during early cures than the other techniques.
17. We have shown that EPR, NMR and FT-IR results provide cure-state parameters for AT resins. These parameters define the unique cure-state in the case of isothermal curing.

V. REFERENCES

1. R. F. Kovar, G. F. L. Ehlers, and F. E. Arnold, *J. Polym. Sci., Chem. Ed.* 15, 1081 (1977).
2. J. M. Pickard, E. G. Jones, and I. J. Goldfarb, *Macromolecules* 12, 895 (1979).
3. A. C. Lind, T. C. Sandreczki, and R. L. Levy, AFWAL TR-84-4075 (1984).
4. E. T. Sabourin, AFWAL-TR-80-4151, Oct. 1980.
5. L. R. Denny, C. Y-C. Lee, and I. J. Goldfarb, *ACS Polym. Prepr.*, 25 (1), 183 (1984).
6. M. E. Husaker, and W. A. Feld, *ACS Polym. Prepr.*, 24 (1), 153 (1983).
7. I. J. Goldfarb, unpublished.
8. W. J. Price, *Sample Handling Techniques*, in Laboratory Methods in Infra-red Spectroscopy, R. G. Miller, and B. C. Stace, eds. (Hayden and Son, London, 1972), p. 118.
9. J. Schaefer and E. O. Stejskal, *J. Am. Chem. Soc.* 98, 1031 (1976).
10. A. Pines, M. G. Gibby, and J. S. Waugh, *J. Chem. Phys.* 59, 569 (1973).
11. J. M. Pickard, S. C. Chatteraj, G. A. Loughran, and M. T. Ryan, *Macromolecules* 13, 1289 (1980).
12. M. D. Sefcik, E. O. Stejskal, R. A. McKay, and Jacob Schaefer, *Macromolecules* 12, 423 (1979).
13. S. Meiboom and D. Gill, *Rev. Sci. Instrum.* 29, 688 (1958).
14. ZXSSQ and complimentary subroutines are copyrighted by IMSL, Inc., NBC Building, 7500 Bellaire Boulevard, Houston TX 77036-5085.
15. D. W. McCall, D. C. Douglass, and E. W. Anderson, *J. Polym. Sci.* 59, 301-316 (1962).
16. A. Charlesby and B. J. Bridges, *Eur. Poly. J.* 17, 645-656 (1981).
17. P. J. Flory, Principles of Polymer Chemistry (Cornell University Press, Ithaca, NY, 1953) Chap. IV.
18. P. W. Atkins, Physical Chemistry (W. H. Freeman and Co., San Francisco, 1978) Chap. 26.
19. B. A. Reinhardt and F. E. Arnold, *Polym. Prepr.* 20 (1), 211 (1979).
20. L. A. Carreira and T. G. Towns, *J. Mol. Struct.* 37, 85 (1977).

21. C. W. Bock, M. Trachtman, and P. George, Chem. Phys. 93, 431 (1985).
22. T. Schaefer and W. J. E. Parr, J. Molec. Spectrosc. 61, 479 (1976).
23. J. E. Almlöf, P. U. Isacsson, P. J. Mjöberg, and W. M. Ralowski, Chem. Phys. Lett. 26 (2), 215 (1974).
24. J. E. Anderson, D. J. D. Barkel, and C. J. Cooksey, Tetrahedron Lett. 24 (10), 1077 (1983).
25. W. M. Whitte, E. T. Kang, P. Ehrlich, J. B. Carroll, Jr., and R. D. Allendoerfer, J. Polym. Sci., Chem. Ed. 19, 1011 (1981).
26. R. L. Levy, Mechanism of Epoxy Moisture Effect, Technical Report, AFML-TR-77-41, April 1977.
27. D. Bloor, R. J. Kennedy, and D. N. Batchelder, J. Polym. Sci., Phys. Ed. 17, 1355 (1979).
28. C. L. Leung, ACS Org. Coat. Plast. Chem. Prepr. 46, 322 (1982).
29. J. J. Ratto, P. J. Dynes, and C. L. Hamermesh, J. Polym. Sci., Polym. Chem. Ed. 18, 1035 (1980).
30. Jack L. Koenig, Spectroscopic Characterization of the Cured State of Acetylene-Terminated Resin, Final Report 1 May 1983, AFWAL/MLBP Contract No. F33615-82-K-5038; Jack L. Koenig and Carl M. Shields, J. Polym. Sci. 23, 845-359 (1985).
31. R. L. Levy and R. P. Wool, Polym. Prepr. 20 (2), 239 (1980).
32. R. L. Levy, Polym. Prepr. 21 (2), 263 (1980).
33. R. L. Levy, Org. Coat. Plast. Chem. 45, 727 (1981).
34. I. J. Goldfarb, private communications, 1984.
35. Ref. 17, pg. 47.
36. C. C. Kuo and C.Y.-C. Lee, AFWAL-TR-82-4037 (1982).